NASA CONTRACTOR REPORT

NASA CR-2569





# DESIGN AND PERFORMANCE OF THE UNIVERSITY OF MICHIGAN 6.6-INCH HYPERSONIC WIND TUNNEL, FINAL REPORT

*James L. Amick*

*Prepared by*
THE UNIVERSITY OF MICHIGAN, Univ.
Ann Arbor, Mich.
*for Langley Research Center*

NATIONAL AERONAUTICS AND SPACE ADMINISTRATION • WASHINGTON, D. C. • JULY 1975

| 1. Report No. | 2. Government Accession No. | 3. Recipient's Catalog No. |
|---|---|---|
| NASA CR-2569 | | |

| 4. Title and Subtitle | 5. Report Date |
|---|---|
| Design and Performance of the University of Michigan 6.6-Inch Hypersonic Wind Tunnel | July 1975 |
| | 6. Performing Organization Code |

| 7. Author(s) | 8. Performing Organization Report No. |
|---|---|
| James L. Amick | None |
| | 10. Work Unit No. |

| 9. Performing Organization Name and Address | 11. Contract or Grant No. |
|---|---|
| The University of Michigan<br>Ann Arbor, Michigan | NGR 23-005-600 |
| | 13. Type of Report and Period Covered |

| 12. Sponsoring Agency Name and Address | 13. Type of Report and Period Covered |
|---|---|
| National Aeronautics and Space Administration<br>Washington, D.C. 20546 | Contractor Report |
| | 14. Sponsoring Agency Code |

15. Supplementary Notes

Appendix C by Nikolay Khvostov.
Final report.

16. Abstract

The tunnel described has several design features intended to maintain laminar flow in the boundary layer of its nozzle. Measurements show that transition to turbulence in the nozzle wall boundary layer begins at the throat and is sensitive to surface roughness, heat transfer rate, and longitudinal radius of curvature. The observed dependence of transition on heat transfer rate is the reverse of that predicted by stability theory for infinitesimal disturbances. Tests include boundary-layer surveys of a contoured nozzle and a conical nozzle with four interchangeable throats.

| 17. Key Words (Suggested by Author(s)) (STAR category underlined) | 18. Distribution Statement |
|---|---|
| Transition Longitudinal curvature<br>Nozzle-wall boundary layers<br>Hypersonic wind tunnel<br>Transition reversal<br>Surface roughness Heat transfer | Unclassified - Unlimited<br><br>Subject Category 34 Fluid Mechanics and Heat Transfer |

| 19. Security Classif. (of this report) | 20. Security Classif. (of this page) | 21. No. of Pages | 22. Price* |
|---|---|---|---|
| Unclassified | Unclassified | 80 | $4.75 |

*Available from { The National Technical Information Service, Springfield, Virginia 22151
STIF/NASA Scientific and Technical Information Facility, P.O. Box 33, College Park, MD 20740

# FOREWORD

The research described herein was conducted at the Gas Dynamics Laboratories, Department of Aerospace Engineering, The University of Michigan, under the direction of Professor J. A. Nicholls. This work was performed under NASA Grant NGR 23-005-600 with Ivan E. Beckwith, Head, Gas Dynamics Section, NASA Langley Research Center, as Project Manager.

Design and construction of the 6.6-inch hypersonic wind tunnel were sponsored jointly by The University of Michigan and the Naval Ordnance Systems Command under Subcontract 181462 with the Applied Physics Laboratory of the Johns Hopkins University, during the period 1962-1966. Initial tests to evaluate the flow were sponsored by the Aerospace Research Laboratories of the U. S. Air Force Office of Aerospace Research under Contract AF33(615)-2407. The boundary-layer surveys reported in Appendix C were conducted in 1968 by Dr. Nikolay Khvostov, a visiting Russian scientist whose work at The University of Michigan was funded by the Ford Foundation and the U. S. Department of State as part of the cultural exchange program with the Soviet Union.

TABLE OF CONTENTS

## LIST OF FIGURES

LIST OF FIGURES (Concluded)

# DESIGN AND PERFORMANCE OF THE UNIVERSITY OF MICHIGAN 6.6-INCH HYPERSONIC WIND TUNNEL

By James L. Amick
The University of Michigan

## SUMMARY

This wind tunnel incorporates several features designed to delay transition to turbulence in the boundary layer of its nozzle, either by minimizing the disturbances to which the boundary layer is exposed or by increasing the stability of the boundary layer. The efficacy of these measures for delaying nozzle boundary-layer transition was evaluated primarily by means of a forward-facing annular step, which detected transition as a jump in the ratio of plateau pressure in the separated region ahead of the step, to the tunnel stagnation pressure. Boundary-layer surveys with a travelling pitot probe confirmed the transition indications of the forward-facing step. The boundary-layer surveys covered a contoured nozzle and a conical nozzle with four interchangeable throat inserts.

Throat transition Reynolds numbers higher than those yet obtained in any other nozzle except the Langley 4-in. Mach 5 nozzle were measured in the conical nozzle. Throat surface roughness appeared to be the cause of transition, since heat transfer from the airstream to the nozzle wall, which thinned the boundary layer, hastened transition. In the absence of surface roughness, stability theory for infinitesimal disturbances would predict the opposite effect of heat transfer. A physical juncture in the nozzle wall at a point where the local Mach number was 2.9 had a step height an order of magnitude larger than the throat roughness, yet did not effect transition. An increase in the throat longitudinal radius of curvature lowered the throat transition Reynolds number.

## INTRODUCTION

The subject wind tunnel is a unique facility with several distinctive features designed to promote low-turbulence flow. This report describes the facility and presents the results of measurements to delineate the tunnel performance and to determine the cause of the boundary-layer transition that limits the range of low-turbulence operation.

Existing hypersonic wind tunnels that operate at moderate-to-high Reynolds numbers have high levels of stream turbulence caused by noise radiated from turbulent boundary layers on the nozzle walls. Such high turbulence has a dominant effect on the boundary-layer transition of models immersed in the stream. Because of this dominant effect of stream turbulence, existing hypersonic tunnels are unsatisfactory for critical investigations of boundary-layer transition on models.

In order to achieve a low level of stream turbulence it is necessary to maintain laminar boundary layers on the walls of the wind tunnel nozzle. Recent progress on laminar wind-tunnel nozzles is discussed in references 1 and 2. Beckwith et al. (ref. 1) summarized the efforts of current investigators, and conducted experiments which showed that transition occurs almost simultaneously in the entire supersonic portion of the nozzle boundary layer. It is believed that bursts of turbulence originate in the boundary layer of the throat region and are convected downstream. Because of the stabilizing effect of the favorable pressure gradient, combined with the large increase in boundary-layer volume with distance downstream, the growth of these turbulent bursts may be insufficient to cause them to coalesce before reaching the nozzle exit. Thus the entire nozzle boundary layer downstream of the throat may exist in a transitional state at a given time.

Since boundary-layer turbulence seems to originate at the throat, the problem of how to make a laminar flow nozzle reduces to that of finding a way to avoid having the throat boundary layer become turbulent. In this respect, the degree of success of various supersonic and hypersonic nozzles can be measured in terms of the throat transition Reynolds number, $Re_t = \rho_* v_* d_* / \mu_*$, where $\rho_*, v_*$, and $\mu_*$ are sonic values of mass density, velocity, and viscosity, respectively, when transition is just beginning, and $d_*$ is the throat diameter. The highest values of $Re_t$ yet reported are those of Stainback et al. (ref. 2), who obtained $Re_t = 1.85 \times 10^6$ in the Langley 4-inch Mach 5 nozzle. This throat Reynolds number is not quite high enough to produce natural transition on an insulated cone model in the test section.

The above results of Stainback et al. were obtained using a careful application of conventional wind tunnel design techniques. On the other hand, the 6.6-inch hypersonic wind tunnel described herein has several unconventional features intended to minimize disturbances of the flow entering the nozzle, and to maximize the boundary layer stability.

The tunnel design minimized incoming flow disturbances by providing:

1. vibration isolation of the tunnel from the throttling valve in the high pressure air supply line,

2. uniform heating of the air,
3. a porous metal filter in the settling chamber,
4. a large contraction from settling chamber to throat, and
5. smooth nozzle wall surfaces.

Stability of the boundary layer in the contoured nozzle was maximized by designing the nozzle to have as short a length as practical, so that large favorable pressure gradients would exist throughout its length. Nozzle design accuracy was maintained at a high level to avoid unwanted local compression regions.

The following sections discuss these design features, the overall tunnel performance, and measurements made to determine the cause of transition. An appendix (Appendix C) presents the results of surveys of the nozzle boundary layer conducted by Dr. Nicolay Khvostov, a Russian exchange scientist.

The unit of pressure used throughout most of this report is the kilopascal (kPa). The pascal is the recently adopted name for the newton per square meter. Useful equivalents are

$$
\begin{aligned}
1\ \text{kPa} &= 1000\ \text{N/m}^2 \\
&= 0.1\ \text{N/cm}^2 \\
&= 0.01\ \text{bar} \\
&= 0.14504\ \text{psia} \\
&= 0.0098692\ \text{atmospheres}
\end{aligned}
$$

## TUNNEL DESCRIPTION

The 6.6-inch hypersonic wind tunnel consists of a metal storage heater, interchangeable contoured or conical nozzles, an open-jet test section, and a fixed diffuser, plus necessary inlet and exhaust piping to connect to a high pressure air supply and a vacuum tank. The general arrangement of these components is shown in figure 1.

### Air Supply

The tunnel is supplied with dry compressed air from a large storage tank at pressures up to 170 atmospheres. Throttling from the storage tank pressure to the desired heater pressure (63 atmospheres or less) is accomplished by means of a dome-loaded pressure regulating valve which is remotely controlled from the tunnel operating console. This throttling

valve is connected to the heater by approximately 7 meters of rigid pipe and a 1.3-meter length of flexible hose. The flexible hose isolates the rest of the tunnel from vibrations originating in the throttling valve.

## Heater

The heater consists of a 54-meter length of 26.6-mm-inside-diameter stainless steel pipe, having a wall thickness of 3.4 mm, which is coiled and surrounded by insulation. A low voltage (15-25 V. ac) electric current is passed through this heater pipe in order to preheat it, by resistance heating, to the desired operating temperature of the tunnel (up to 800 K). During a run, cold air enters one end of the heated pipe and emerges from the other end at almost the pipe temperature. The emerging air stream maintains a substantially constant temperature over a long period of time (of the order of a minute), while it is being heated almost entirely by transfer of heat from the upstream portions of the pipe. It is believed that the temperature uniformity of the air stream is very good, because of the large amount of turbulent mixing that takes place downstream of the region where most of the heat is added.

This type of heater was apparently originated at Princeton University, and is described by Zarin in reference 3.

## Settling Chamber

The downstream end of the heater pipe is welded directly to a 100-mm-inside-diameter settling chamber (see fig. 2). Separate resistance heaters are used to preheat this settling chamber to approximately the same temperature as the heater pipe, so that air flowing along the settling chamber walls will maintain nearly the same temperature as that flowing along the axis. Temperatures at various points on the settling chamber and heater pipe are monitored by means of iron-constantan thermocouples. Stagnation air temperature is measured by an iron-constantan thermocouple installed in the center of the settling chamber. An insulating gasket consisting of five layers of Inconel alternating with six layers of wire-mesh-reinforced asbestos is used to seal the flanged joint between the settling chamber and the nozzle, while minimizing heat transfer to the nozzle.

## Spherical Filter

At the downstream end of the settling chamber a porous stainless steel filter is fitted into the nozzle entrance. The filter has a constant thickness of 6 mm and spherical inner and

outer surfaces. The edge of the filter was machined on a lathe to fit the entrance of the nozzle, so that the downstream surface of the filter is perpendicular to the nozzle surface at a point where the local Mach number is 0.0068 (for a 11.1-mm throat diameter). Leakage of air between the filter edge and the nozzle surface is prevented by a thin coating of a high-temperature thread compound.

The spherical filter, with its relatively large pressure drop, effectively obliterates the previous history of the flow. A convergent conical flow begins just downstream of the filter, where all streamlines are perpendicular to the spherical filter surface. Thus, the spherical filter makes possible a nozzle entrance of extremely wide angle ($166^{\circ}$ included angle in this case), which produces a very favorable pressure gradient tending to stabilize the boundary layer. Without the filter, such a wide entrance would cause separation.

It might be thought that the porous material of the spherical filter would be a source of serious turbulence, because of the known tendency of the small jets emerging from the pores to coalesce into larger jets in a repeatable pattern (ref. 4). However, in the case of the present wind tunnel the flow velocity through the porous material is so low that the resulting turbulence can amount to only a few hundredths of one percent of the flow velocity at the throat. Pimenta and Moffat (ref. 4) made hot wire traverses 3 mm downstream from the surface of a porous material sintered from particles of approximately 0.1 mm diameter (a particle size similar to that used in the present spherical filter). They found a mean flow velocity non-uniformity of approximately $\pm$ 3 percent of the average velocity of 0.1 m/s. Applying this same percentage to the spherical filter in combination with a 11.1-mm-diameter throat gives a mean flow velocity non-uniformity of $\pm$ 0.06 m/s, which is only $\pm$ 0.02 percent of the throat velocity. The rms turbulent velocity fluctuation resulting from this mean flow velocity non-uniformity would be an even smaller percentage of the throat velocity.

## Nozzles

Two axisymmetric nozzles have been used with this wind tunnel: 1) a contoured nozzle designed for Mach 8, and 2) a conical nozzle with four interchangeable throat inserts to give Mach numbers between 7 and 10.

The contoured nozzle was carefully designed to have a short length (to maximize the favorable pressure gradient) and yet produce uniform, parallel flow at its exit. The nozzle design procedure is described in Appendix A. The important transonic region was calculated by means of extended Friedrichs method equations given in Appendix B.

The technique of fabrication chosen for the contoured nozzle was that of electroforming. In this process, the nozzle wall is formed by electroplating over a mandrel. When the desired wall thickness is reached, after several weeks of plating, the mandrel is removed. The inside surface of the resulting nozzle duplicates closely the surface finish and shape of the mandrel.

The mandrel for the nozzle was turned from an aluminum billet on a tape-controlled lathe, to a nominal accuracy of 0.025 mm. The tape that controlled the lathe had been generated by a computer program that approximated the calculated nozzle contour by a series of 295 straight-line or circular-arc segments. After machining, the mandrel was hand polished with three grades of silicon carbide paper and two grades of diamond paste.

The electroforming was begun with nickel. After a thin layer of nickel had been built up, the remainder of the electroforming was done with copper, reaching a thickness of 15 to 25 mm. After mating surfaces were machined on both ends of the nozzle, the aluminum mandrel was removed by dissolving with hot sodium hydroxide, leaving a thick-walled copper nozzle with excellent heat-sink characteristics.

Unfortunately, one of the preliminary steps by the electroforming contractor resulted in a rough finish on the nozzle. Some of the roughness in the throat region was subsequently removed by hand polishing.

In place of the contoured nozzle just described, the conical nozzle shown in figure 3 may be installed. This nozzle has an $11^{\circ}$ total cone angle and consists of three major parts: 1) a stainless steel throat insert, 2) a brass piece into which the throat insert fits, and 3) an aluminum downstream piece. The pieces are secured to each other by set screws or bolts, and the joints between them are sealed with O-rings. This nozzle has the same entrance angle as the contoured nozzle ($166^{\circ}$), and can therefore be used with the spherical filter.

There are four interchangeable throat inserts for the conical nozzle. The throat diameters of these inserts, and the theoretical one-dimensional inviscid Mach numbers at the insert downstream end (first juncture), brass piece downstream end (second juncture), and nozzle exit are given in table I.

The smaller diameter throat inserts produce flow static temperatures lower than the equilibrium condensation temperature, for supply temperatures that can be achieved by the heater. However, according to Daum's results (ref. 5) at stagnation pressures in the operating range of this wind tunnel the gas in the nozzle supercools and does not condense.

TABLE I. - CONICAL NOZZLE GEOMETRIC PARAMETERS

| Throat Diameter $d_*$, mm | Nominal Throat Radius of Curvature mm | Supersonic Length mm | One-Dimensional Mach Number at | | |
|---|---|---|---|---|---|
| | | | First Juncture | Second Juncture | Exit |
| 13.18 | 68.5 | 800 | 2.02 | 4.13 | 7.72 |
| 11.1 | 46.5 | 815 | 2.41 | 4.53 | 8.33 |
| 8.7 | 29.5 | 825 | 2.92 | 5.12 | 9.24 |
| 6.83 | 18 | 835 | 3.44 | 5.85 | 10.24 |

The stainless-steel throat inserts were hand polished using diamond polishing compound, but visible circumferential grooves remain. At the junctures between the three nozzle pieces step heights are less than 0.05 mm.

### Diffuser

Flow from the axisymmetric nozzle issues into the test chamber as a free jet, which is collected by the converging supersonic diffuser shown in figure 1. This supersonic diffuser, having a half-angle of $7^{\circ}$, is followed by a 71-cm-long second throat of 18-cm diameter and a $3^{\circ}$ half-angle subsonic diffuser. The diffuser exhausts into a 25-cm diameter pipe which then enlarges to 30-cm diameter and connects to a vacuum tank. The vacuum tank has a volume of 370 $m^3$ and can be evacuated to 0.003 atmosphere.

## TUNNEL PERFORMANCE

With the Mach 8 contoured nozzle installed the tunnel can run for 20 sec or longer over the stagnation pressure range of 100 to 4700 kPa. At intermediate stagnation pressures much longer runs, exceeding two minutes under some conditions, are possible.

The vacuum tank size determines maximum run length at the lower stagnation pressures. A 90 sec run can be made at a stagnation pressure of only 200 kPa.

Run times at the higher stagnation pressures are limited by the heat storage capacity of the coiled-pipe heater. After 20 sec of running at the maximum stagnation pressure of 4700 kPa the heater outlet temperature has fallen about 2 K. Further running results in

increasingly faster temperature drops.

The maximum operating stagnation pressure of 4700 kPa for a nozzle throat diameter of 11.1 mm, results from the 6300-kPa working pressure limitation of the heater and a 1600-kPa pressure drop across the spherical porous-metal filter at this heater pressure. The filter pressure drop is proportional to the heater pressure, for a given nozzle throat area.

Flow uniformity in the contoured nozzle has not been extensively investigated. From a limited number of tests with a 5-prong pitot probe near the nozzle exit, it appears that the Mach number deviations from an average value at a given station are less than ± 2 percent.

## INSTRUMENTATION FOR TRANSITION DETECTION

Transition of the nozzle wall boundary layer in this tunnel has been detected by three kinds of instrumentation: 1) travelling pitot probe traversed through the boundary layer, 2) annular forward-facing step, and 3) pitot pressure fluctuation. The three methods appear to give similar results.

### Travelling Pitot Probe

Boundary-layer surveys in the downstream half of each nozzle were conducted by Dr. Nicolay Khvostov, a Russian exchange scientist sponsored by the State Department. These boundary-layer surveys are described in detail in Appendix C. Briefly, the pressure picked up by a travelling pitot probe was plotted on an x-y recorder as a function of distance from the nozzle wall. Laminar or turbulent boundary-layer states were easily distinguished by the boundary-layer profile shape and relative thickness.

### Annular Step

In order to detect transition near the throat of the conical nozzle an annular forward-facing step was installed at the downstream end of the throat insert, as shown in figure 4. This annular step has a height of 0.84 mm. The step is the front face of a cone frustum which fits tightly into the conical nozzle. It is held in place by three tubes which extend back to the nozzle exit, where they are clamped.

An orifice in the step face senses the plateau pressure $p_p$ in the separated flow ahead of the step. With a laminar boundary layer approaching the step the plateau pressure is considerably smaller than it is when the boundary layer is transitional or turbulent. Thus, a

sudden rise in plateau pressure as the tunnel stagnation pressure $p_o$ is gradually increased signals the beginning of transition.

### Pitot Pressure Fluctuation

A marked increase in pressure fluctuations throughout the supersonic part of the nozzle occurs when the boundary layer becomes transitional, and this can be sensed by a pitot probe as reported in reference 2. For the present tests, a 5.6-mm-diameter quartz piezoelectric transducer was flush mounted at the forward end of an 8-mm-diameter pitot probe. A charge amplifier and rms integrator conditioned the signal for an x-y recorder which plotted the fluctuation level as a function of tunnel stagnation pressure.

## NOZZLE BOUNDARY-LAYER TRANSITION

In order to determine the cause of nozzle boundary-layer transition, tests were conducted in the conical nozzle with the $d_* = 8.7$ mm throat insert in three different surface conditions.

### Nozzle Conditions

Condition A of the $d_* = 8.7$ mm throat insert represents the original condition corresponding to the boundary-layer surveys of Appendix C. The throat region had been polished with a diamond compound, but visible circumferential grooves remained. A profilometer tracing of a portion of the surface 5 mm ahead of the throat, taken in the streamwise direction, is shown as figure 5. Roughness peaks projecting 0.1 $\mu$m above the average surface are present, and a circumferential groove 0.3 $\mu$m deep and 400 $\mu$m wide is seen.

For Condition B the throat insert was polished with a motor-driven endless leather cord threaded through the throat and dressed with a stainless steel buffing compound. This polishing resulted in a greatly decreased roughness height of 0.01 $\mu$m as shown in figure 6, but it produced many pits of diameters ranging up to 100 $\mu$m (not shown in figure 6). Each pit was followed by a long tapering groove extending downstream.

The nozzle throat contour in Condition B was measured by means of a wax replica viewed at 50 times size on an optical comparator, with the result shown in figure 7. The 30-mm longitudinal radius of curvature does not join the conical supersonic portion tangentially but rather at an angle of $7.2^\circ$. The juncture is rounded with radii of 6-28 mm. Presumably this same shape existed in Condition A.

For Condition C the small radius of curvature at the throat in Condition B was increased by removing material until the throat diameter had increased by 0.8 mm to a new throat diameter of 9.5 mm, as shown in figure 7. The new contour was polished with diamond compounds, finishing with the 1/4-$\mu$m grade. However, microscopic examination of a wax impression of the throat region revealed many pits (without tails) ranging up to 100 $\mu$m in diameter and 1 $\mu$m in depth, as well as circumferential grooves about 1 $\mu$m deep.

## Transition Results

Transition data for the three nozzle insert conditions are shown in figure 8. The plateau pressure $p_p$ on the forward-facing annular step is plotted as a function of tunnel stagnation pressure $p_o$. On each curve an increase in the rate of change of step pressure with stagnation pressure above the initial proportional rate indicates the beginning of transition.

Results of pitot pressure fluctuation measurements for Condition B, with the pitot tube located on the nozzle centerline 145 mm downstream of the throat, are compared in figure 9 with annular step pressures. The pitot pressure fluctuation curve represents rms pitot pressures integrated over a 0.1-sec time period, plotted to an arbitrary ordinate scale. The sudden rise in fluctuation level at a stagnation pressure of about 650 kPa indicates the beginning of transition, in agreement with the annular step data.

The results shown in figures 8 and 9 are for room temperature air flowing through the nozzle, with almost no heat transfer to the nozzle wall. When the air was heated to about 500 K and the nozzle was kept near room temperature, the results depicted in figure 10 were obtained. In each of the two runs shown, the tunnel stagnation pressure was increased and decreased through several cycles. Each sudden rise in step pressure (marking the beginning of transition) occurred at a higher stagnation pressure than the preceeding one. Thus the nozzle transition Reynolds number increased monotonically during each run, whereas during the cold flow runs it had remained constant.

The increase in transition Reynolds number during the runs with heated air is believed to be due to the diminishing heat transfer rate interacting with the throat surface roughness. At the beginning of a run the nozzle throat is relatively cold and there exists a high rate of heat transfer to the wall, which thins the boundary layer, making the surface roughness appear relatively large. Later in the run the heat transfer rate has decreased because the wall is hotter, so that the boundary layer is thicker and less susceptible to disturbance by the surface roughness. (See Appendix C for similar results.)

The transition data of figures 8 and 10 are summarized in figure 11, and compared with data from the Langley 4-in. Mach 5 tunnel (ref. 2). The abscissa in this plot is the nozzle wall temperature minus the stagnation temperature, $T_w - T_o$. This temperature difference gives a rough measure of the rate of heat transfer from the nozzle wall to the airstream. The values plotted are based on the estimated nozzle wall temperature before each run, with no allowance for the actual change in wall temperature at the throat during the run. To minimize the error due to this approximation, the transition Reynolds numbers $Re_t$ plotted are those observed near the beginning of each run.

The data points in figure 11 at a temperature difference of -470 K represent transition near the nozzle exit as determined by the boundary-layer surveys of Appendix C. These results are in general agreement with the other results of the present tests, which were obtained with the forward-facing step. Since the forward-facing step data were taken ahead of the juncture between dissimilar metals in the conical nozzle, while the boundary-layer surveys were made downstream of the junctures, any irregularities at these junctures must have had no effect on boundary-layer transition. Step heights at the first and second junctures are less than 50 $\mu$m and the local Mach numbers are 2.9 and 5.1, respectively.

General agreement is indicated in figure 11 between the present tests and the Langley 4-in. Mach 5 results, as to the effect of heat transfer on nozzle transition. The heat transfer effect is such as to implicate throat surface roughness as the immediate cause of transition in both tunnels.

Figure 11 indicates a significant decrease in transition Reynolds number in this tunnel when the longitudinal radius of curvature $r_c$ in the immediate neighborhood of the throat is increased (Condition C compared with Condition A and B), since the effective surface roughnesses of the three conditions are believed to be similar. The contoured nozzle also had a relatively large throat longitudinal radius of curvature, and a correspondingly low transition Reynolds number.

## CONCLUSIONS

From the results of tests of The University of Michigan 6.6-in. hypersonic wind tunnel it is concluded that:

1. Nozzle boundary-layer transition in this wind tunnel is caused by throat roughness.

2. For a given throat roughness, decreasing the longitudinal radius of curvature in the immediate throat region can raise the throat transition Reynolds number.

3. Contrary to expectations based on stability theory for infinitesimal disturbances, heat transfer from the airstream to the nozzle wall decreases the throat transition Reynolds number, when significant surface roughness is present.

4. Throat transition Reynolds numbers obtained in this tunnel under zero heat transfer conditions are higher than those reported for any other nozzle except the Langley 4-in. Mach 5.

## APPENDIX A

## DESIGN OF A SHORT-LENGTH NOZZLE FOR MACH 8

A Mach 8 axisymmetric nozzle was designed to produce uniform flow in an unusually short length, so that a laminar nozzle boundary layer might exist at high Reynolds numbers. The design methods used are described in the following.

Calculation of the inviscid flow began with an assumed centerline Mach number distribution (fig. A1). The flow field was calculated outward from the centerline, using the Friedrichs method (ref. 6) for subsonic and transonic regions, and the characteristics method in the supersonic region.

The Friedrichs method is a series solution of the exact flow equations, expanded about the throat. The method therefore gives very good accuracy near the throat, and becomes less accurate with increasing distance from the centerline. Accuracy also depends on the number of terms carried in the series. To increase accuracy, several additional terms beyond those given by Friedrichs were calculated. The equations used are shown in Appendix B; resulting streamlines for the centerline distribution of figure A1 are shown in figure A2. An enlarged view of the throat region flow is shown in figure A3.

The supersonic region was calculated by the usual axisymmetric method of characteristics, except that parabolic, rather than linear, extrapolation along Mach lines was used. Each point was iterated several times (usually 4 or 5 but sometimes as many as 22 times). This work (as well as the Friedrichs calculations) was done on the University's high-speed digital computer.

Part of the computed network of Mach lines is shown in figure A4. The region where nearly-horizontal Mach lines come together is shown in closer view in figure A5. Some of these Mach lines coalesce into an impossible sudden-expansion singularity.

Two streamlines of the flow are also shown in figure A5, as calculated by the Friedrichs method and as calculated by the method of characteristics. The two methods tend toward agreement as the throat is approached or as the centerline is approached. The discrepancies between the two methods are better seen in figure A6. Here the circles represent the radial differences between characteristics and Friedrichs calculations, in the region where the two results overlap. It was assumed that the characteristics results are correct. The dashed

curve for $\eta = .028$ (the chosen streamline for the inviscid nozzle wall) was used as a correction to the Friedrichs method results in the region between the throat and the first characteristics point.

The $\eta = .028$ streamline was chosen for the wall after weighing several factors. On the one hand, it was desired to have the largest possible value of $\eta$, in order to maximize the favorable pressure gradient. On the other hand, a large value of $\eta$ would mean that the correction shown in figure A6 would be large and therefore less accurate; also $\eta$ must be small enough to avoid the singularity shown in figure A5. (Actually, it is wise to keep some distance from the singularity so that the rapid turning and localized expansion associated with closely spaced Mach lines is lessened, since these would tend to make construction of a satisfactory nozzle more difficult, and the boundary layer correction less accurate.)

Coordinates of the $\eta = .028$ streamline are given in table AI. This streamline has a maximum inclination to the axis of $24^{\circ}$. The resulting value of L (fig. 2) is 19.75 cm, for a 15.23 cm inviscid exit diameter, and the axial distance from the sonic point on the axis to the exit plane is 5.26 times the inviscid exit diameter.

The actual physical contour of the nozzle was obtained by adding a laminar boundary layer displacement thickness, as calculated by the method of Cohen and Reshotko (ref. 7), to the inviscid flow streamline. The boundary layer calculations were made for stagnation conditions of 2760 kPa and 728 K. The resulting displacement thickness at the exit is .76 cm giving a final exit diameter of 16.76 cm (6.60 in.).

Table AI. Inviscid Streamline Data, $\eta = .028$

| x/L | r/L | M | $\theta$, rad |
|---|---|---|---|
| -.1544 | .20863 | .0068 | -1.4180 |
| -.1492 | .16843 | .0111 | -1.4125 |
| -.1447 | .14250 | .0164 | -1.3713 |
| -.1407 | .12425 | .0225 | -1.3186 |
| -.1368 | .11087 | .0297 | -1.2568 |
| -.1331 | .10066 | .0375 | -1.1888 |
| -.1295 | .09264 | .0456 | -1.1163 |
| -.1261 | .08616 | .0537 | -1.0457 |
| -.1227 | .08081 | .0620 | -.9802 |
| -.1195 | .07633 | .0703 | -.9202 |
| -.1164 | .07253 | .0788 | -.8664 |
| -.1135 | .06926 | .0875 | -.8183 |
| -.1107 | .06642 | .0965 | -.7757 |
| -.1081 | .06395 | .1058 | -.7367 |
| -.1056 | .06178 | .1154 | -.7024 |
| -.1032 | .05986 | .1253 | -.6719 |
| -.1010 | .05814 | .1355 | -.6451 |
| -.0871 | .04896 | .1971 | -.5085 |
| -.0716 | .04123 | .2892 | -.3916 |
| -.0549 | .03524 | .4127 | -.2844 |
| -.0514 | .03426 | .4433 | -.2630 |
| -.0479 | .03335 | .4757 | -.2418 |
| -.0443 | .03251 | .5101 | -.2209 |
| -.0407 | .03175 | .5465 | -.2003 |
| -.0371 | .03105 | .5849 | -.1799 |
| -.0335 | .03043 | .6254 | -.1597 |
| -.0298 | .02988 | .6678 | -.1397 |
| -.0261 | .02940 | .7124 | -.1200 |
| -.0224 | .02899 | .7589 | -.1005 |
| -.0187 | .02865 | .8075 | -.0812 |
| -.0150 | .02838 | .8581 | -.0621 |
| -.0113 | .02818 | .9108 | -.0431 |
| -.0075 | .02806 | .9653 | -.0243 |
| -.0038 | .02800 | 1.0219 | -.0057 |
| -.0000 | .02802 | 1.0803 | .0128 |
| .0036 | .02810 | 1.1409 | .0313 |
| .0074 | .02825 | 1.2034 | .0499 |
| .0111 | .02848 | 1.2680 | .0685 |
| .0149 | .02877 | 1.3349 | .0873 |
| .0186 | .02914 | 1.4041 | .1063 |
| .0223 | .02957 | 1.4756 | .1255 |
| .0260 | .03008 | 1.5498 | .1451 |
| .0297 | .03066 | 1.6268 | .1651 |
| .0334 | .03131 | 1.7071 | .1858 |

| x/L | r/L | M | $\theta$, rad |
|---|---|---|---|
| .0363 | .03187 | 1.7720 | .2028 |
| .0389 | .03244 | 1.8354 | .2194 |
| .0419 | .03313 | 1.9108 | .2393 |
| .0453 | .03400 | 2.0047 | .2649 |
| .0491 | .03512 | 2.1298 | .3007 |
| .0537 | .03666 | 2.3165 | .3568 |
| .0590 | .03879 | 2.4764 | .3917 |
| .0653 | .04143 | 2.6013 | .4053 |
| .0725 | .04455 | 2.7210 | .4115 |
| .0808 | .04819 | 2.8419 | .4132 |
| .0904 | .05242 | 2.9667 | .4115 |
| .1016 | .05728 | 3.0982 | .4072 |
| .1147 | .06287 | 3.2354 | .4002 |
| .1300 | .06927 | 3.3832 | .3908 |
| .1481 | .07658 | 3.5334 | .3792 |
| .1694 | .08490 | 3.6957 | .3656 |
| .1946 | .09433 | 3.8676 | .3500 |
| .2246 | .10498 | 4.0494 | .3326 |
| .2603 | .11695 | 4.2417 | .3136 |
| .3030 | .13030 | 4.4445 | .2934 |
| .3539 | .14508 | 4.6578 | .2721 |
| .4146 | .16128 | 4.8807 | .2500 |
| .4868 | .17883 | 5.1127 | .2275 |
| .5724 | .19760 | 5.3523 | .2049 |
| .6731 | .21733 | 5.5972 | .1826 |
| .7908 | .23770 | 5.8450 | .1608 |
| .9269 | .25827 | 6.0926 | .1398 |
| 1.0825 | .27855 | 6.3364 | .1199 |
| 1.2574 | .29797 | 6.5722 | .1015 |
| 1.4525 | .31610 | 6.7980 | .0844 |
| 1.6647 | .33236 | 7.0081 | .0689 |
| 1.8913 | .34641 | 7.2001 | .0552 |
| 2.1282 | .35805 | 7.3712 | .0432 |
| 2.3697 | .36722 | 7.5196 | .0330 |
| 2.6109 | .37412 | 7.6454 | .0243 |
| 2.8444 | .37898 | 7.7481 | .0173 |
| 3.0647 | .38218 | 7.8293 | .0118 |
| 3.2669 | .38413 | 7.8911 | .0075 |
| 3.4479 | .38521 | 7.9360 | .0044 |
| 3.6060 | .38575 | 7.9666 | .0023 |
| 3.7418 | .38597 | 7.9857 | .0010 |
| 3.8585 | .38604 | 7.9958 | .0002 |
| 3.9623 | .38606 | 7.9995 | .0000 |
| 4.0642 | .38606 | 7.9999 | .0000 |

## APPENDIX B

## FRIEDRICHS METHOD EQUATIONS FOR AXISYMMETRIC FLOW

In order to increase accuracy, the equations given in Friedrichs' original reports (refs. 8 and 9) were extended to include higher order terms. The extended expansions are given below, including new equations for the coefficients of the higher order terms.

### Definitions

| | |
|---|---|
| $x$ | axial coordinate, measured from sonic point on axis |
| $r$ | radial coordinate |
| $L$ | centerline distance from sonic line to beginning of test section |
| $\bar{x}$ | non-dimensional axial coordinate, $x/L$ |
| $\bar{y}$ | non-dimensional radial coordinate, $r/L$ |
| $\xi$ | potential line coordinate, value of $\bar{x}$ where potential line crosses axis |
| $\eta$ | streamline coordinate, value of $\bar{y}$ where streamline crosses $\bar{x} = 0$ line |
| $M_o$ | Mach number on centerline |
| $h_o$ | centerline stream tube height, $\left[(M_o^2 + 5)^3/(216\ M_o)\right]^{1/2}$ |
| $q/q_o$ | velocity ratio |
| $\theta$ | flow angle |
| $b$ | $M_o^2 - 1$ |

## Expansions

$$\bar{x} = \xi + x_2 \eta^2 + x_4 \eta^4 + x_6 \eta^6 + \cdots$$

$$\bar{y} = h_o \eta + y_3 \eta^3 + y_5 \eta^5 + \cdots$$

$$\theta = \theta_1 \eta + \theta_3 \eta^3 + \theta_5 \eta^5 + \cdots$$

$$q/q_o = 1 + q_2 \eta^2 + q_4 \eta^4 + \cdots$$

## Coefficients

$$\theta_1 = h_o'$$

$$q_2 = \frac{h_o h_o''}{2}$$

$$y_3 = \frac{h_o}{4}\left[b\, q_2 - \frac{\theta_1^2}{2}\right]$$

$$\theta_3 = \frac{\theta_1 q_2}{60\, b}(47\, M_o^4 + 20\, M_o^2 + 5) + \frac{h_o^2 h_o'''}{8} b - \frac{\theta_1 y_3}{3\, h_o}$$

$$q_4 = \frac{q_2}{20\, b}\left[\frac{q_2}{2}(29\, M_o^4 + 20\, M_o^2 - 25) + \frac{\theta_1^2}{6}(19\, M_o^4 + 20\, M_o^2 - 15)\right.$$

$$\left. + \frac{\theta_1^2 M_o^2 (M_o^2 + 5)}{15\, b^2}(47\, M_o^4 - 94\, M_o^2 - 25)\right]$$

$$+ \frac{h_o^2}{160}\left[\frac{\theta_1 h_o'''}{b}(28\, M_o^4 + 10\, M_o^2 + 10) + 5\, b\, h_o h_o''''\right]$$

$$x_4 = -\frac{h_o}{32}\left[b\, h_o^2 h_o''' + \frac{2\theta_1 q_2}{5b}(29\, M_o^4 - 20\, M_o^2 + 15)\right]$$

$$y_5 = \frac{h_o}{6}\left[\frac{q_2^2}{80}(41\, M_o^4 - 10\, M_o^2 + 65) + b\, q_4 - \frac{5b\, q_2 \theta_1^2}{16} - \frac{\theta_1^4}{192} - \theta_1 \theta_3\right]$$

$$x_2 = -\frac{h_o \theta_1}{2}$$

$$\theta_5 = \frac{1}{240}\left[\frac{\theta_1 q_2^2}{10\, b^2}(2781\, M_o^8 + 3080\, M_o^6 - 7390\, M_o^4 - 400\, M_o^2 - 375)\right.$$

$$+ \frac{\theta_1^3 q_2 M_o^2}{25\, b^4}(1134\, M_o^{10} + 2303\, M_o^8 - 10268\, M_o^6 + 3630\, M_o^4 + 16150\, M_o^2 + 875)$$

$$+ \frac{q_2 h_o^2 h_o'''}{2}(127\, M_o^4 + 80\, M_o^2 - 15) + \frac{5 h_o^4 h_o V_b^2}{4}$$

$$+ \frac{\theta_1^2 h_o^2 h_o'''}{20\, b^2}(770\, M_o^8 + 729\, M_o^6 - 1875\, M_o^4 - 125\, M_o^2 - 75)$$

$$\left. + \theta_1 h_o^3 h_o''''(14\, M_o^4 + 5\, M_o^2 + 5) + \frac{9\, \theta_1^5}{8}\right]$$

$$x_6 = -\frac{h_o}{6}\left[\theta_5 - \frac{\theta_1^2 \theta_3}{2} + \frac{\theta_1^5}{120} + b\, q_2 \theta_3 - b\, q_2 \frac{\theta_1^3}{6} + \frac{\theta_1 q_2}{10}(7\, M_o^4 - 5\, M_o^2 + 10) + \theta_1 q_4 b + 4\frac{y_3 x_4}{h_o^2} - \theta_1 \frac{y_5}{h_o}\right]$$

## APPENDIX C

## NOZZLE BOUNDARY-LAYER SURVEYS AT M = 6 - 9

by Nikolay Khvostov

In order to obtain information on boundary layer growth in hypersonic wind tunnel nozzles, and on the location and causes of boundary layer transition in nozzles, a series of boundary layer surveys was conducted in the conical nozzle at M = 5.8 - 9.2 and in the contoured nozzle (M = 7.8).

### Instrumentation and Tests

The boundary layer surveys made use of a traveling pitot probe consisting of a square-ended stainless steel tube of 1.1 mm outside diameter and .8 mm inside diameter, with a length of 48 mm. It was connected to a pressure transducer by a 180-mm length of 1.1 mm inside diameter tubing and a 500-mm length of 2.3 mm inside diameter tubing.

The calibration of the pressure transducer and recording equipment at low differential pressures was performed with a water manometer having a micrometer scale and inclined index. For differential pressures higher than 150 mm of water a mercury manometer was used.

The pitot probe was mounted on a traversing mechanism driven by a reversible alternating current motor. To record the probe location with respect to the nozzle wall, a ten-turn potentiometer geared to the traversing mechanism was used.

The signals from the pitot-pressure transducer were recorded by an x-y plotter as ordinates, while the signals from the ten-turn potentiometer (proportional to distance from the wall) were used as abscissa values. The pitot-pressure profile through the boundary layer at a fixed nozzle station was thus plotted directly.

The experiment was conducted in the following way: At the beginning of a run the probe touched the nozzle wall; after the flow in the nozzle had become stable the probe was moved along the nozzle radius for a distance of 20 - 35 mm and then returned to its original position. At the moment the probe made electrical contact with the wall, the electric motor used to move the probe was shut down automatically. Due to the large friction in the probe gear

and the fast response of the motor, the probe stopped almost instantaneously when the current supply was shut off.

## Data Reduction

Mach number in the flow core was determined from the ratio of the measured value of the pitot pressure (total pressure behind the normal shock) to the stagnation pressure $p_o'/p_o$ and the isentropic flow tables. Then the static pressure $p_{st}$ in the flow core was calculated and assumed to remain constant through the boundary layer at a given nozzle station. Mach number distribution in the boundary layer was obtained from the static pressure and the measured values of $p_o'$.

A pressure lag was observed near the nozzle wall due to the response of the measuring line to the low pitot pressure. In this case the data reduction used an average of the readings taken with the probe moving toward the wall and away from the wall.

## Boundary-Layer Profiles

General test results are presented as the variation of Mach number with a nondimensional distance from the nozzle wall y/R, where R is the nozzle radius in the plane of measurements. In figures C1 and C2 test data are presented for the conical nozzle with the throat diameter $d_* = 11.1$ mm, at a distance x = 770 mm from the throat and at different Reynolds numbers, $Re_x = (\rho v x)/\mu$, where $\rho$, v, $\mu$ are the density, velocity, and viscosity in the isentropic flow core, respectively. Reynolds number is changed by the supply pressure variation. The stagnation temperature varies only slightly from test to test and is equal approximately to 710 K $\pm$ 10%.

The test results for the laminar nozzle flow are shown in figure C1. At the supply pressure $p_o$ = 164 kPa ($Re_x = 0.38 \times 10^6$) separation occurred in the nozzle, which did not effect the core flow, but induced the local pressure increase at the edge of the boundary layer. In defining Mach numbers from the ratio $p_{st}/p_o'$ under the assumption that $p_{st}$ is constant throughout any nozzle cross section, Mach numbers at the boundary of the separated region are overestimated. This fact is shown in figure C1 (Run No. 30). As the supply pressure increases, the separated zone disappears and the Mach number profile varies smoothly.

Near the wall, Mach numbers vary slowly with distance from the wall. As Reynolds number increases, the boundary layer thickness reduces, the isentropic core dimension becomes larger, and the Mach number profile is found to be more steep.

Turbulent boundary layer results are presented in figure C2. The turbulent velocity profile is much different from the laminar one, having significantly increased velocity near the wall and decreased velocity near the outer edge of the boundary layer, and having twice the total thickness. Mach number in the core decreases to M = 7.55 as compared with M = 7.7 for a laminar flow at the maximum Reynolds number.

Mach number profiles at nozzle station x = 570 mm, for the conical nozzle with the same throat diameter ($d_*$ = 11.1 mm), are presented in figures C3 and C4. Profiles for the three other throat diameters ($d_*$ = 8.7, 6.83, and 13.18 mm) are presented in figures C5-C20.

For Mach numbers exceeding 8.5 a viscous interaction between the isentropic flow and the boundary layer is evident. This appears as an increase of the pressure measured by the probe near the boundary layer edge. The pressure increases as the probe moves from the nozzle axis to the boundary layer edge due to the streamline curvature, reaches a maximum, and decreases near the nozzle wall due to the viscous effect. The streamline curvature is inevitably accompanied by a static pressure variation across the nozzle. Thus, the evaluation of Mach number in the boundary layer from the core static pressure may result in an appreciable error.

Therefore the test results for Mach numbers exceeding 8.5 are presented as the variation of the pressure ratio (measured pressure $p_0'$ to supply pressure $p_0$) against the nondimensional distance from the nozzle wall y/R.

The test data for the boundary layer in the contoured nozzle are presented in figures C21-C23. The stability of the boundary layer in the contoured nozzle appears to be less than in the conical one.

## Transition Reversal

In tests of the conical nozzle with throat diameter of $d_*$ = 11.1 the transition of a turbulent boundary layer to a laminar one (transition reversal) was observed. Recorder traces are shown on figure C24 for two runs, when the transition of the turbulent nozzle flow to the laminar one occurred at constant supply conditions.

In run No. 20 (supply pressure and temperature were 689 kPa and 635 K, respectively) the probe touched the wall at the initial moment of the experiment (y = 0) and moved along the nozzle radius to the axis during the test. The direction of the probe movement is shown by arrows. As the probe moved from the wall, a typical "turbulent" pressure profile was recorded. At some distance from the wall pressure oscillations appeared which were not

observed in the preceding tests. As the external limit of the boundary layer was approached, these pulsations disappeared. As the probe moved to the wall, a typical laminar pressure profile was obtained. The boundary layer thickness reduced significantly.

Almost analogous results were obtained in run No. 21 (supply pressure $p_o$ = 689 kPa, supply temperature $T_o$ = 645 K). However, at the moment of tunnel starting the probe was within the core, at a distance greater than the turbulent boundary layer thickness (point 1 in figure C24). As the probe moved to the wall, it passed through a pressure oscillation region and the boundary layer became laminar. The probe having touched the nozzle wall, it was introduced again into the core (line 2) and then moved back to the wall (line 3). During this period the flow remained laminar without visible pressure oscillations. The discrepancy between the lines (2) and (3) near the wall is due to the response of measuring lines when low pressures are measured.

The pressure values obtained outside the boundary layer differ significantly. The pressure $p_o'$ in the laminar flow is lower than in the turbulent one. This fact defines a difference of Mach number outside the boundary layer. Thus, in the turbulent flow, M = 6.76; in the laminar, M = 6.92.

In spite of the fact that the Mach number variation in the nozzle is only 2%, the area of the uniform Mach number field increased approximately by 60%. Such an appreciable variation of the boundary layer thickness shows that the transition includes a significant part of the nozzle or the whole nozzle and not only the station which is considered.

The transition of the turbulent flow to a laminar one is apparently due to wall heating in the transonic region of the nozzle. As the nozzle wall temperature increases, the boundary layer thickness also increases. The effect of wall roughness (which produces turbulence) decreases, and the boundary layer no longer becomes turbulent downstream. This transition is accompanied by oscillations of the boundary layer thickness which are observed by the pressure variation near the outer edge of the boundary layer.

Although the supply pressure and temperature are constant in figure C24, the local Reynolds numbers are different: the turbulent value is $Re_x = 1.62 \times 10^6$ and the laminar $Re_x = 1.52 \times 10^6$. This difference is due to the nozzle Mach number variation.

This anomalous behavior of the boundary layer was subsequently observed in tests of the conical nozzle with other throat diameters. Examples of transition reversal are seen in the boundary layer profiles for runs No. 71 (fig. C7), No. 162 (figs. C14 and C15), No. 224 (fig. C16), and No. 243 (fig. C20).

To evaluate the rate of change of the turbulent flow to a laminar one, the process of the pressure variation at a given point of the boundary layer was investigated in the conical nozzle with throat diameter $d_* = 13.18$ mm. The probe was placed at a distance 5.4 mm from the nozzle wall ($y/R = 0.11$) and at $x = 440$ mm from the throat. The supply pressure was $p_o = 470$ kPa, as in run No. 243 (fig. C20). The pressure history is shown in figure C25. It is evident that the measured pressure remained steady during the first 20 sec and then began to increase smoothly. This increase terminated at $t > 90$ sec. The transition region was characterized by pressure oscillations which reached 3-4%.

## Displacement Thickness

In figure C1 the vertical bars show the displacement thickness $\delta^*$ related to the nozzle radius R at a given station by

$$\delta^*/R = 1 - (d_*/2R)\sqrt{A/A_*}$$

where $A/A_*$ is the area ratio corresponding to the Mach number in the core.

The variation of displacement thickness against Mach number for the laminar boundary layer in the conical nozzle is plotted in figure C26. The curve represents the equation

$$(\delta^*/x)\sqrt{Re_x} = 0.32\ M^{1.8} \qquad \text{(laminar)}$$

A similar plot for the turbulent boundary layer yielded the equation

$$(\delta^*/x)(Re_x)^{1/5} = 0.0133\ M^{3/2} \qquad \text{(turbulent)}$$

These empirical relations are plotted in figure C27 along with all the displacement thickness data as a function of Reynolds number.

The effect of inlet turbulence on boundary layer transition in nozzles was evaluated in tests conducted without the spherical filter in place. Removing the filter resulted in appreciable pressure oscillations near the outer edge of the boundary layer, and a shift of the transition region to lower Reynolds numbers. This transition region shift to lower Reynolds numbers is shown in figure C27. Similar results were obtained for $d_* = 13.18$ mm (not shown).

Area ratios calculated from the empirical laminar and turbulent displacement thickness relations for $Re_x = 1.5 \times 10^6$ are compared in figure C28 with one-dimensional theory.

When these results are used, it should be taken into account that the data were obtained not for an adiabatic wall but at the temperature factor $T_w/T_o = 0.43 - 0.52$, where $T_w$ is the nozzle wall temperature at a distance 400 - 430 mm from the throat.

## Conclusions

Laminar, turbulent, and transitional boundary layers have been surveyed in the conical nozzle at Mach numbers 5.8 - 9.2, and in the contoured nozzle at M = 7.8. The wall temperature to stagnation temperature ratio at the nozzle mid-length station was $T_w/T_o = 0.43 - 0.52$.

Simple empirical equations fitted to the experimental data express the displacement thickness in terms of the length Reynolds number and core Mach number, for either laminar or turbulent flow in the conical nozzle.

Transition reversal (a change from turbulent to laminar flow as heat transfer rate is decreased) occurs in the conical nozzle at certain Reynolds numbers.

Without the spherical filter in place at the nozzle entrance, appreciable pressure fluctuations are noted near the outer edge of the boundary layer, and transition begins at lower Reynolds numbers.

## APPENDIX D

## SYMBOLS

| | |
|---|---|
| $A$ | cross section area of air stream |
| $A_*$ | sonic cross section area |
| $d_*$ | throat diameter of nozzle |
| $L$ | length of nozzle from throat to beginning of test section on axis |
| $M$ | Mach number |
| $p_o$ | stagnation pressure |
| $p_o'$ | pitot pressure |
| $p_p$ | plateau pressure |
| $p_{st}$ | static pressure |
| $R$ | radius of nozzle cross section |
| $Re_t$ | transition Reynolds number, $\rho_* v_* d_*/\mu_*$ |
| $Re_x$ | Reynolds number based on distance from throat, $\rho vx/\mu$ |
| $r_c$ | longitudinal radius of curvature at throat |
| $r_*$ | throat cross section radius, $d_*/2$ |
| $T_o$ | stagnation temperature |

| | |
|---|---|
| $T_w$ | wall surface temperature |
| v | velocity |
| $v_*$ | sonic velocity |
| x | distance from throat |
| y | distance from wall, perpendicular to axis |
| $\delta^*$ | displacement thickness |
| $\eta$ | streamline coordinate |
| $\theta$ | flow angle |
| $\mu$ | viscosity |
| $\mu_*$ | sonic viscosity |
| $\rho$ | mass density |
| $\rho_*$ | sonic mass density |

## REFERENCES


1. Beckwith, I. E.; Harvey, W. D.; Harris, J. E.; and Holley, B. B.: Control of Supersonic Wind-Tunnel Noise by Laminarization of Nozzle-Wall Boundary Layers. NASA TM X-2879, 1973.

2. Stainback, P. C.; Anders, J. B.; Harvey, W. D.; Cary, A. M.; and Harris, J. E.: An Investigation of Boundary-Layer Transition on the Wall of a Mach 5 Nozzle. Pts. I and II. AIAA Paper No. 74-136, Jan. 1974.

3. Zarin, N. A.: The Development of a Hypersonic Air Tunnel and Some Preliminary Experimental Results. Princeton University Aeronautical Engineering Report No. 666, March 1963.

4. Pimenta, M.; and Moffat, R. J.: Stability of Flow Through Porous Plates: Coalescent Jets Effect. AIAA J., vol. 12, no. 10, Oct. 1974, pp. 1438-1440.

5. Daum, F. L.: Air Condensation in a Hypersonic Wind Tunnel. AIAA J., vol. 1, no. 5, May 1963, pp. 1043-1046.

6. Hopkins, D. F.; and Hill, D. E.: Effect of Small Radius of Curvature on Transonic Flow in Axisymmetric Nozzles. AIAA J., vol. 4, no. 8, Aug. 1966, pp. 1337-1343.

7. Cohen, C. B.; and Reshotko, E.: The Compressible Laminar Boundary Layer with Heat Transfer and Arbitrary Pressure Gradient. NACA Report 1294, 1956.

8. Friedrichs, K. O.: Theoretical Studies on the Flow Through Nozzles and Related Problems. Applied Mathematics Group, New York University, Rept. 82.1R, AMG-NYU 43, 1944.

9. Friedrichs, K. O.: On Supersonic Compressors and Nozzles. Applied Mathematics Group, New York University, Rept. 82.2, AMG-NYU 77, 1944.

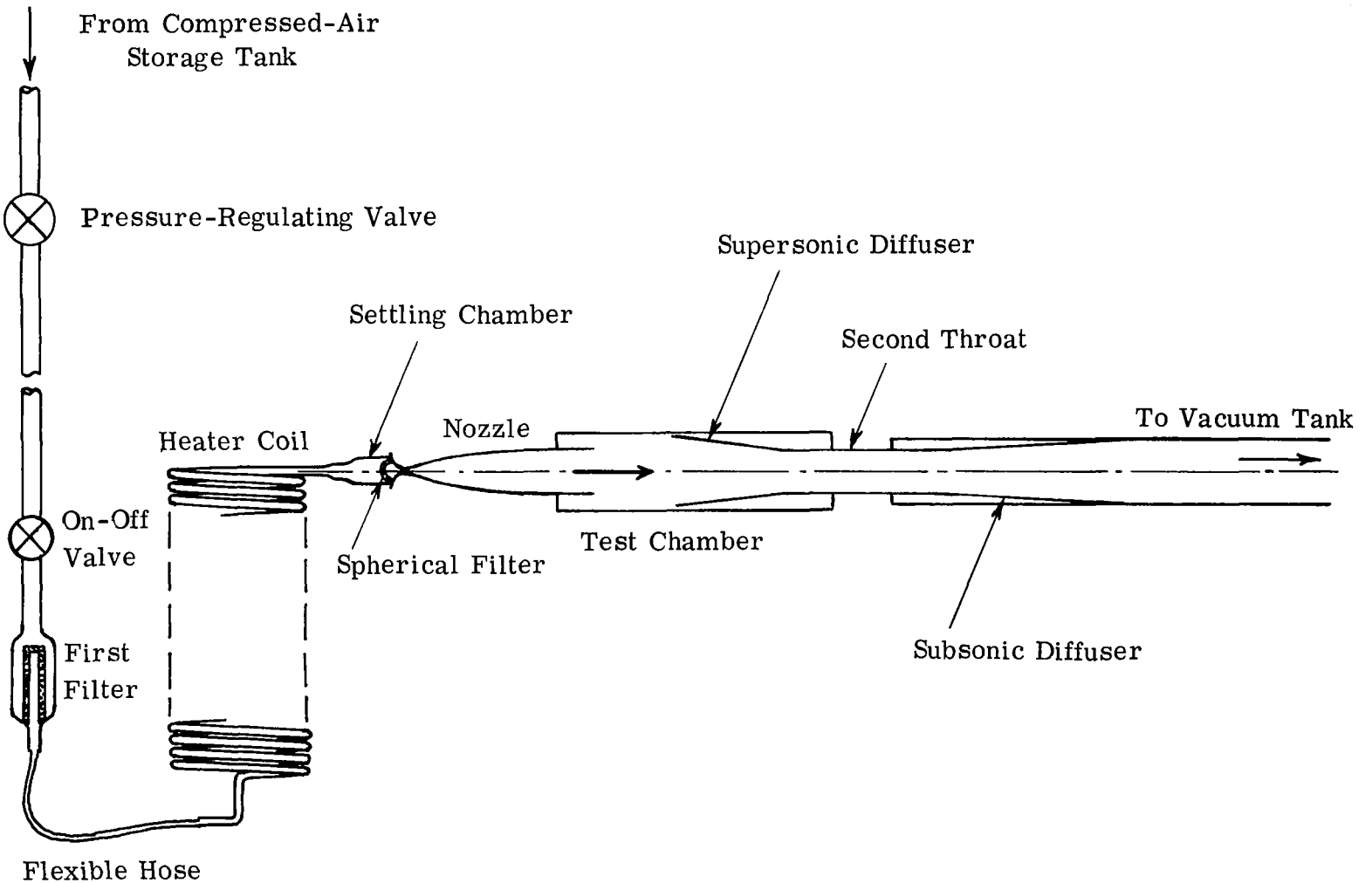


Figure 1. Arrangement of Wind-Tunnel Components. 1/25-Size.

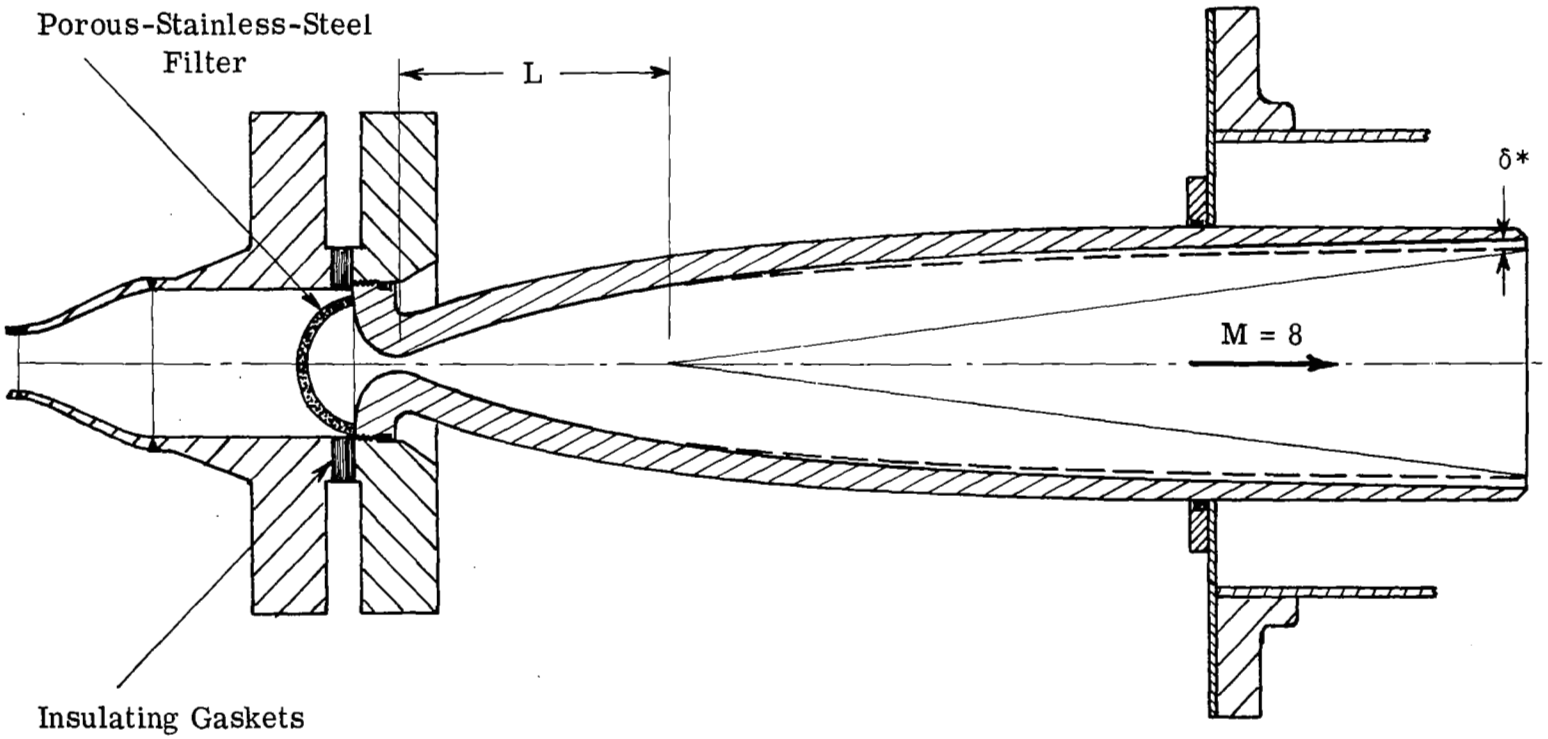


Figure 2. Section Through Contoured Mach 8 Nozzle Installation. 1/5-Size.

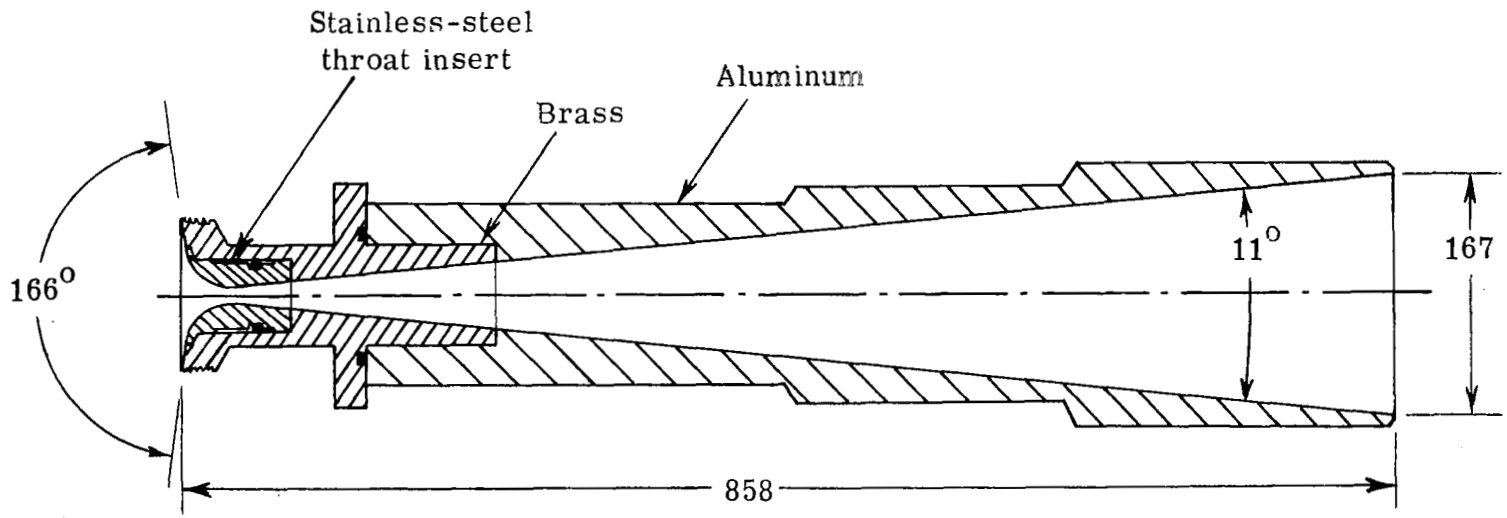


Figure 3. Section Through Conical Nozzle. 1/5-Size. Dimensions in mm.

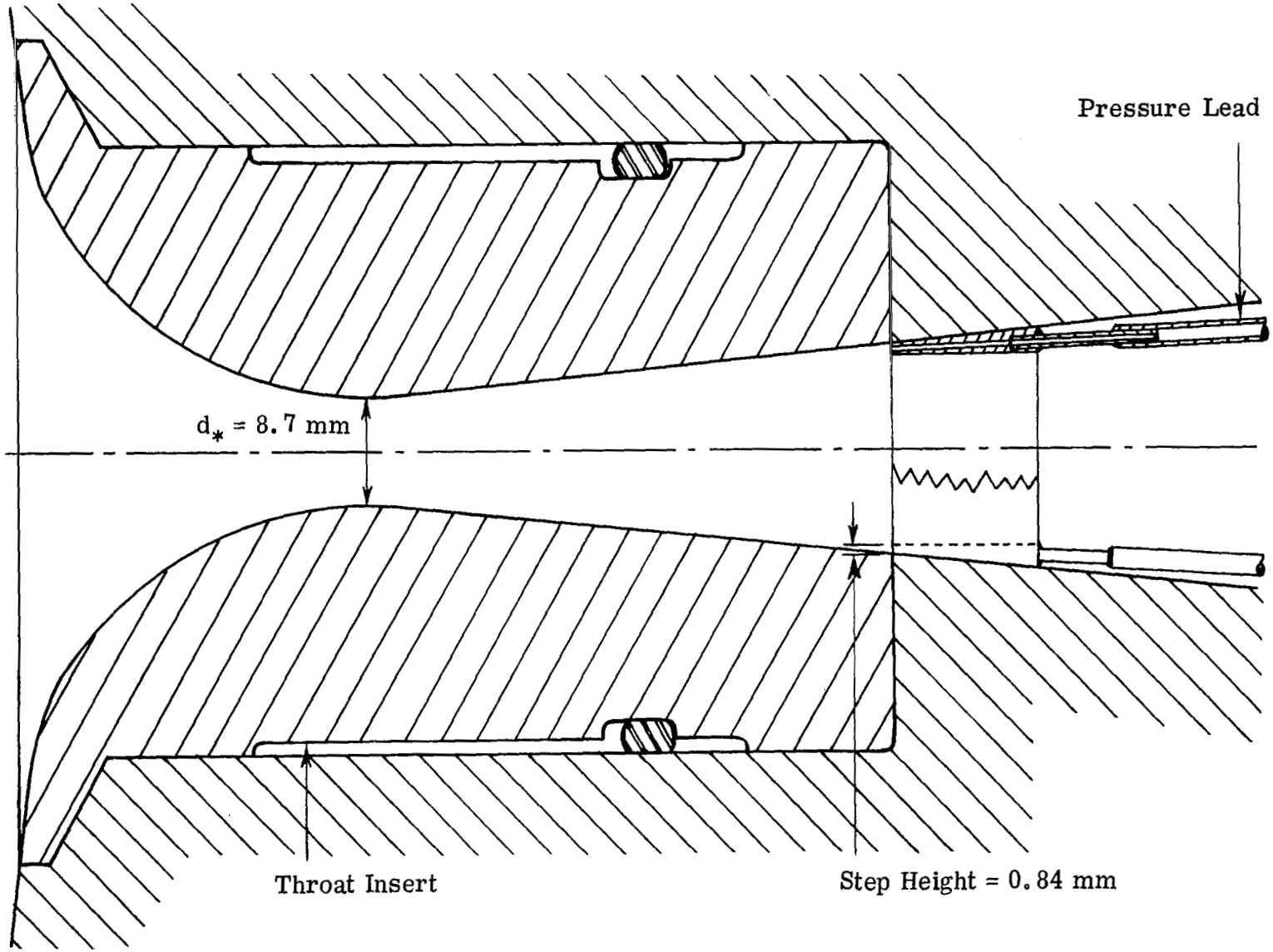


Figure 4. Annular Forward-Facing Step Installed in Conical Nozzle. Twice Size.

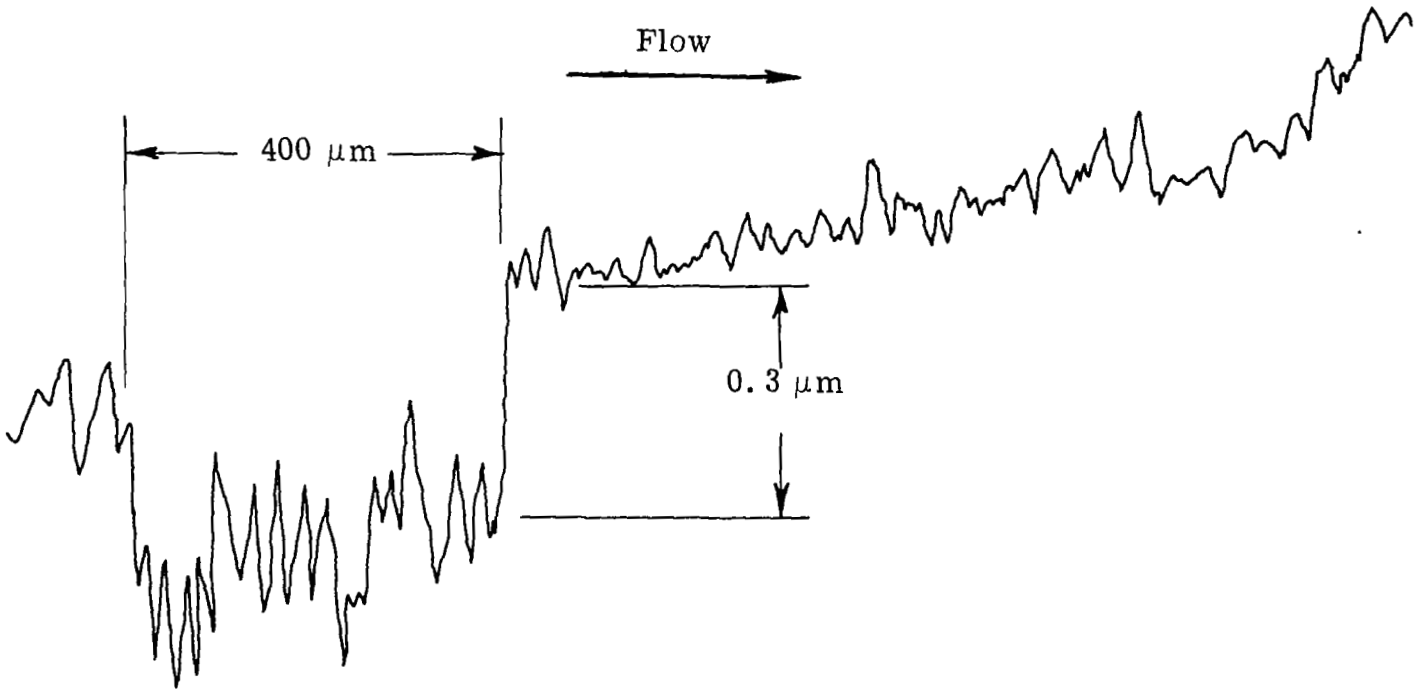


Figure 5. Proficorder Trace of Throat Surface in Condition A.

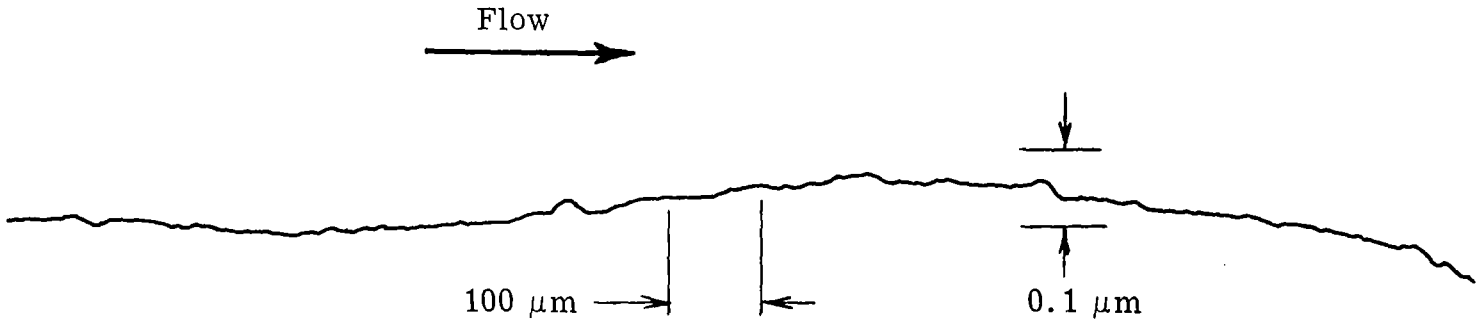


Figure 6. Proficorder Trace of Throat Surface in Condition B.

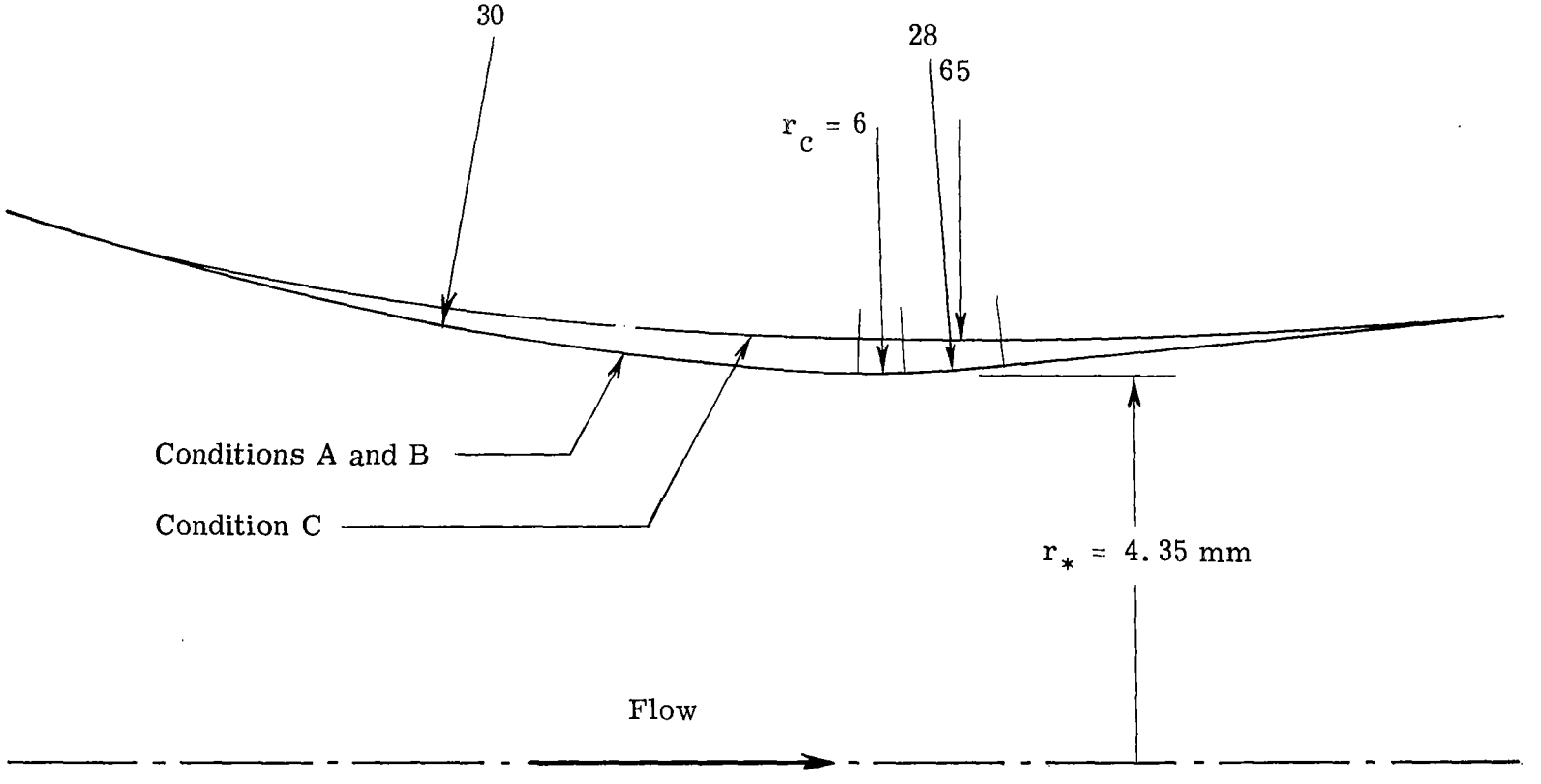


Figure 7. Throat Contours. Longitudinal Radii of Curvature in mm.

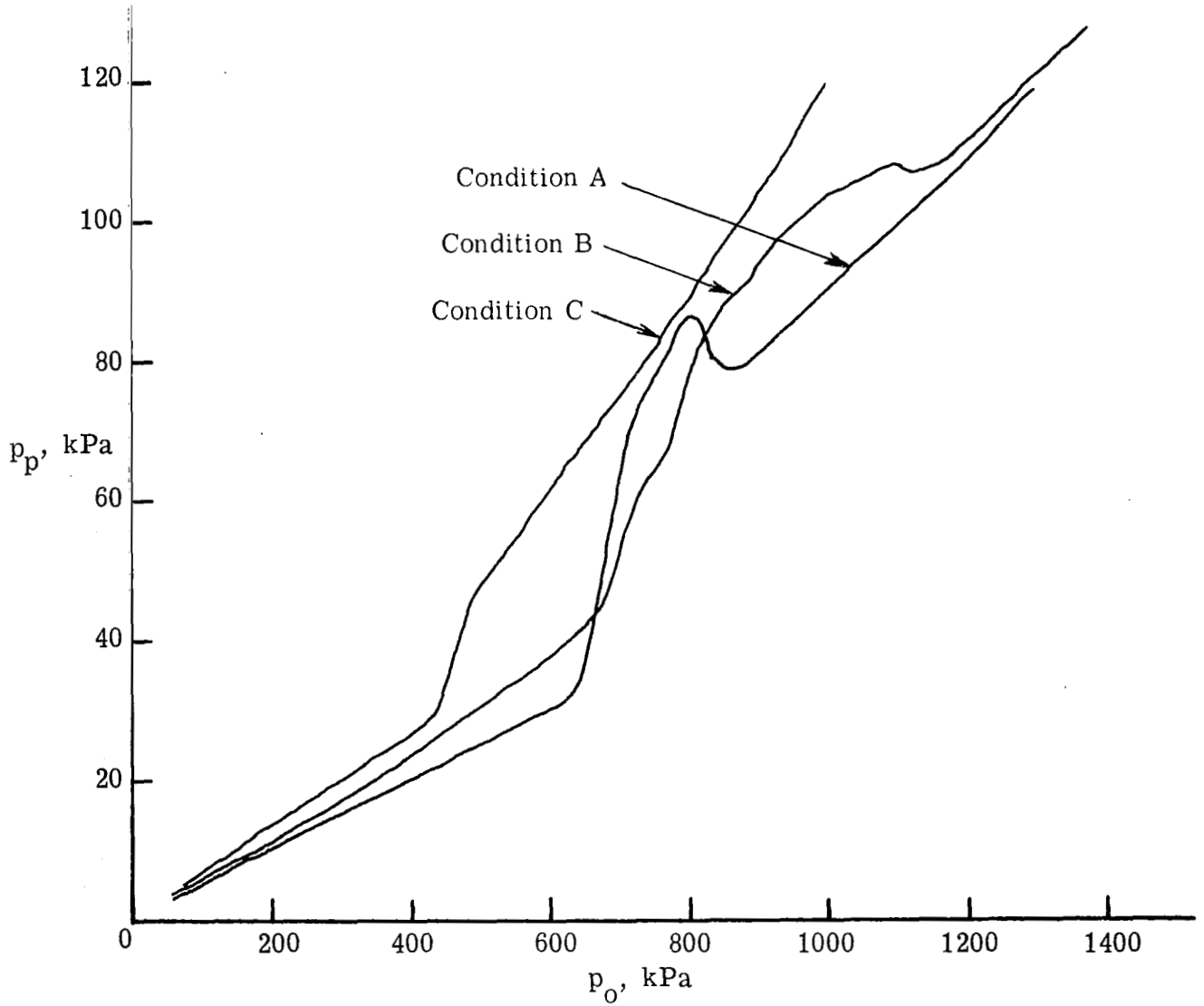


Figure 8. Plateau Pressure on Annular Step as a Function of Tunnel Stagnation Pressure. Unheated Air.

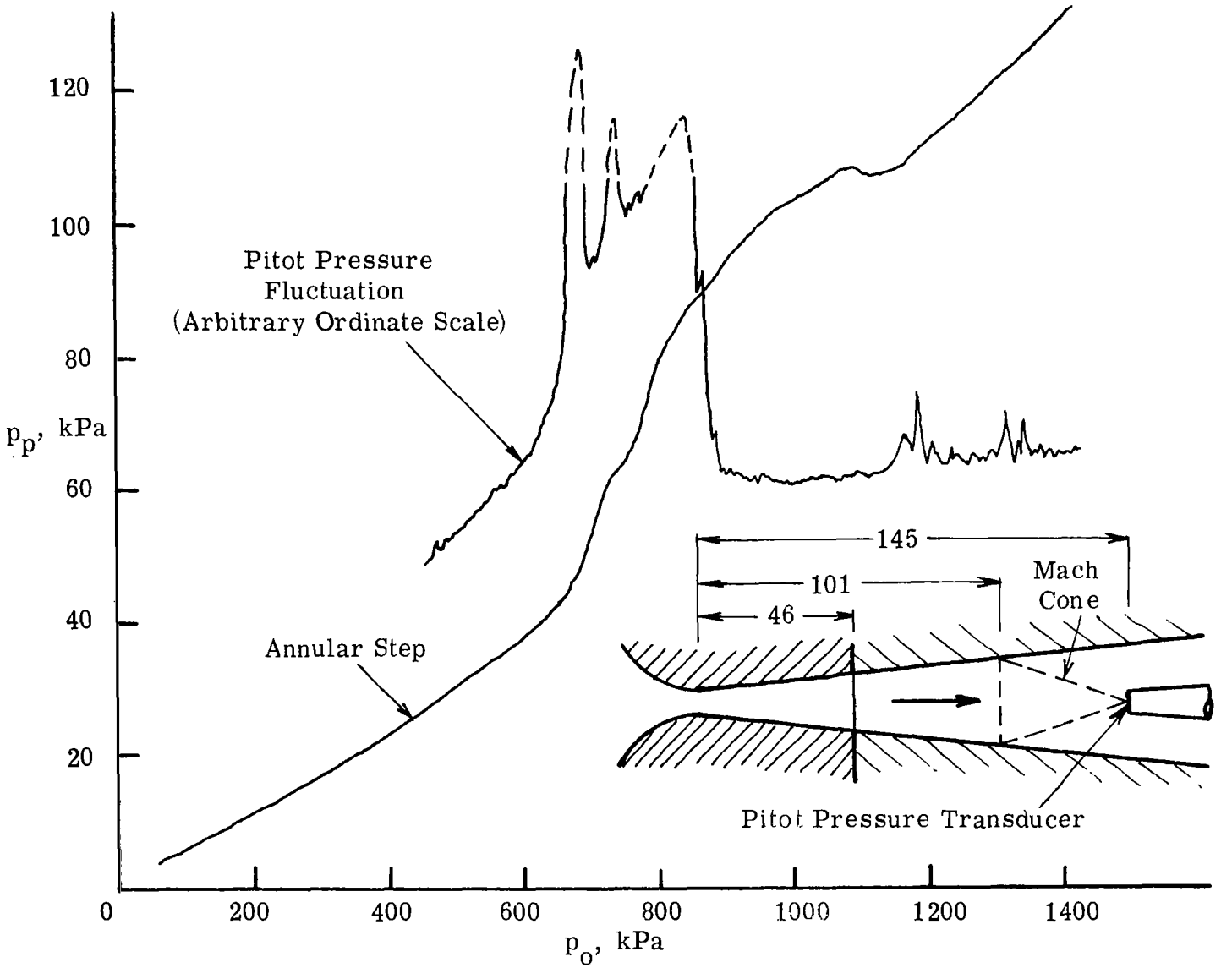


Figure 9. Pitot Pressure Fluctuation Compared with Plateau Pressure on Annular Step. Condition B, Unheated Air.

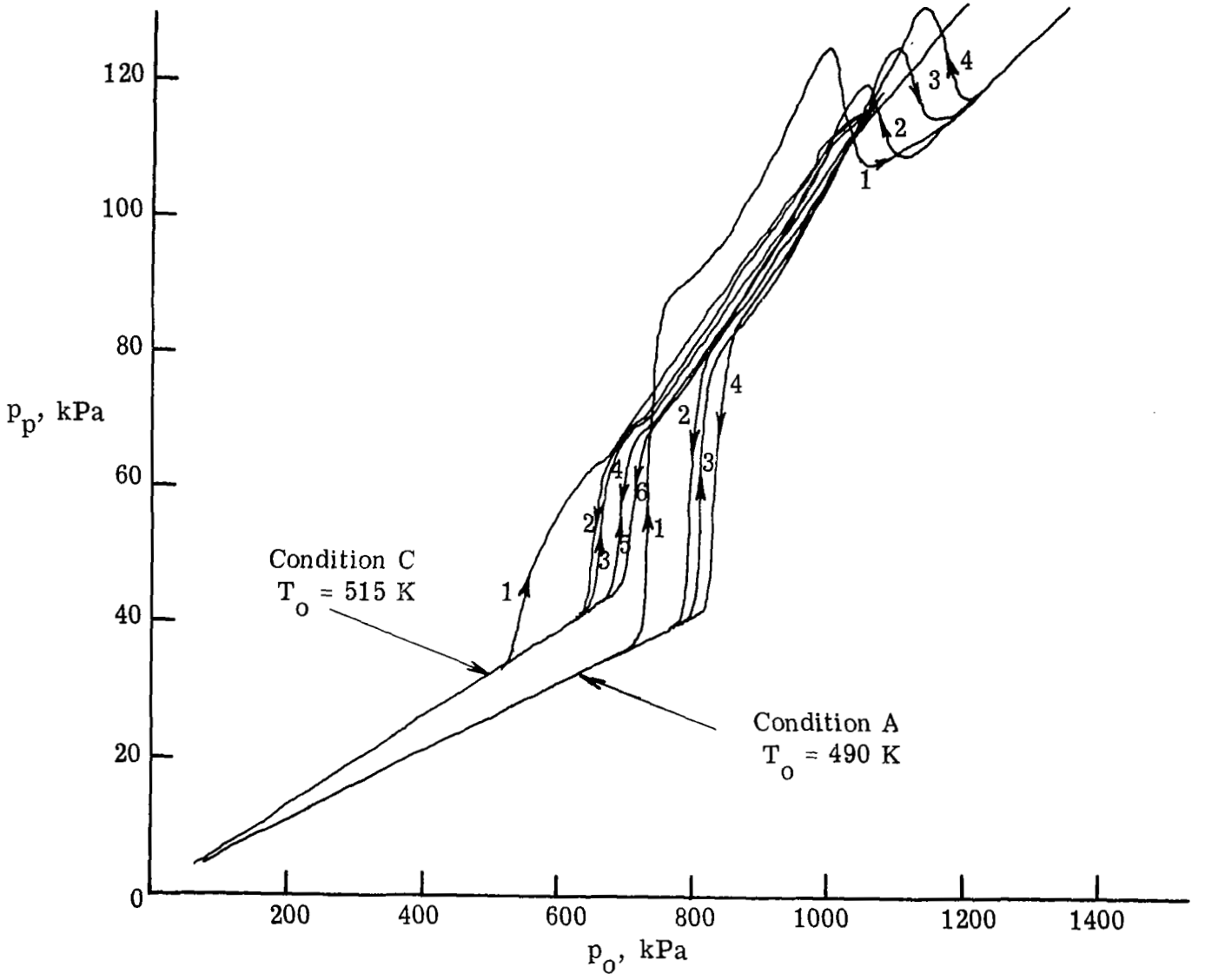


Figure 10. Plateau Pressure on Annular Step as a Function of Tunnel Stagnation Pressure, Heated Air.

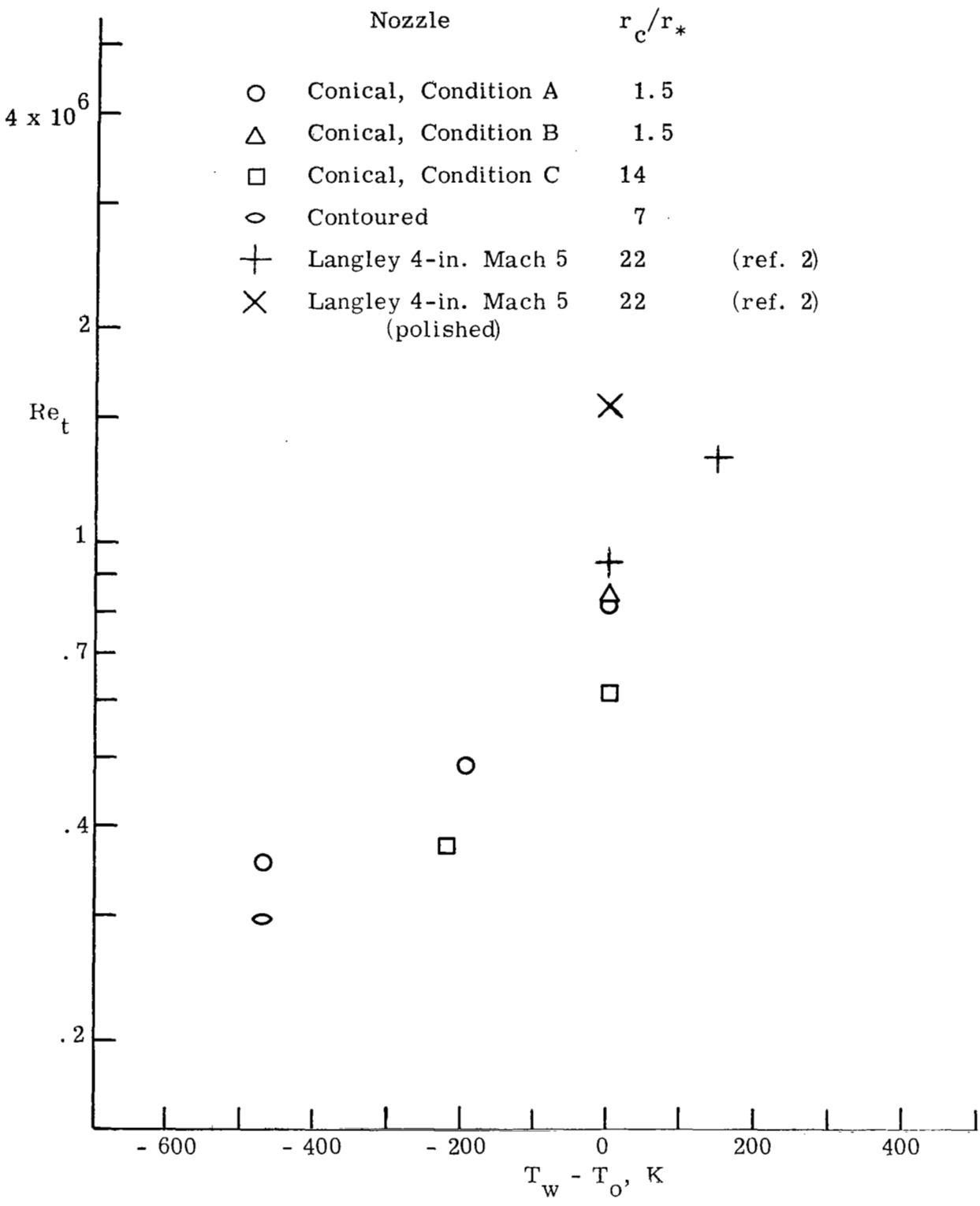


Figure 11. Variation of Throat Transition Reynolds Number with Heat Transfer Rate.

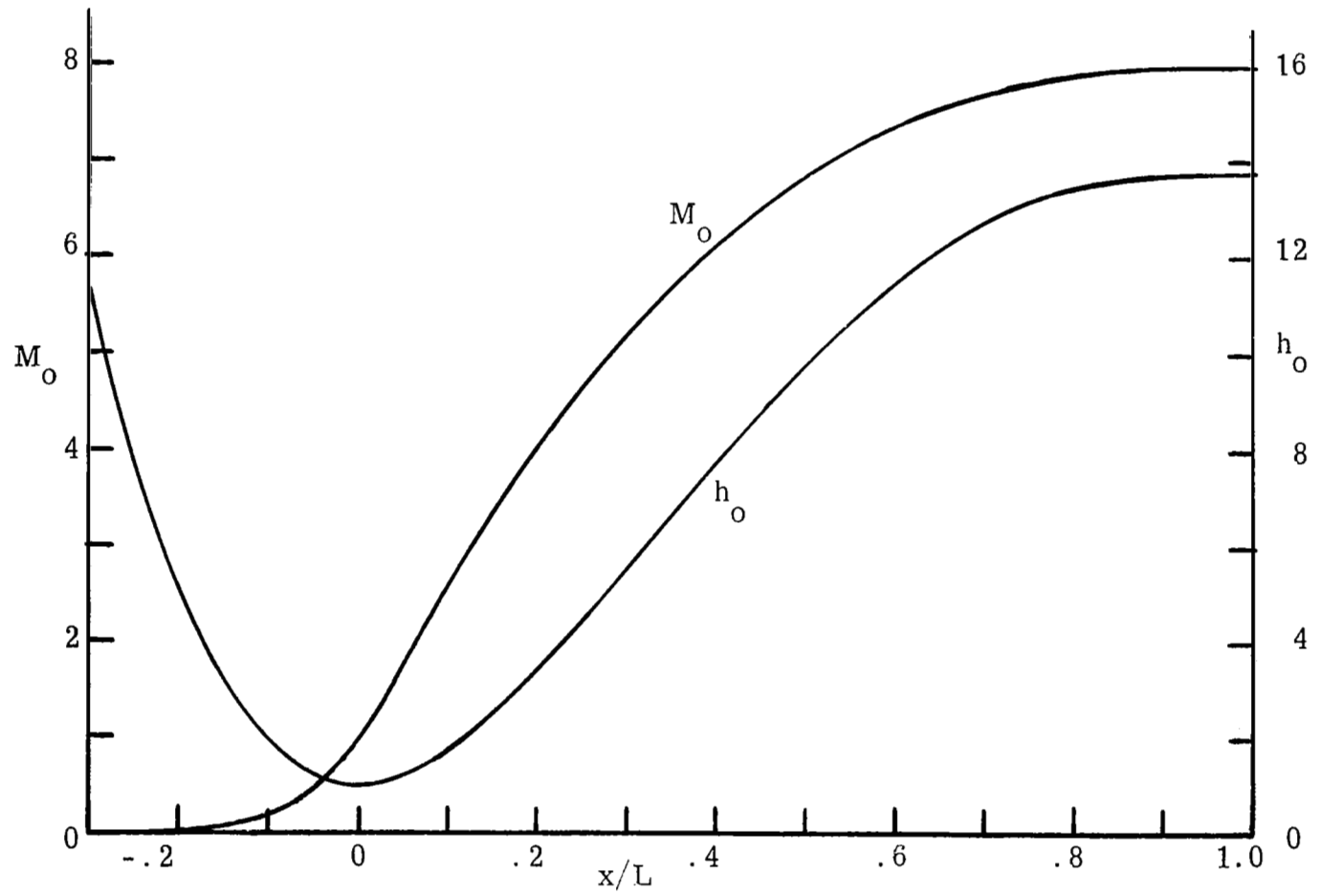


Figure A1. Prescribed Distribution of Centerline Area Ratio Parameter, $h_o$ ($\equiv [(M_o^2 + 5)^3/(216\ M_o)]^{1/2}$), and Resulting Centerline Mach Number Distribution. $h_o = 1 + 12.788\ (x/L)^2\ [6 - 8\ (x/L) + 3\ (x/L)^2]$

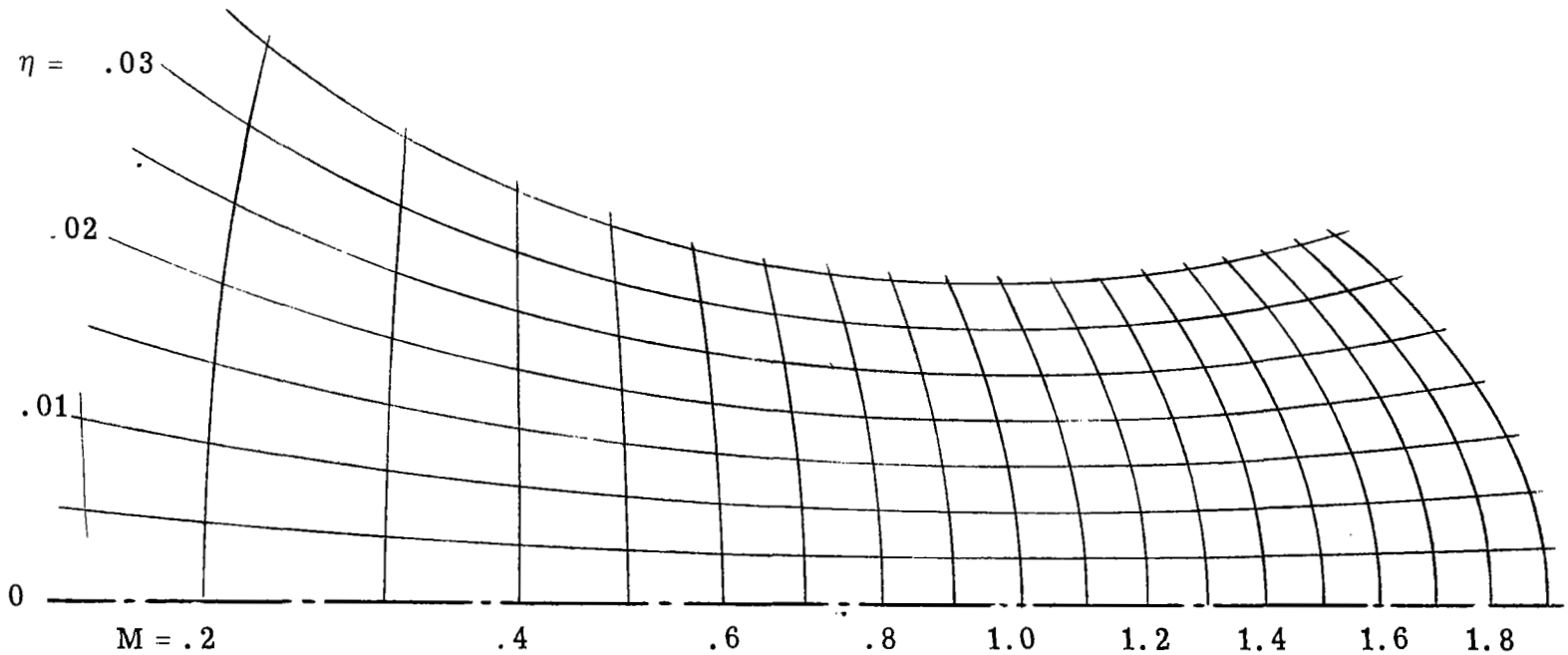


Figure A2. Streamlines and Constant Mach Number Lines in Throat Region, as Calculated by Friedrichs Method.

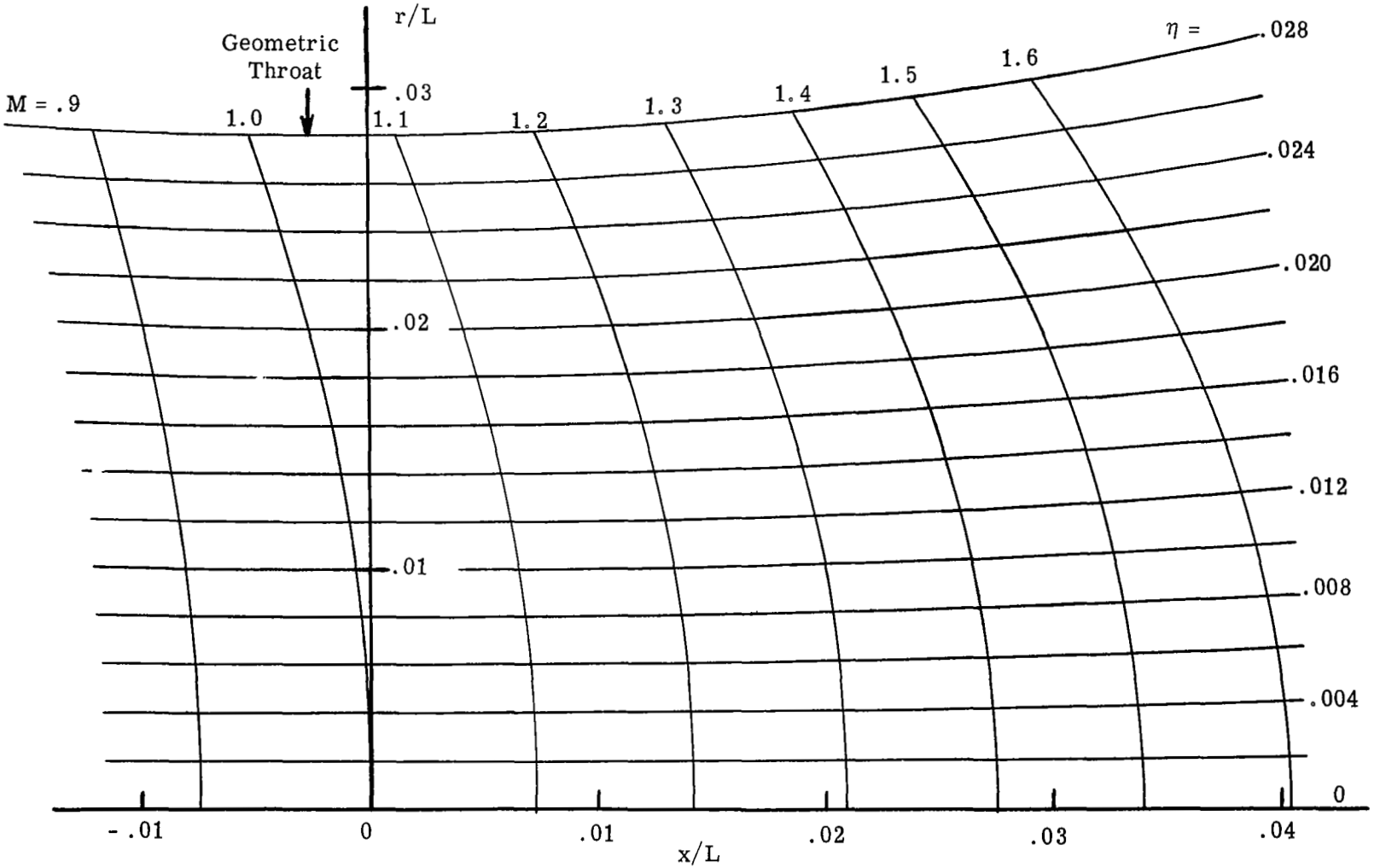


Figure A3. Enlarged View of Throat Streamlines and Constant Mach Number Lines by Friedrichs Method.

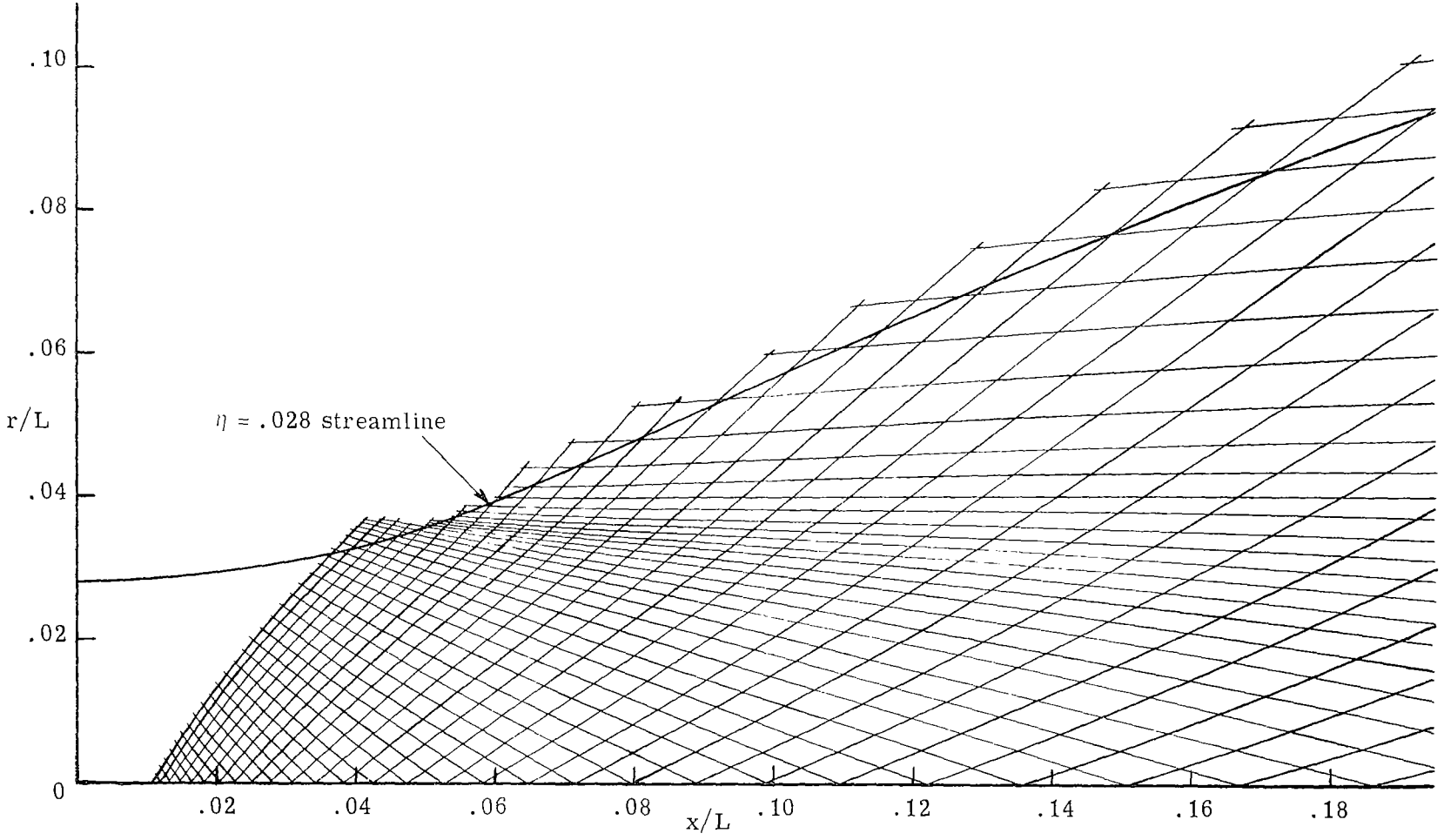


Figure A4. Characteristics Network Near Throat

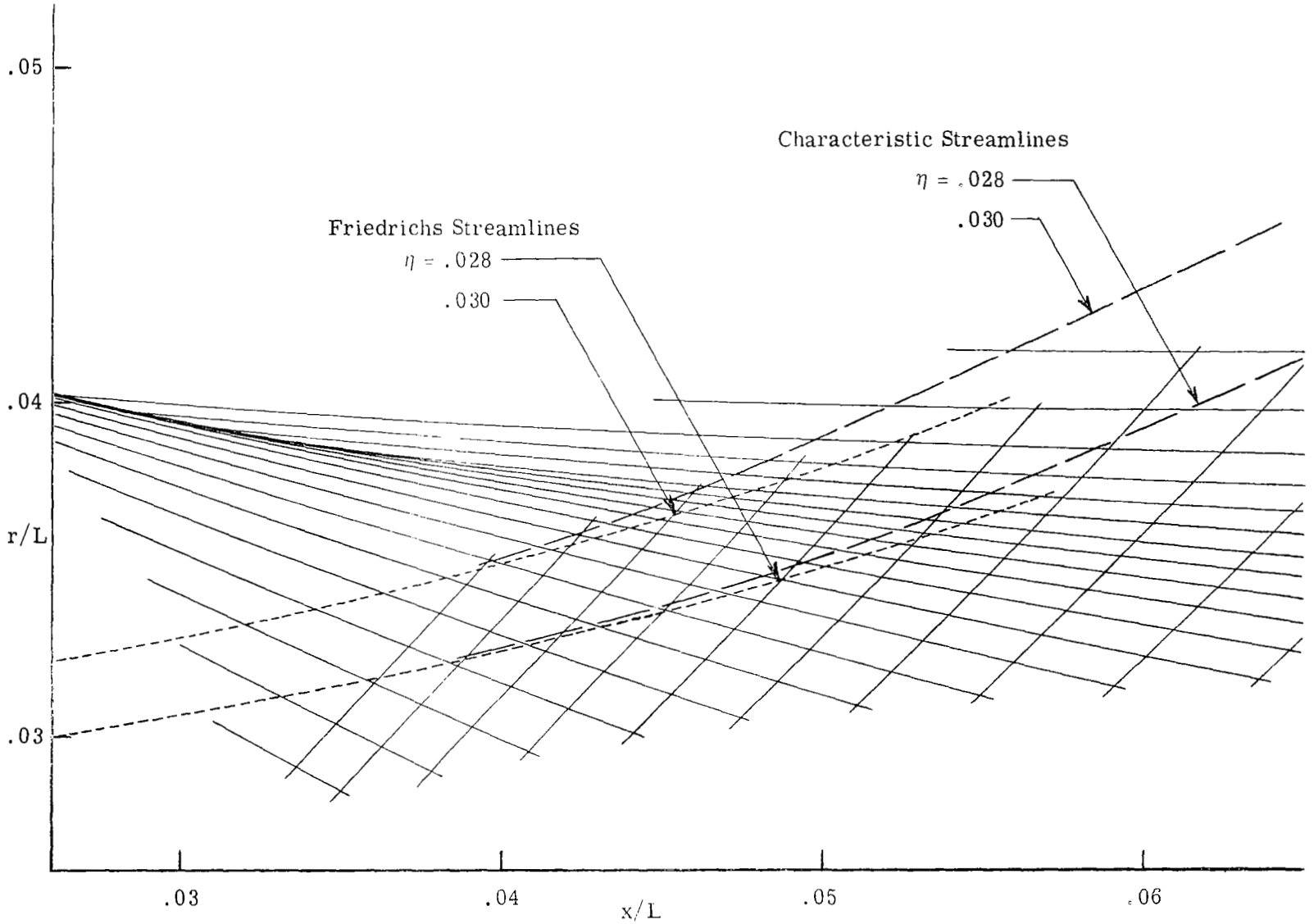


Figure A5. Coalescence of Mach Lines.

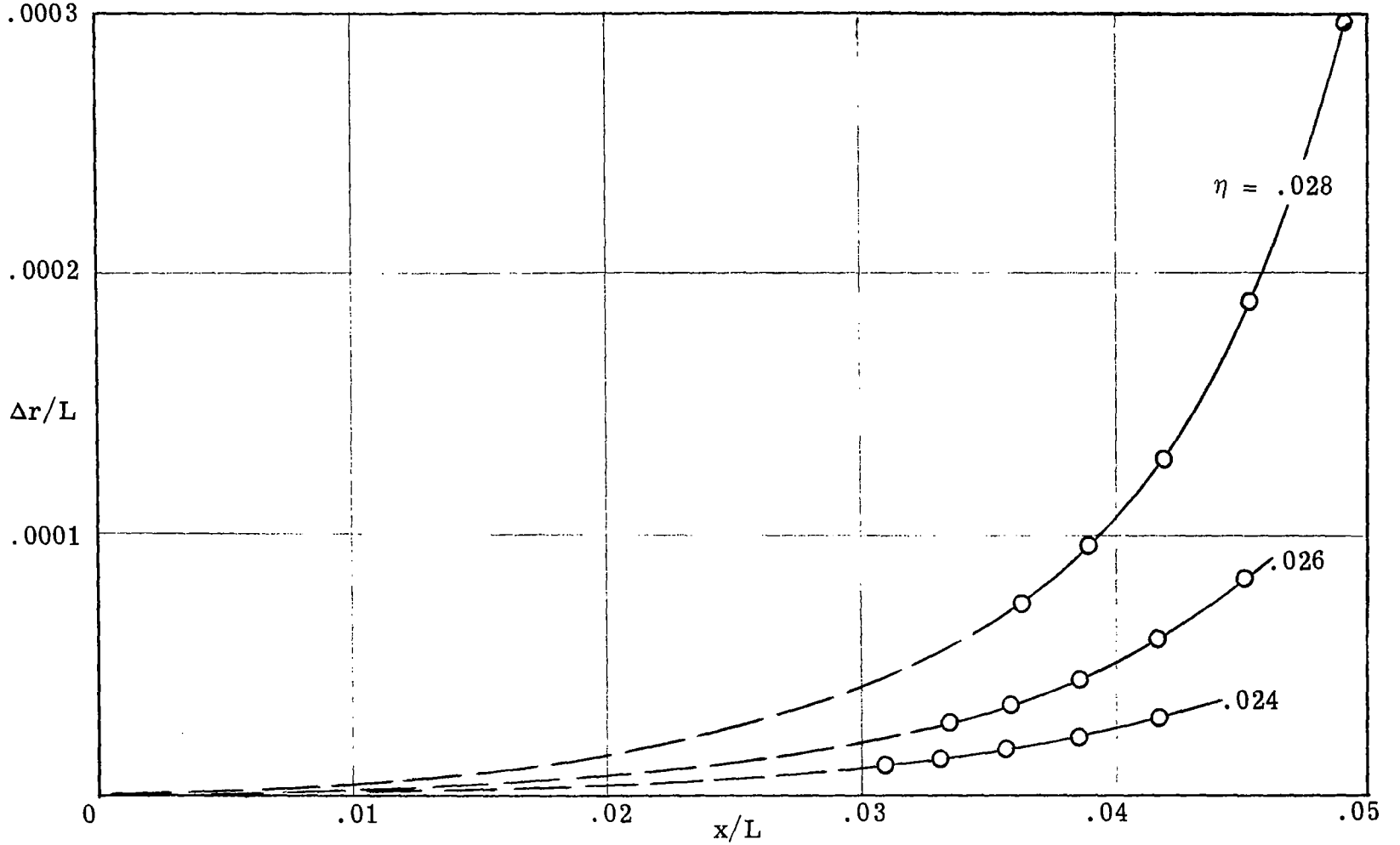


Figure A6. Discrepancy Between Streamlines from Friedrichs Method and Method of Characteristics.

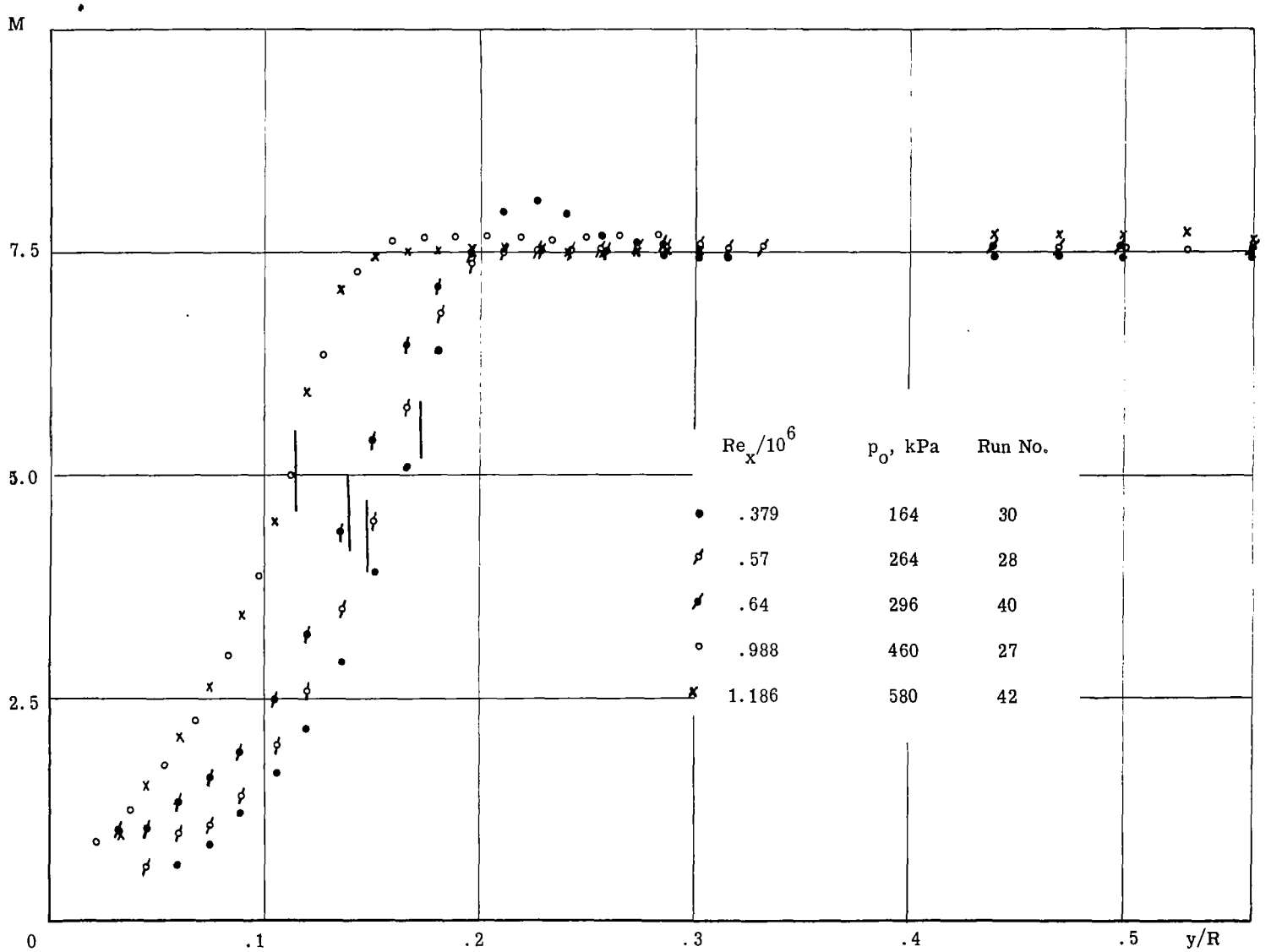


Figure C1. Laminar Mach Number Profiles for Conical Nozzle. $d_* = 11.1$ mm, x = 770 mm, R = 79.5 mm

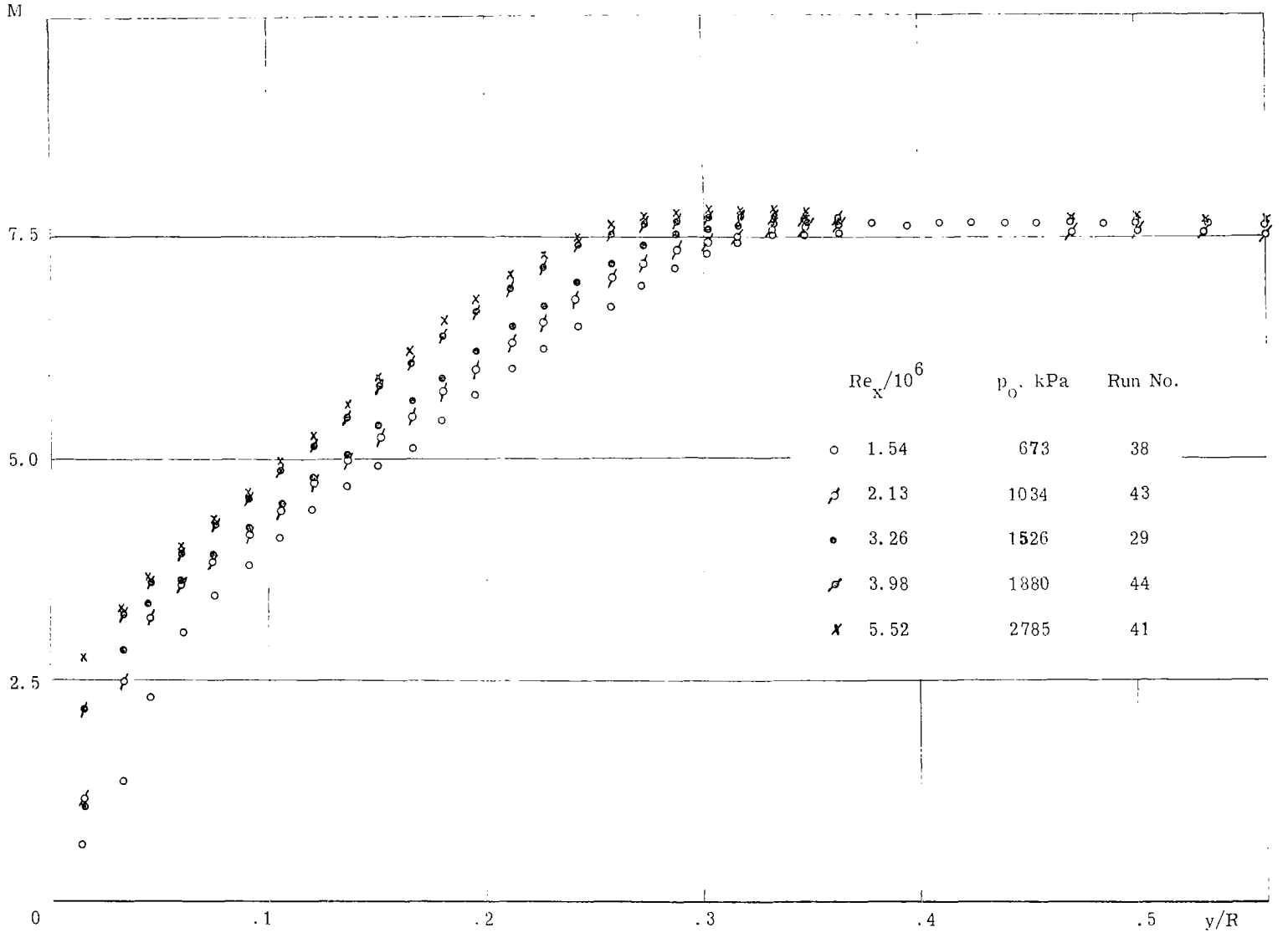


Figure C2. Turbulent Mach Number Profiles for Conical Nozzle. $d_* = 11.1$ mm, $x = 770$ mm, $R = 79.5$ mm

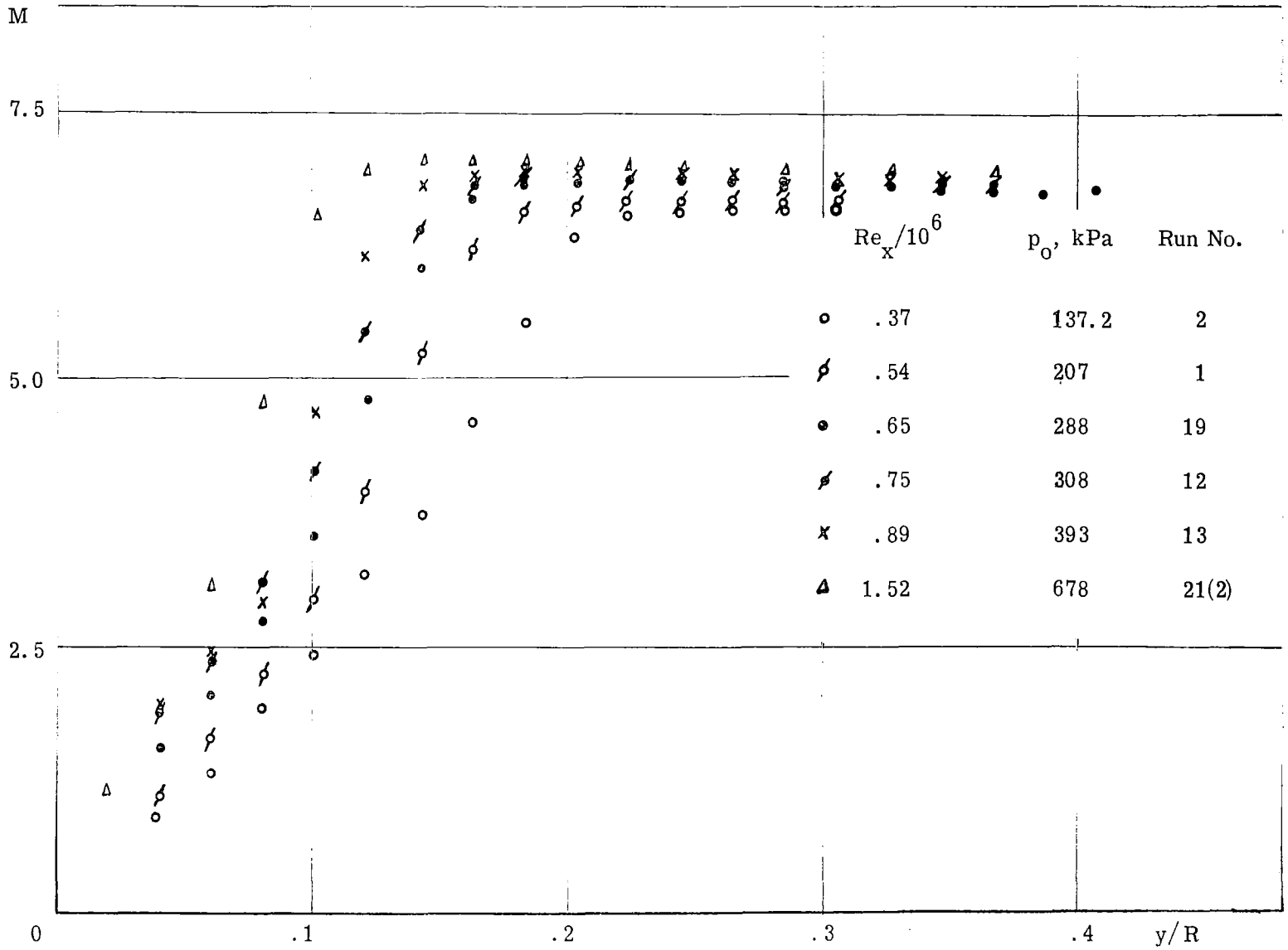


Figure C3. Laminar Mach Number Profiles for Conical Nozzle. $d_* = 11.1$ mm, $x = 570$ mm, $R = 59$ mm

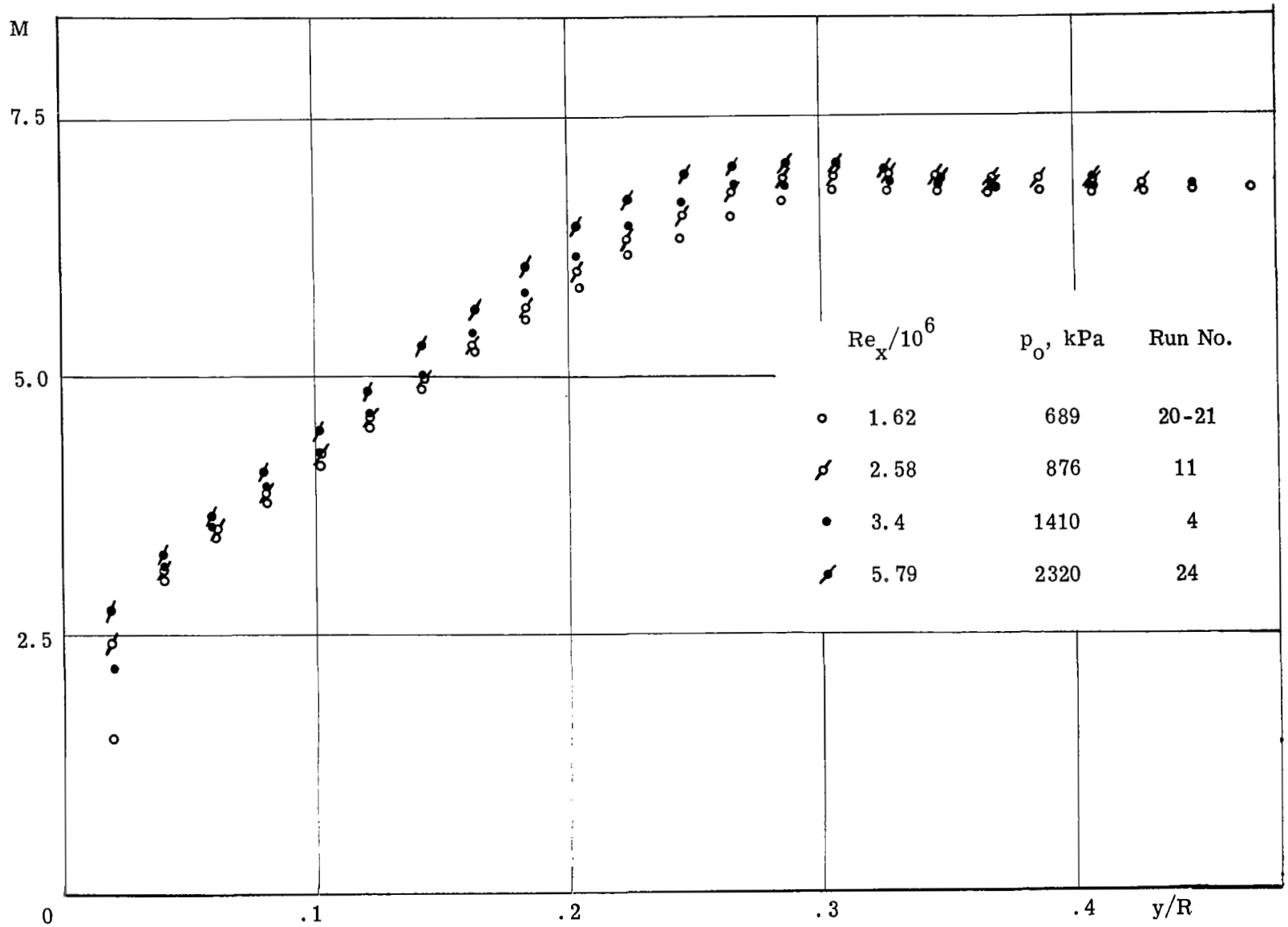


Figure C4. Turbulent Mach Number Profiles for Conical Nozzle. $d_* = 11.1$ mm, x = 570 mm, R = 59 mm

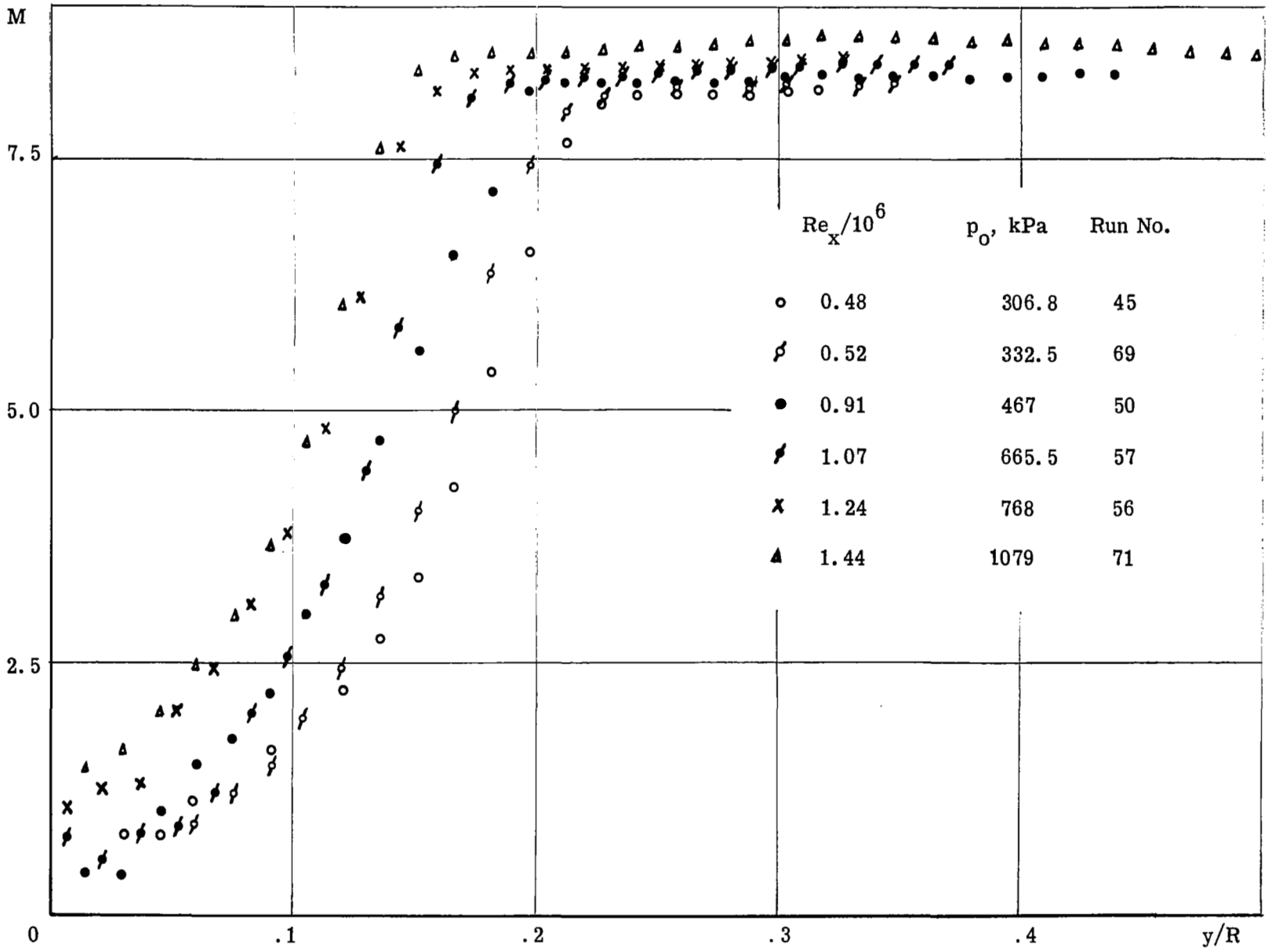


Figure C5. Laminar Mach Number Profiles for Conical Nozzle. $d_* = 8.7$ mm, x = 780 mm, R = 79.2 mm

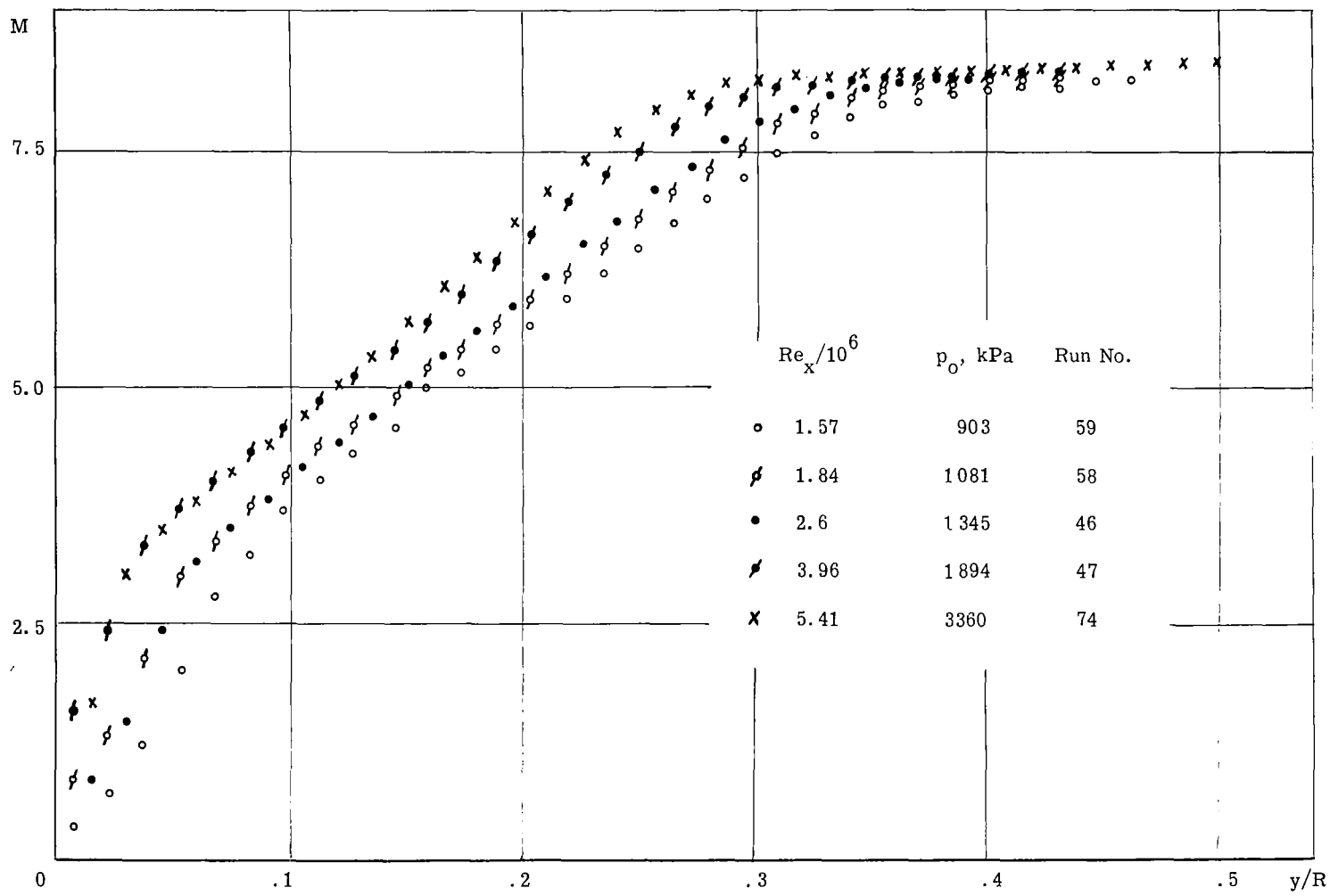


Figure C6. Turbulent Mach Number Profiles for Conical Nozzle. $d_* = 8.7$ mm, x = 780 mm, R = 79.2 mm

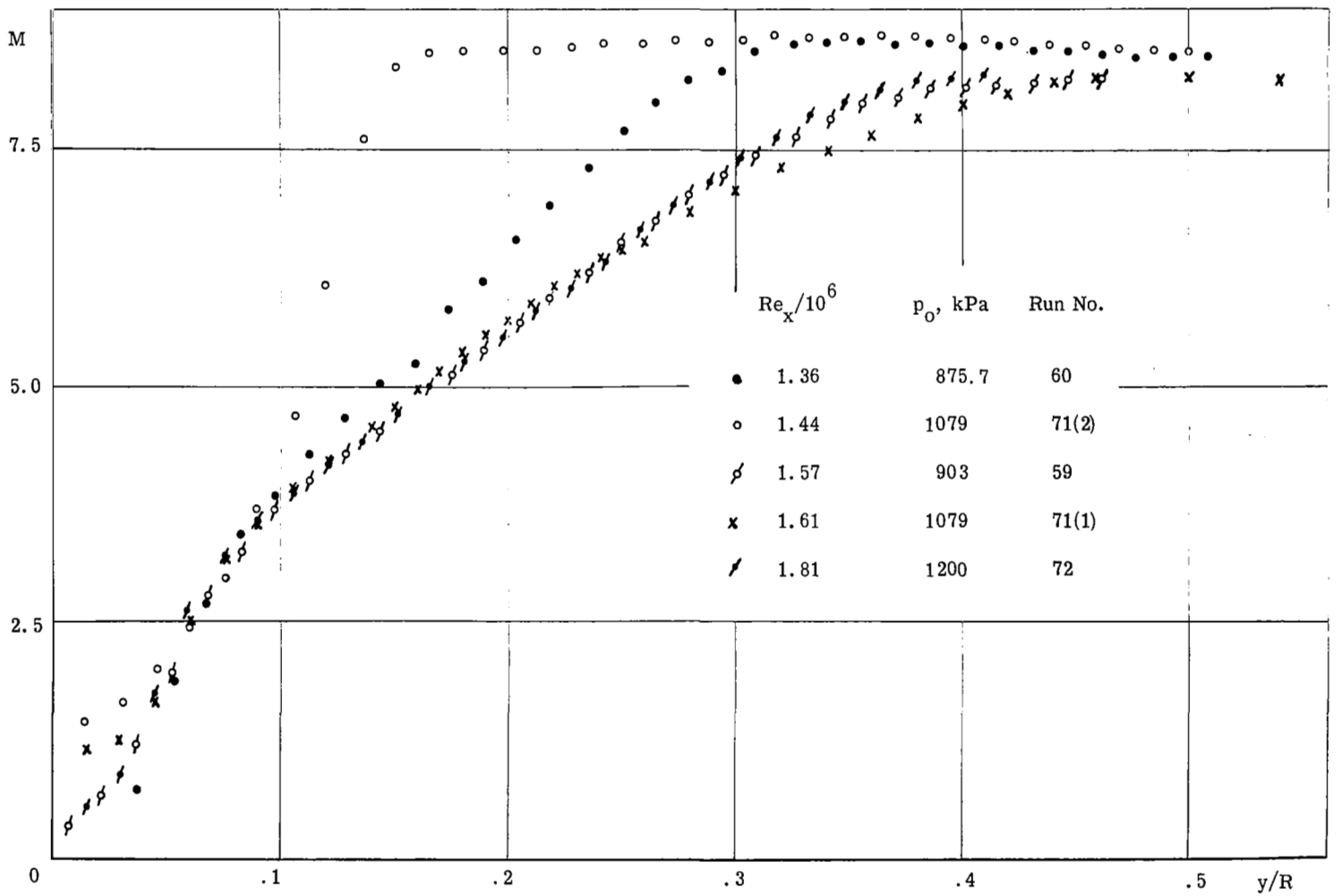


Figure C7. Transitional Mach Number Profiles for Conical Nozzle. $d_* = 8.7$ mm, x = 780 mm, R = 79.2 mm

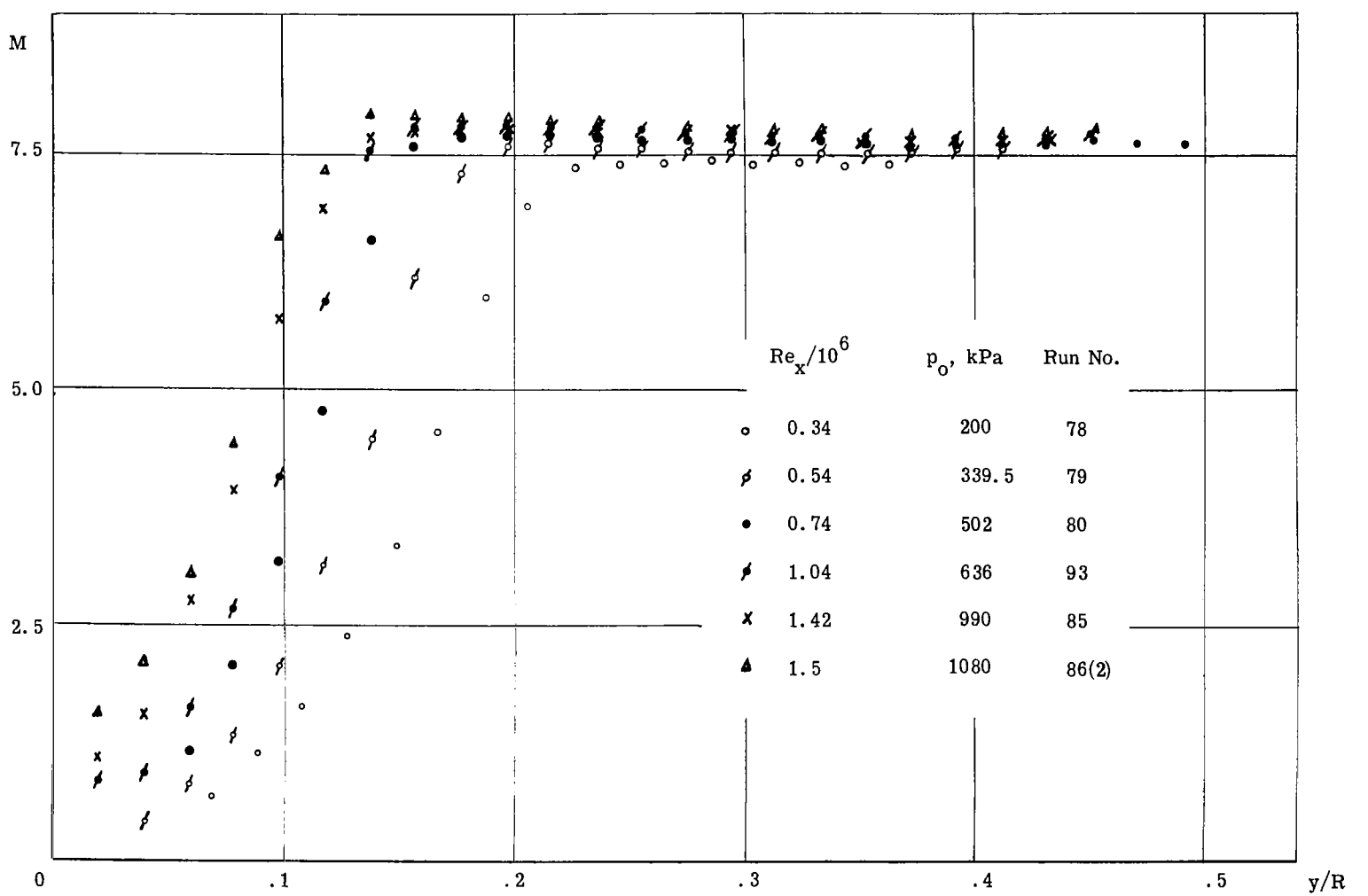


Figure C8. Laminar Mach Number Profiles for Conical Nozzle. $d_* = 8.7$ mm, x = 585 mm, R = 61 mm

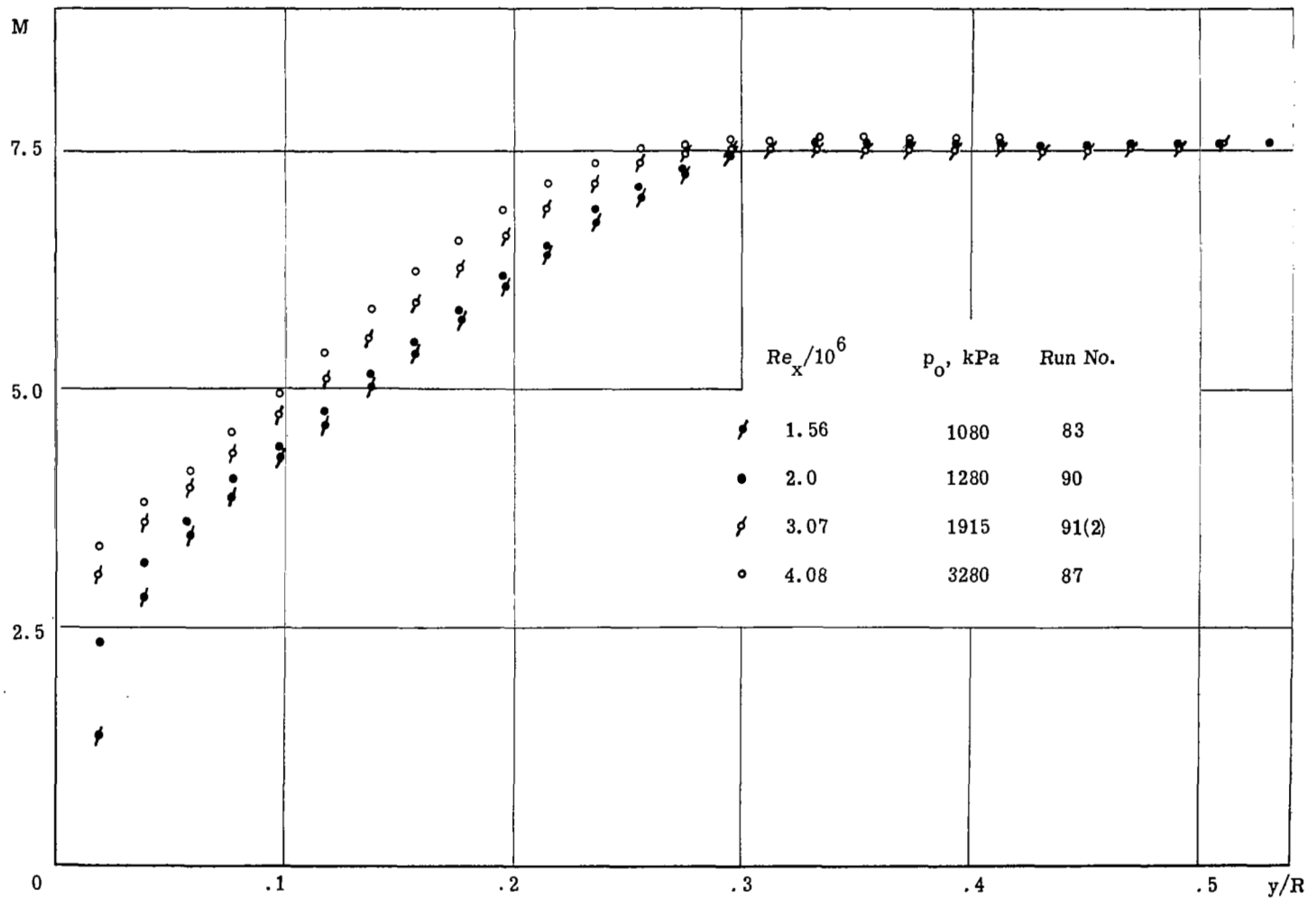


Figure C9. Turbulent Mach Number Profiles for Conical Nozzle. $d_* = 8.7$ mm, $x = 585$ mm, $R = 61$ mm

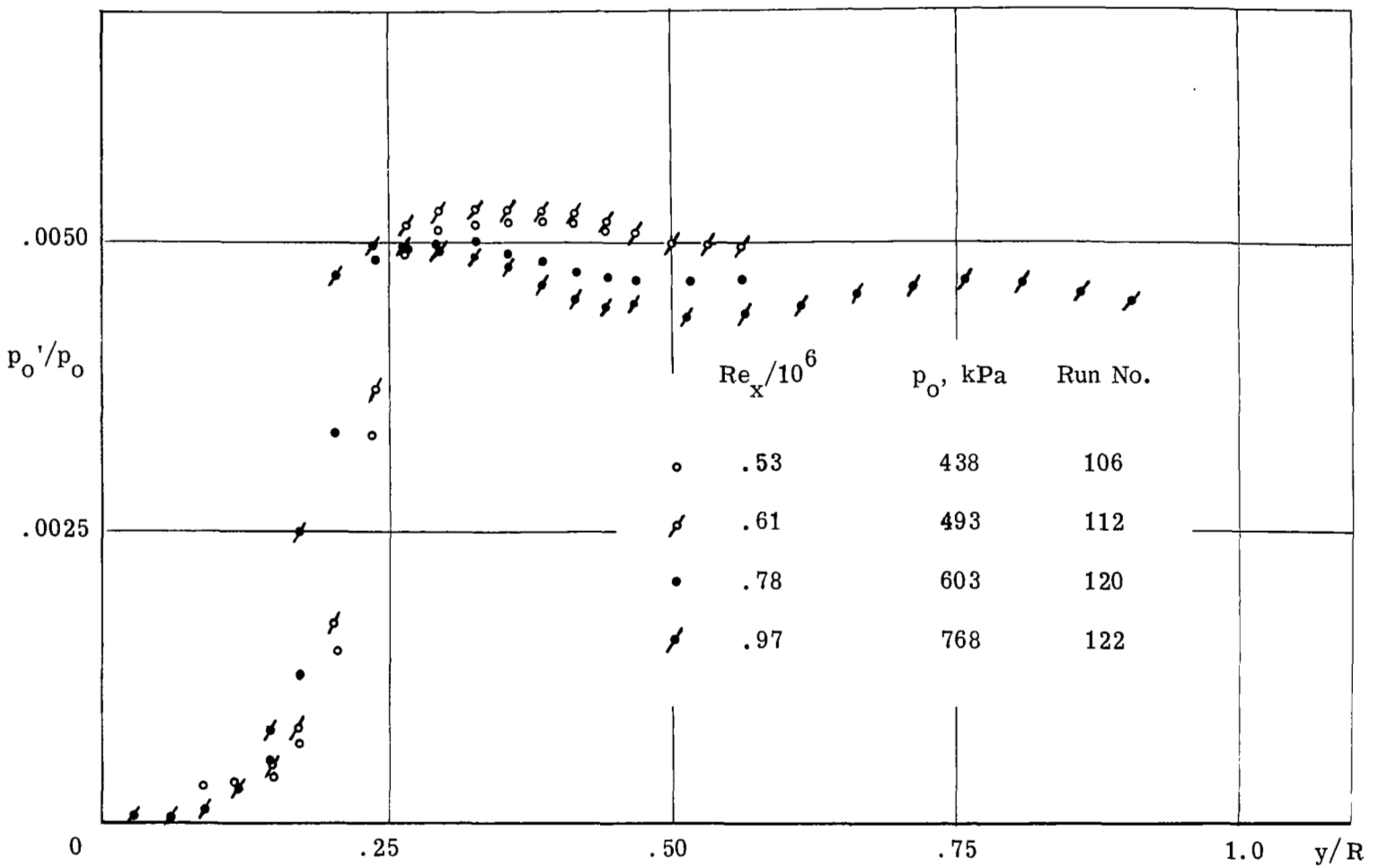


Figure C10. Laminar Pitot Pressure Profiles for Conical Nozzle. $d_* = 6.83$ mm, x = 790 mm, R = 79.2 mm

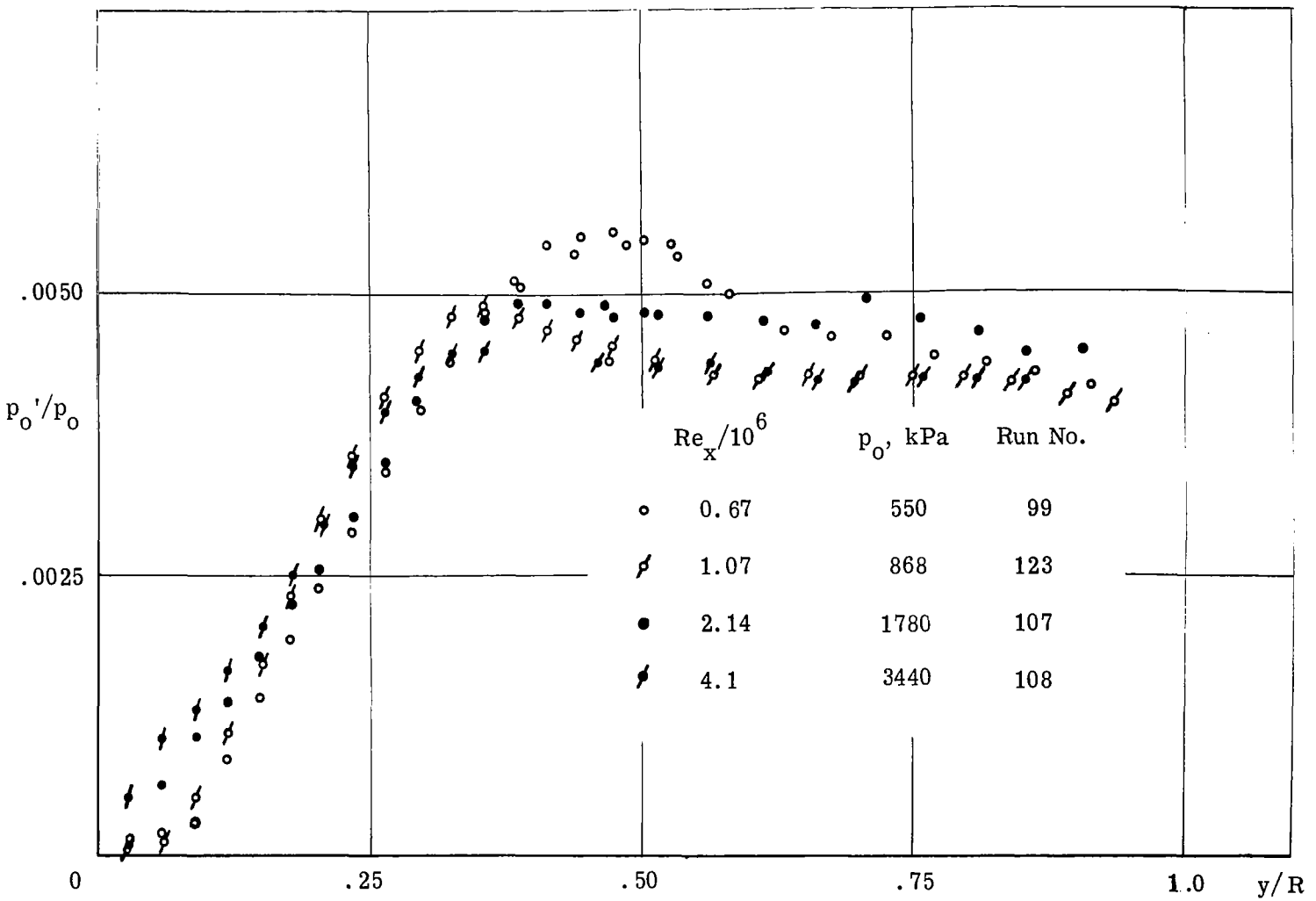


Figure C11. Turbulent Pitot Pressure Profiles for Conical Nozzle. $d_* = 6.83$ mm, x = 790 mm, R = 79.2 mm

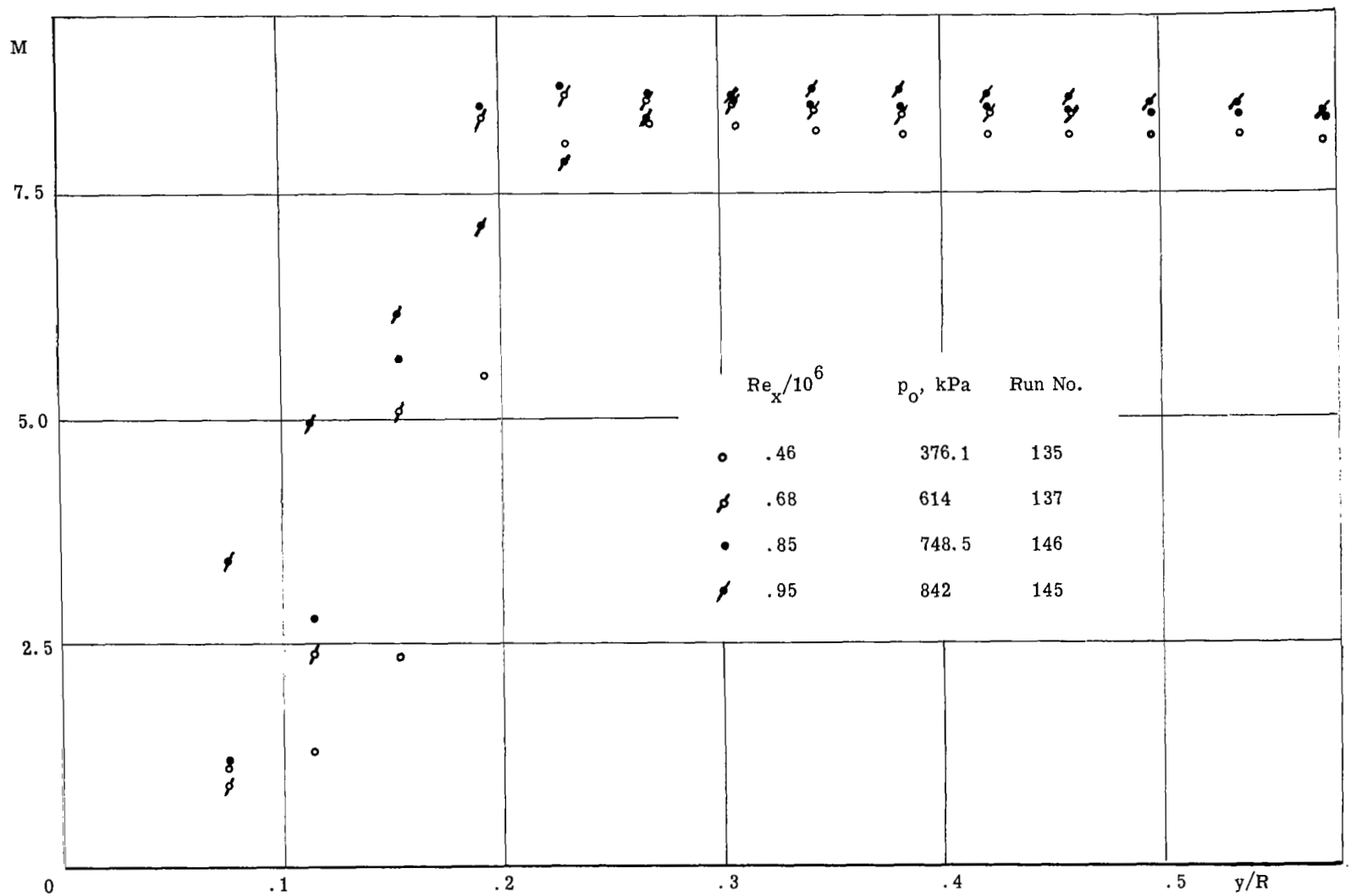


Figure C12. Laminar Mach Number Profiles for Conical Nozzle. $d_* = 6.83$ mm, x = 590 mm, R = 61 mm

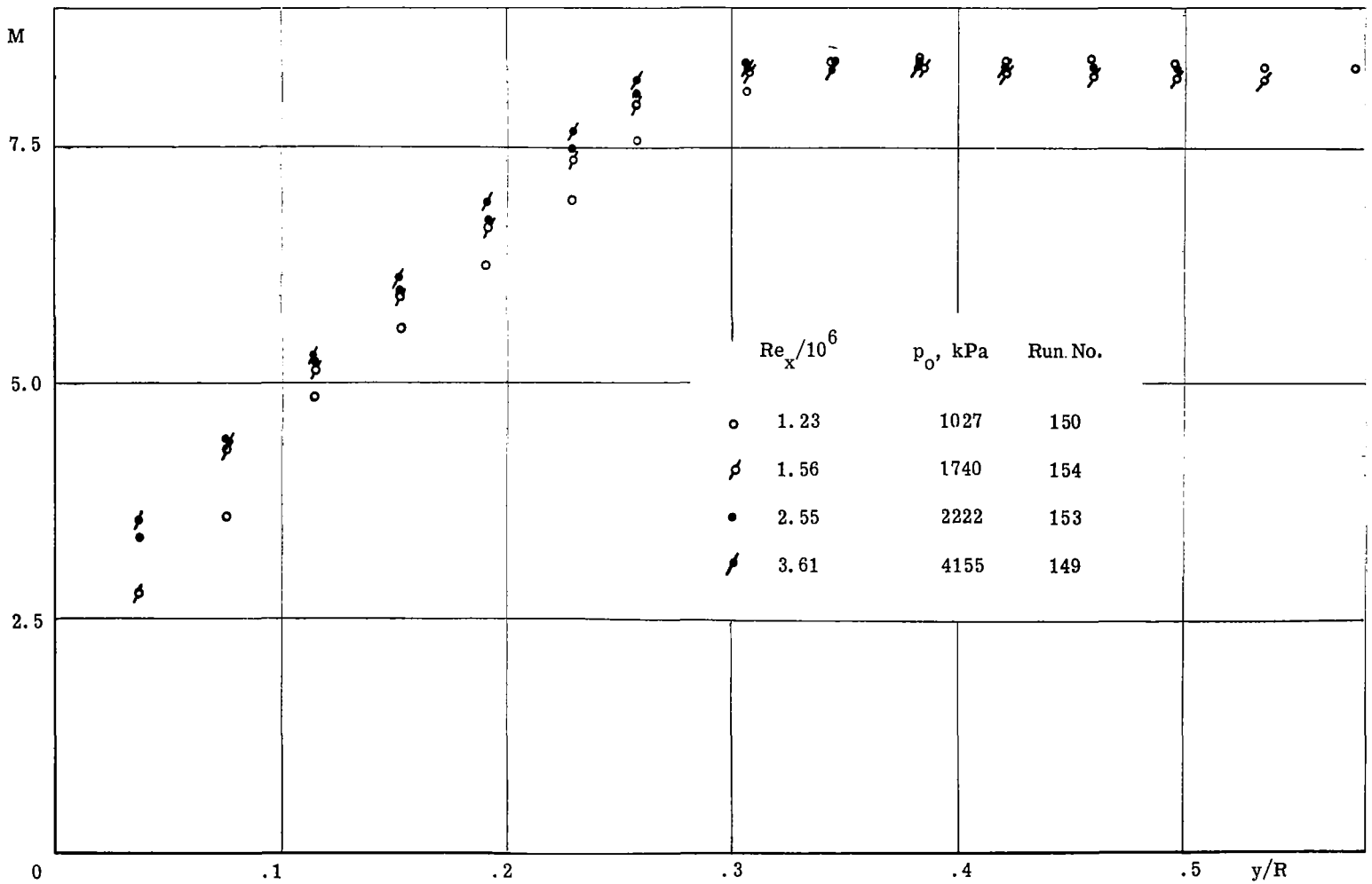


Figure C13. Turbulent Mach Number Profiles for Conical Nozzle. $d_* = 6.83$ mm, x = 590 mm, R = 61 mm

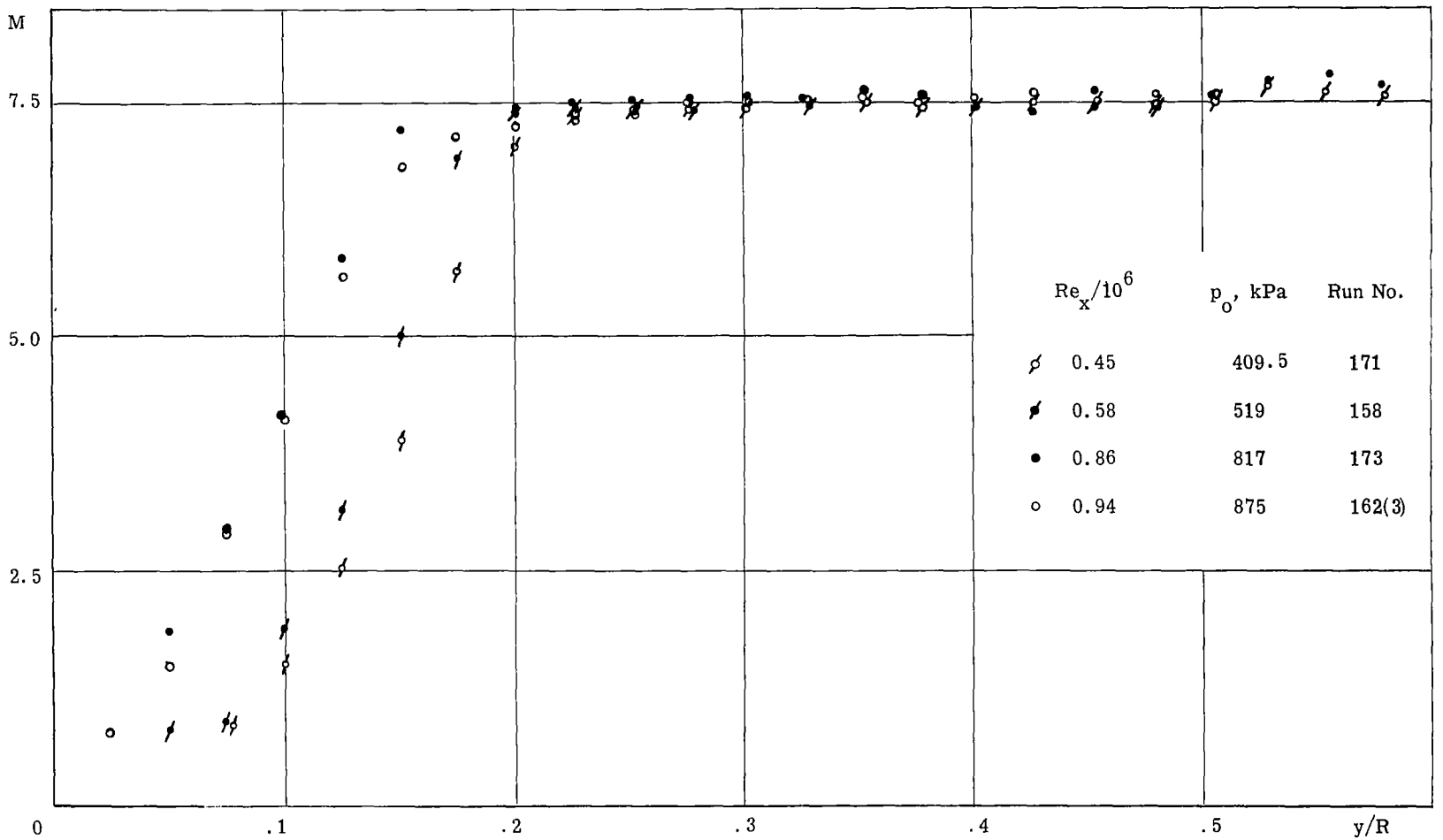


Figure C14. Laminar Mach Number Profiles for Conical Nozzle. $d_* = 6.83$ mm, x = 460 mm, R = 47.6 mm

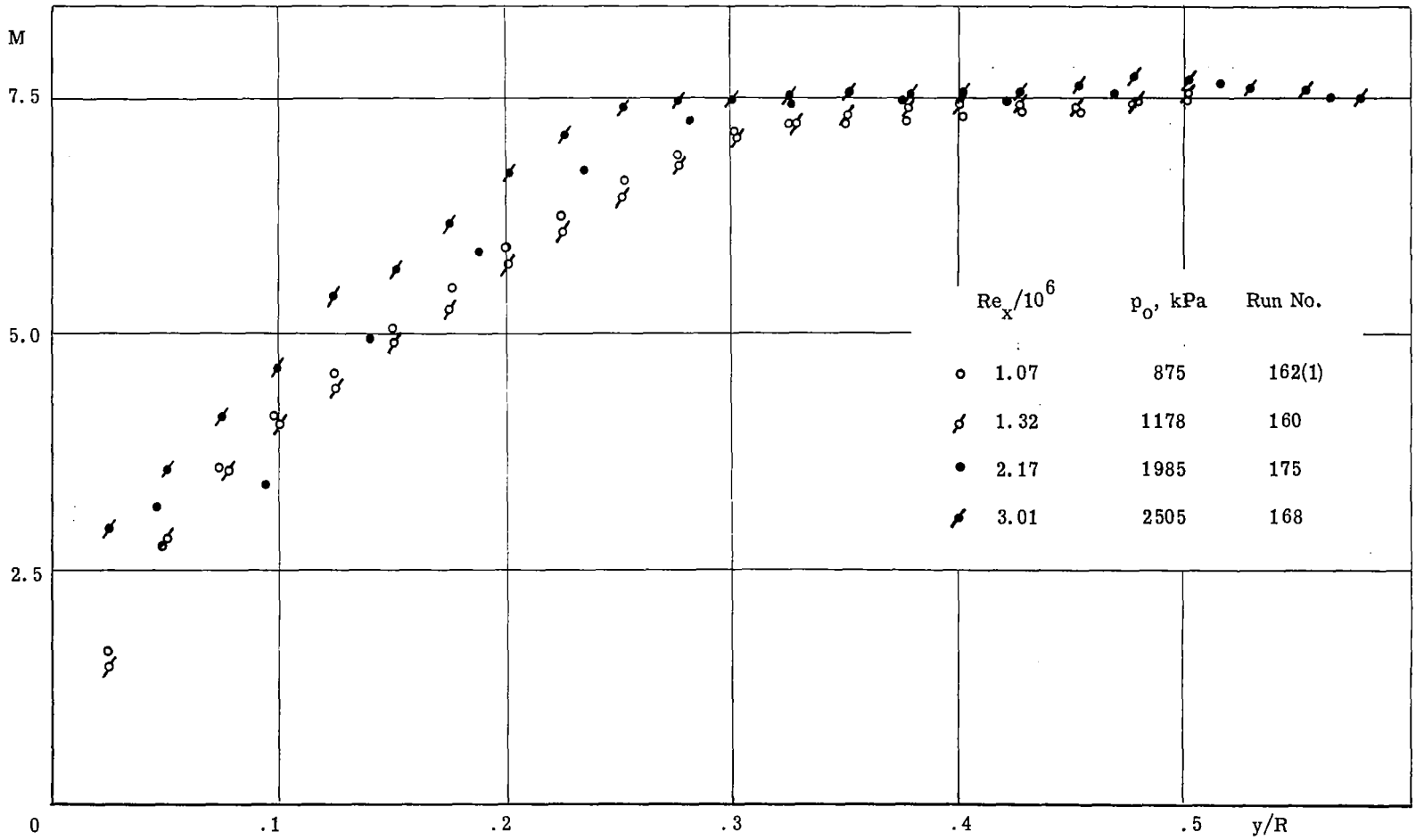


Figure C15. Turbulent Mach Number Profiles for Conical Nozzle. $d_* = 6.83$ mm, x = 460 mm, R = 47.6 mm

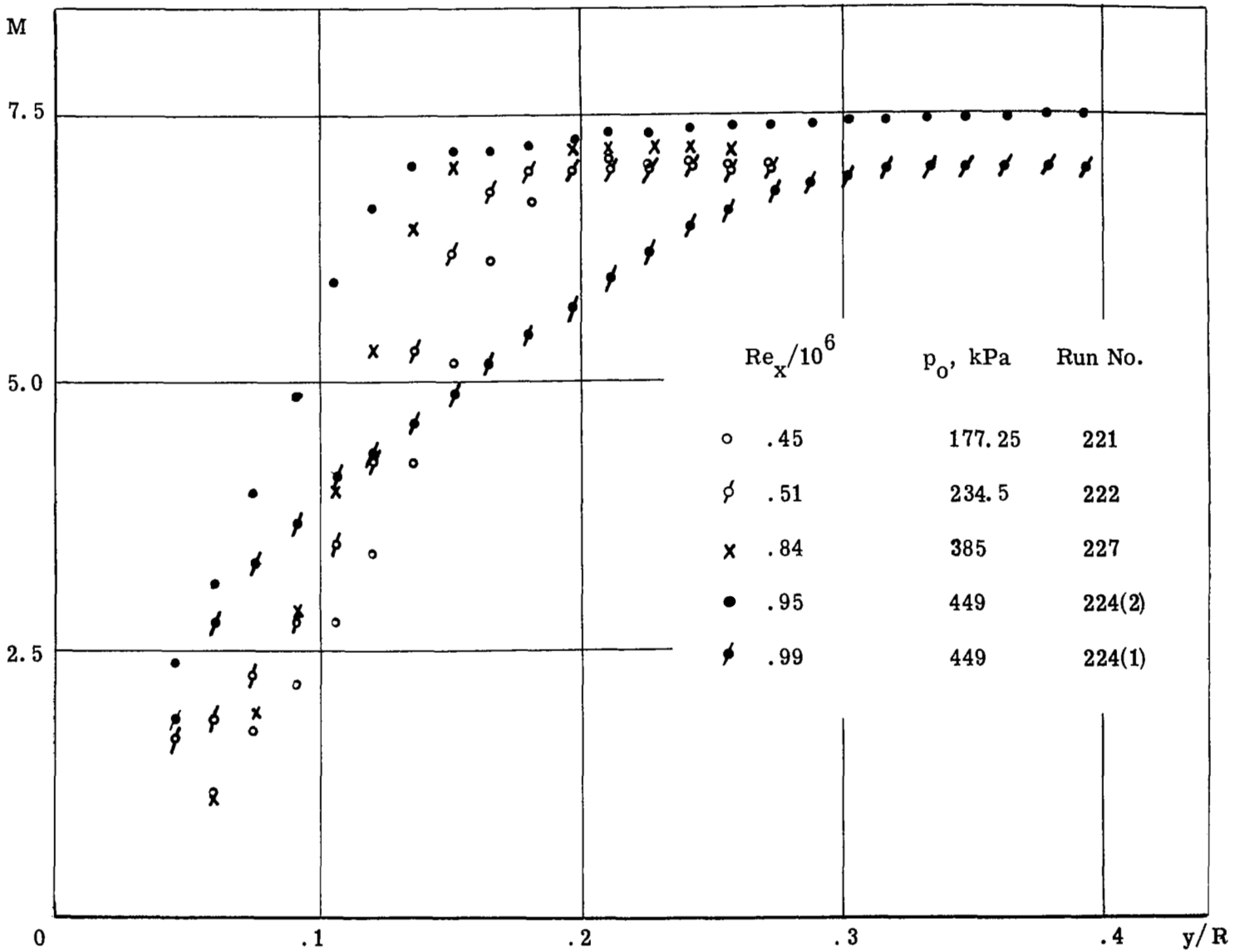


Figure C16. Laminar Mach Number Profiles for Conical Nozzle. $d_* = 13.18$ mm, $x = 755$ mm, $R = 79.2$ mm

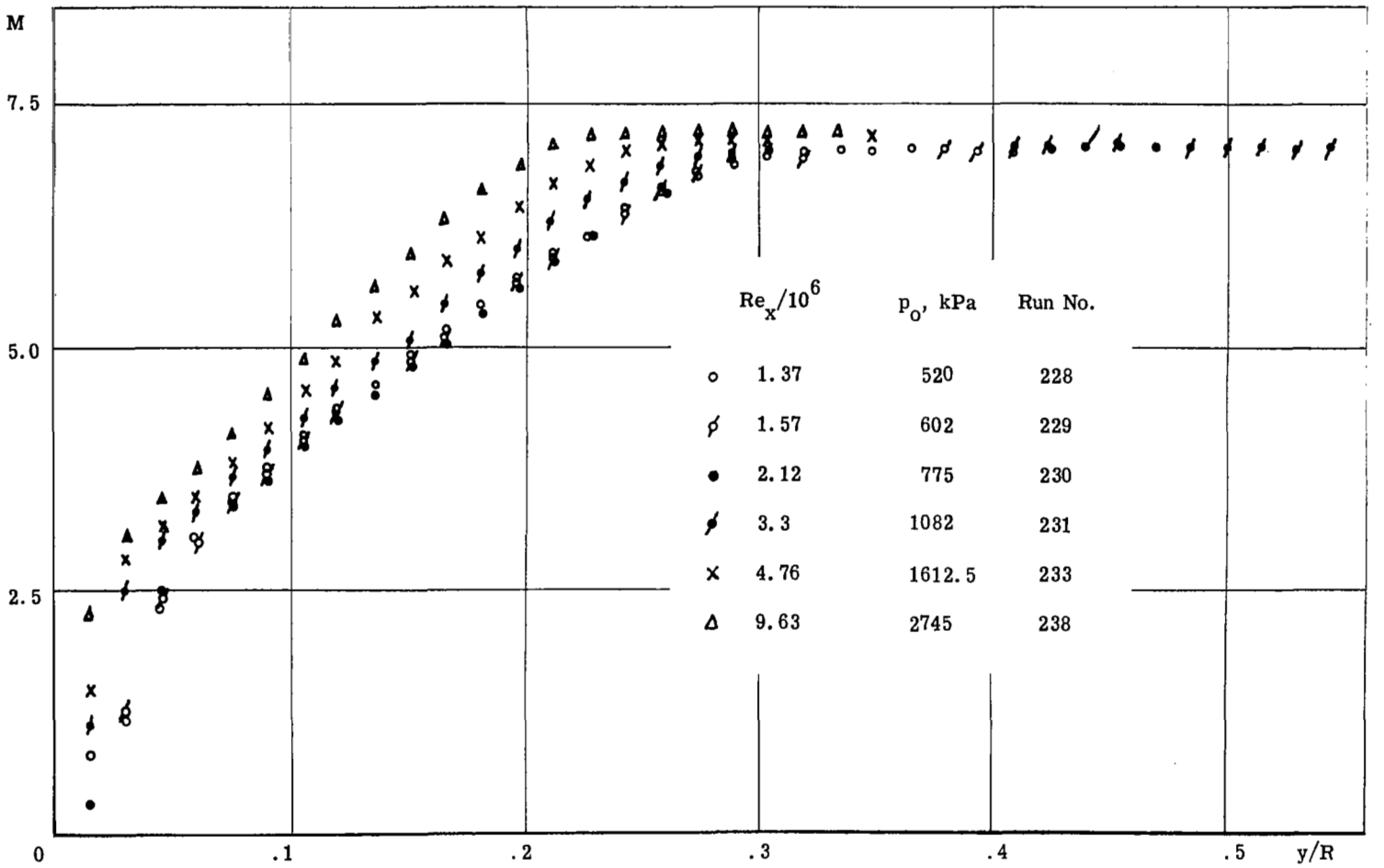


Figure C17. Turbulent Mach Number Profiles for Conical Nozzle. $d_* = 13.18$ mm, $x = 755$ mm, $R = 79.2$ mm

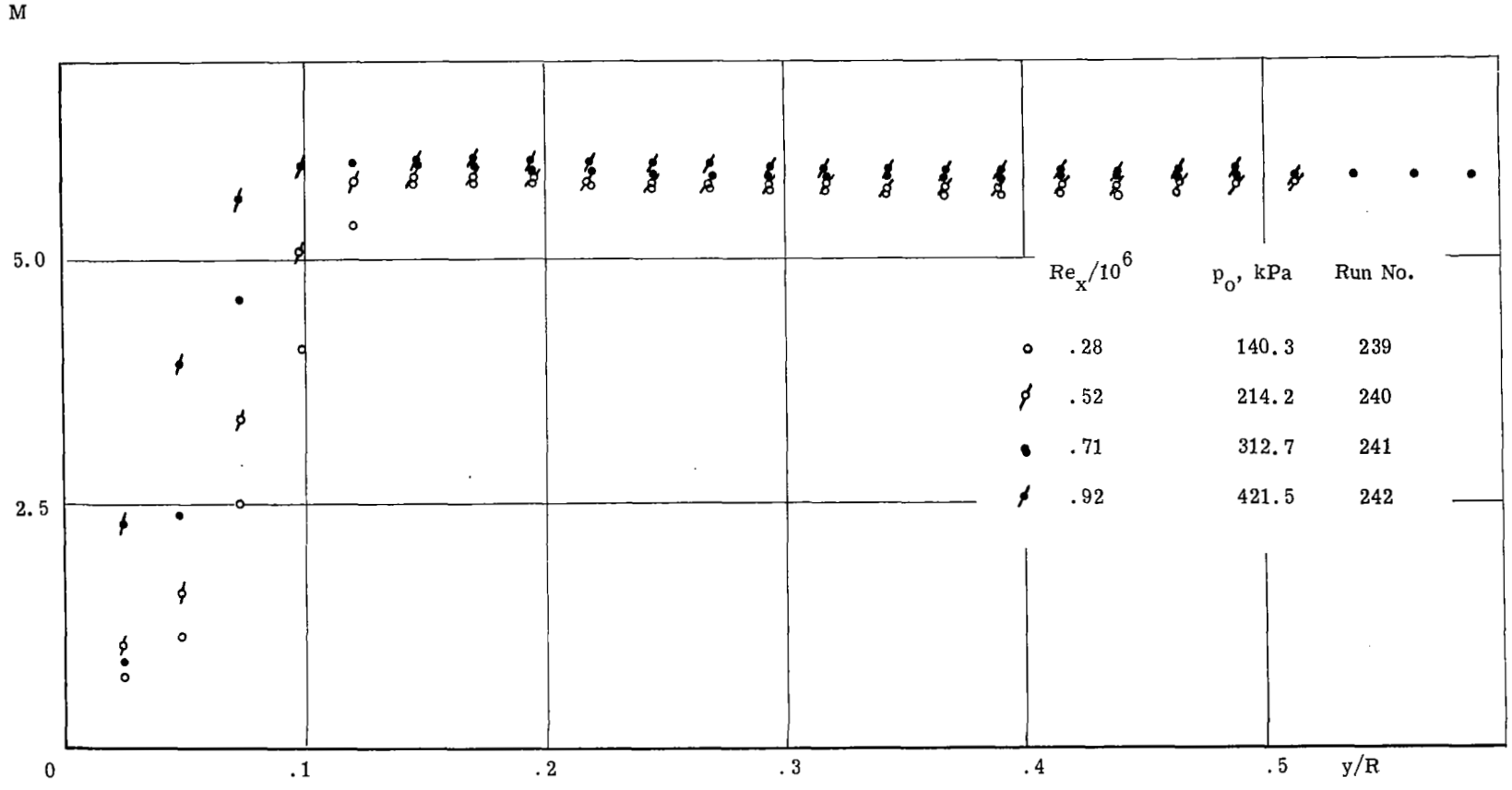


Figure C18. Laminar Mach Number Profiles for Conical Nozzle. $d_* = 13.18$ mm, x = 440 mm, R = 49 mm

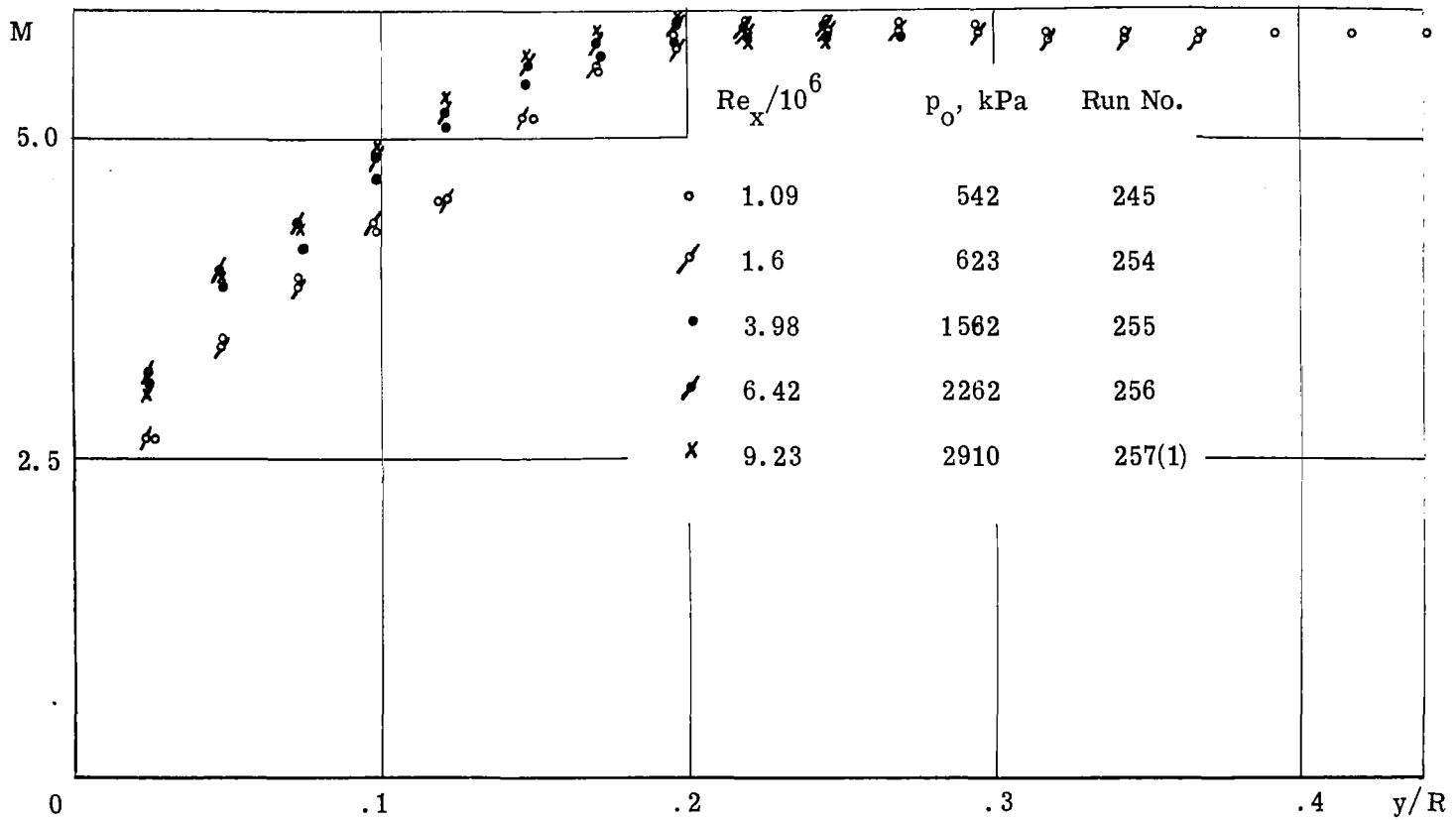


Figure C19. Turbulent Mach Number Profiles for Conical Nozzle. $d_* = 13.18$ mm, $x = 440$ mm, $R = 49$ mm

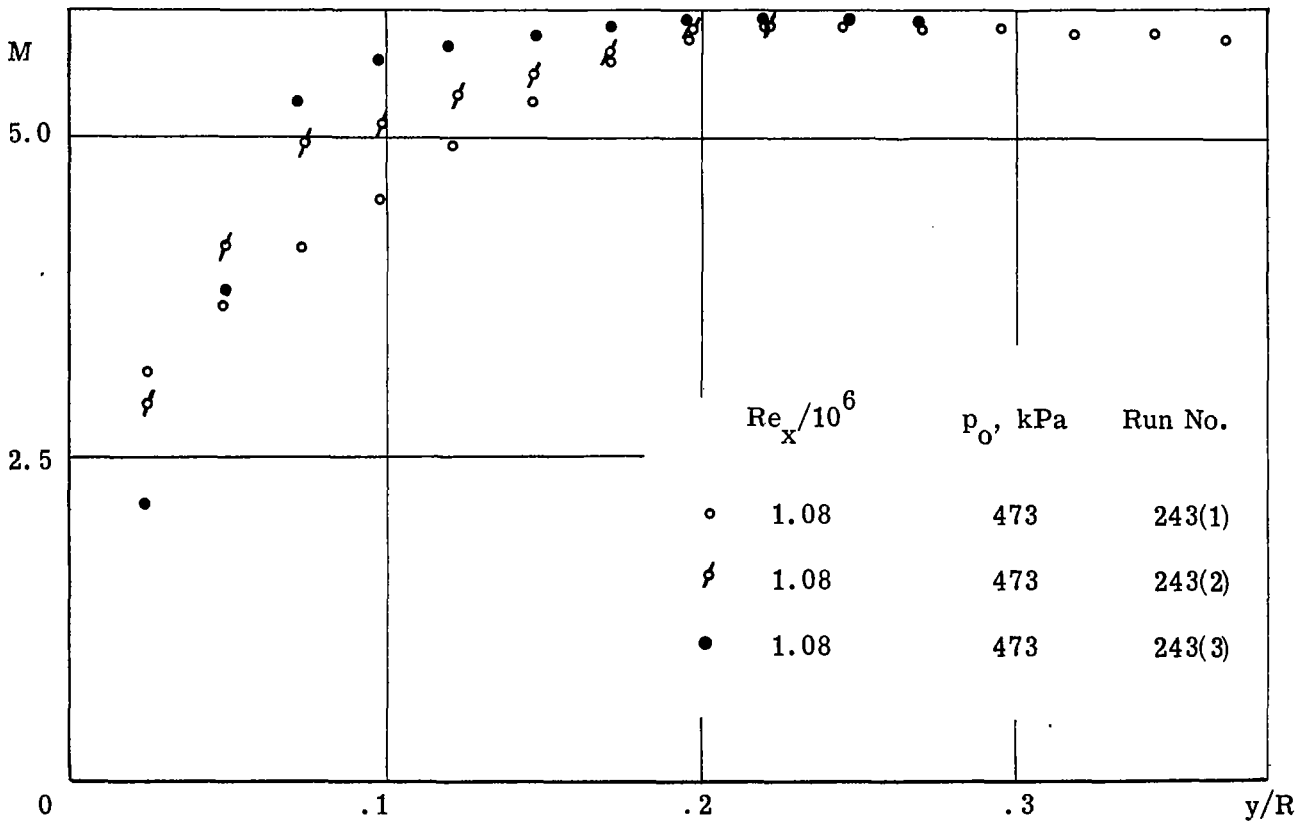


Figure C20. Transitional Mach Number Profiles for Conical Nozzle.
$d_* = 13.18$ mm, x = 440 mm, R = 49 mm

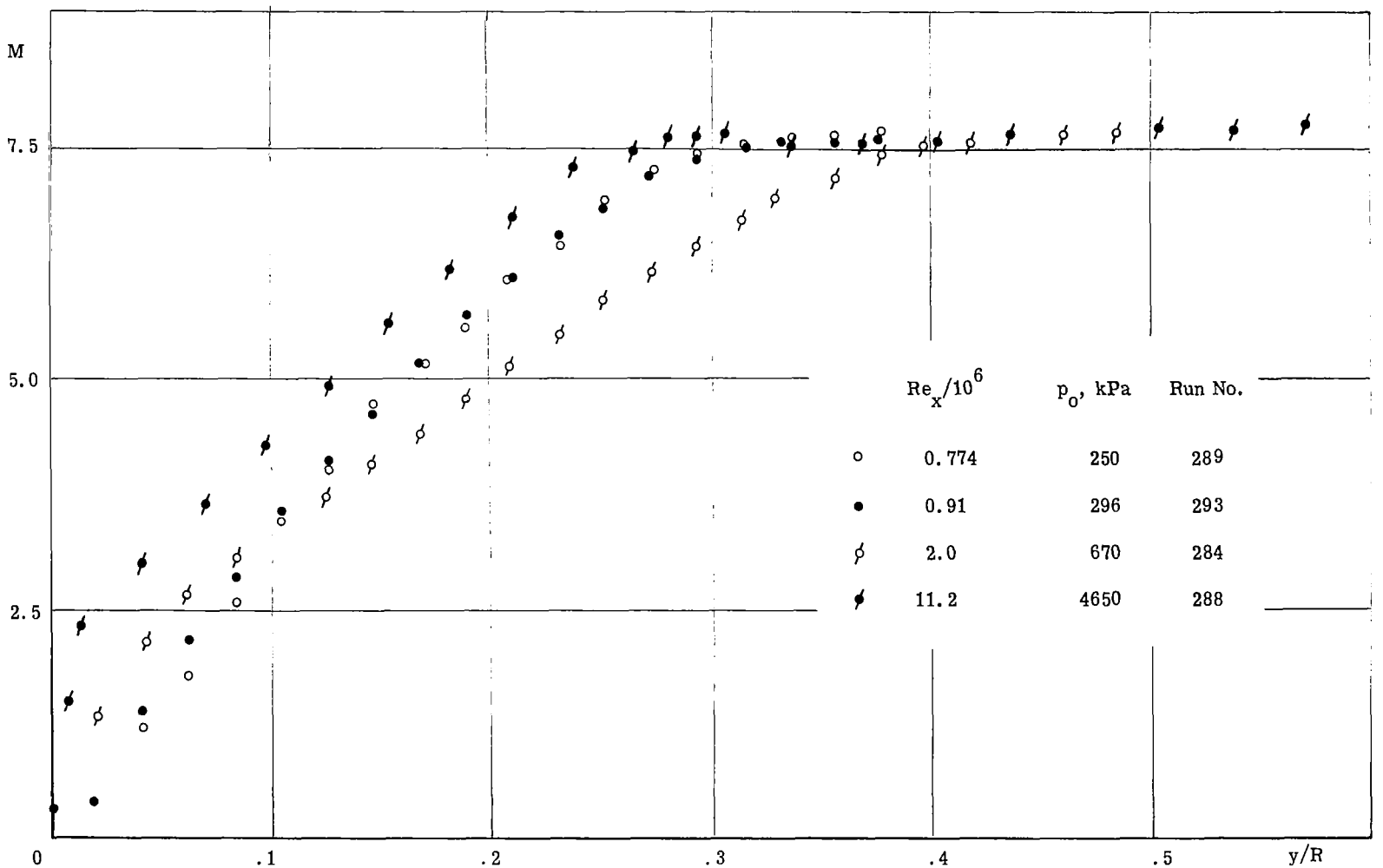


Figure C21. Mach Number Profiles for Contoured Nozzle. x = 770 mm, R = 83 mm

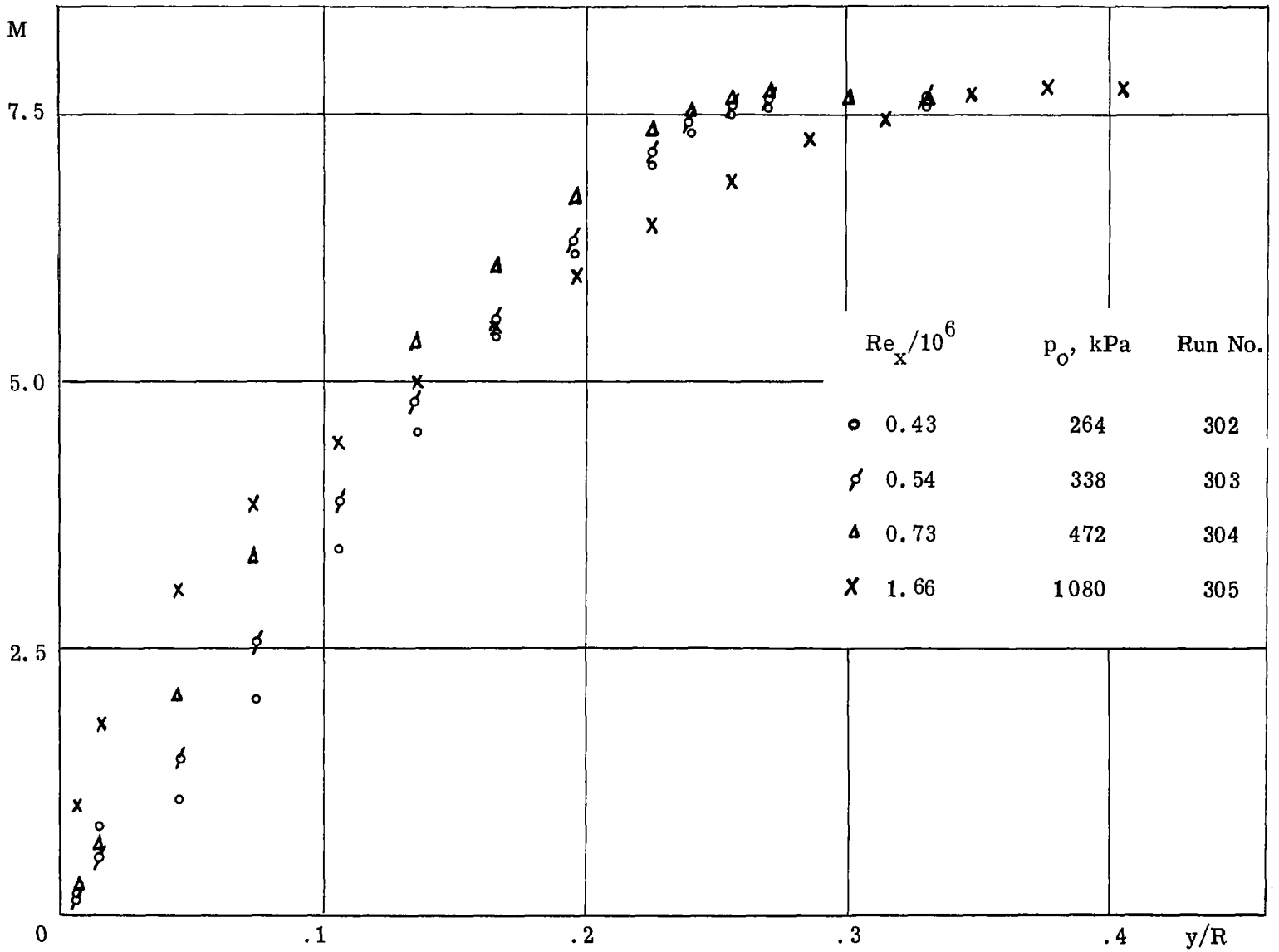


Figure C22. Mach Number Profiles for Contoured Nozzle. x = 570 mm, R = 77 mm

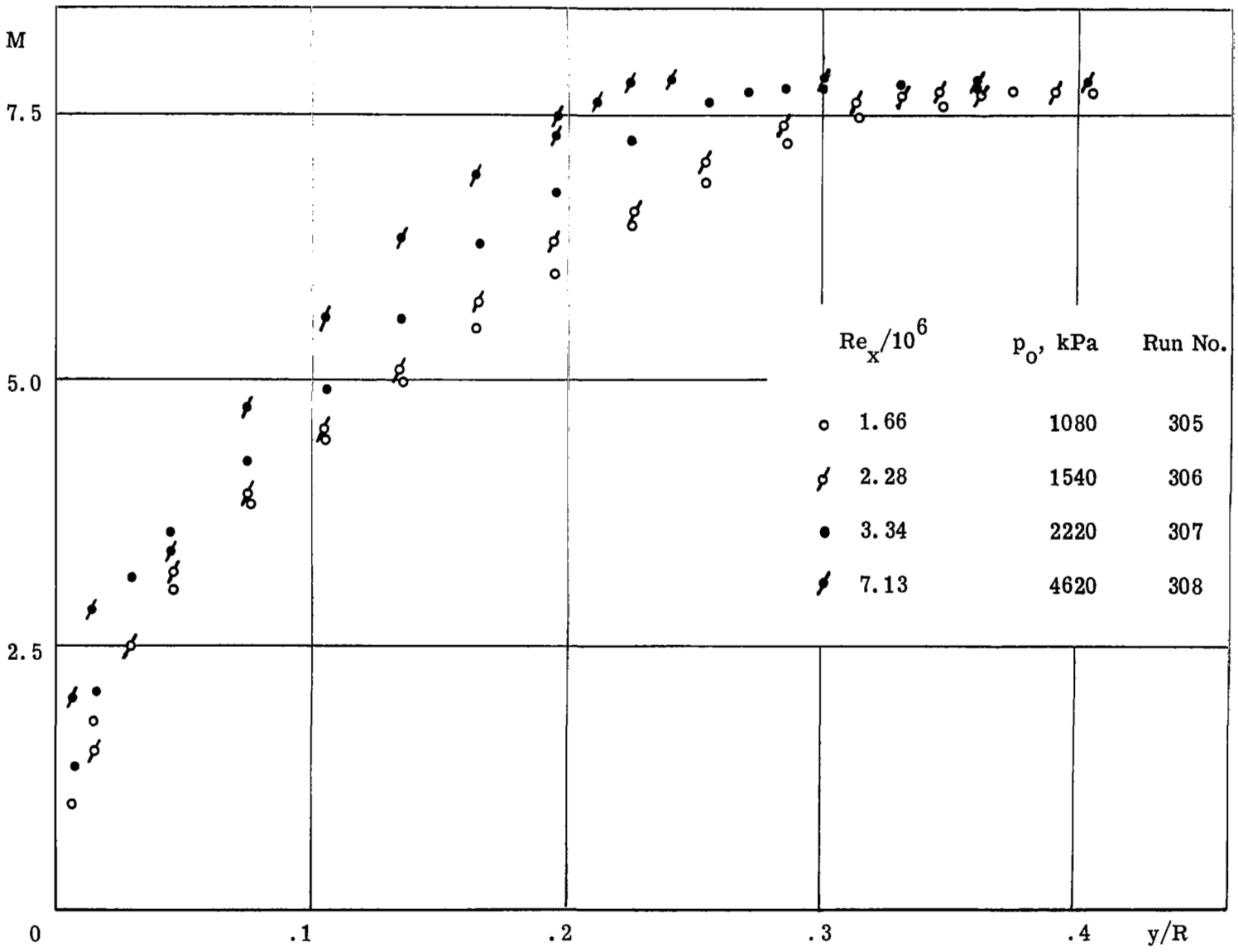


Figure C23. Turbulent Mach Number Profiles for Contoured Nozzle. x = 570 mm, R = 77 mm

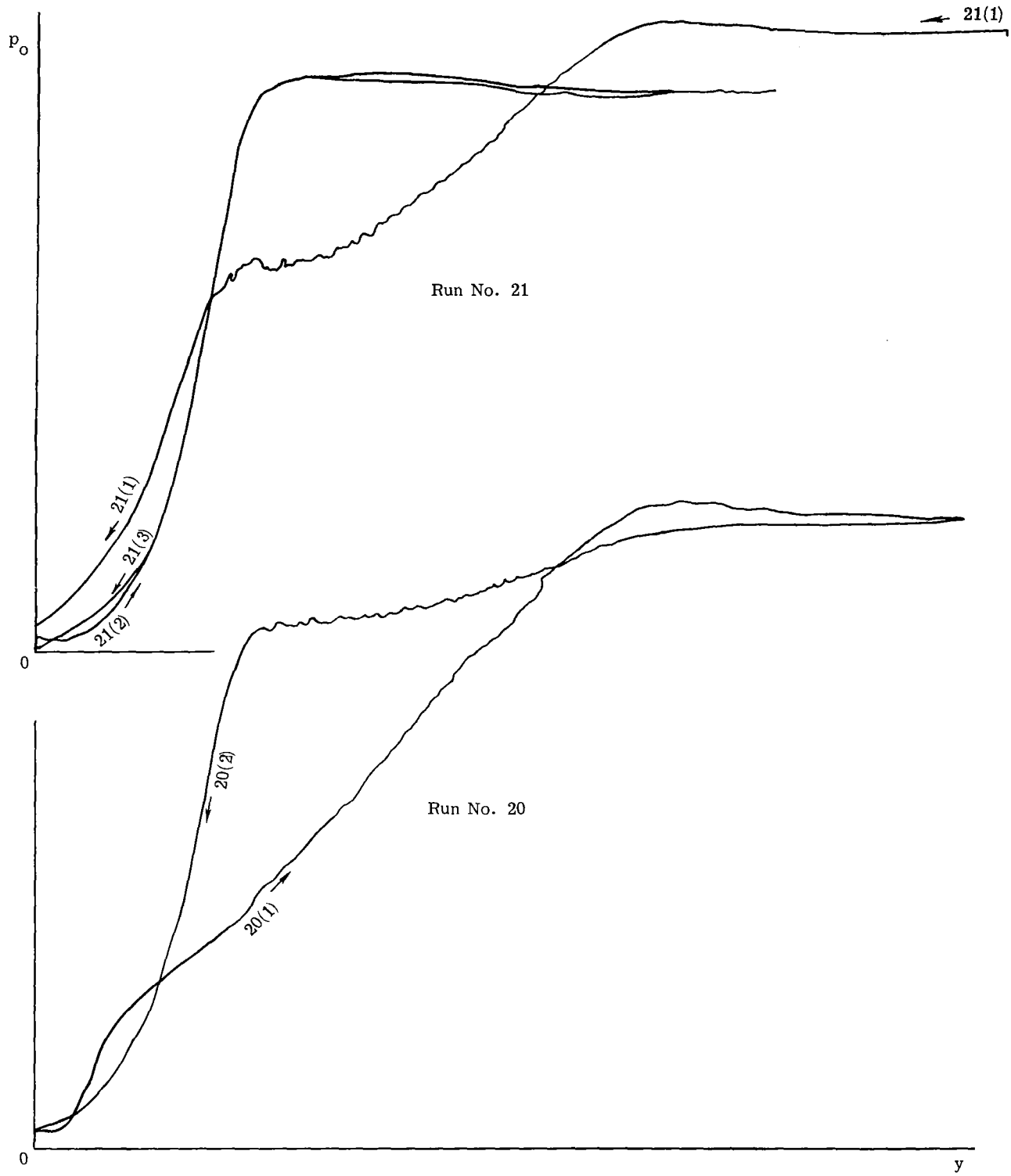


Figure C24. Recorder Traces of Transition Reversal in Conical Nozzle
$d_* = 11.1$ mm, $x = 570$ mm, $p_o = 689$ kPa

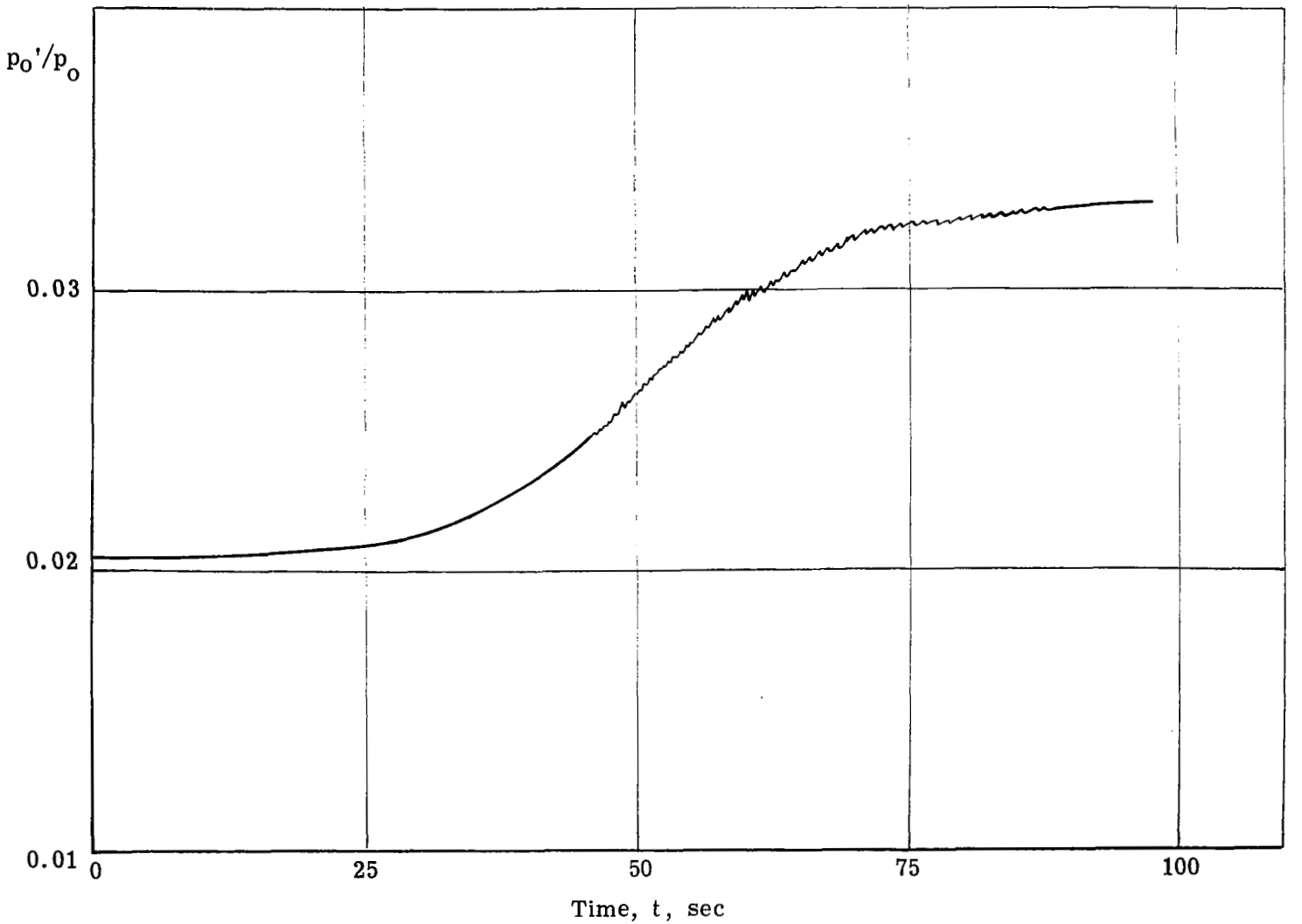


Figure C25. Pitot Pressure Variation During a Transition Reversal Run in Conical Nozzle. $d_* = 13.18$ mm, $x = 440$ mm, $y/R = .11$, $p_o = 470$ kPa.

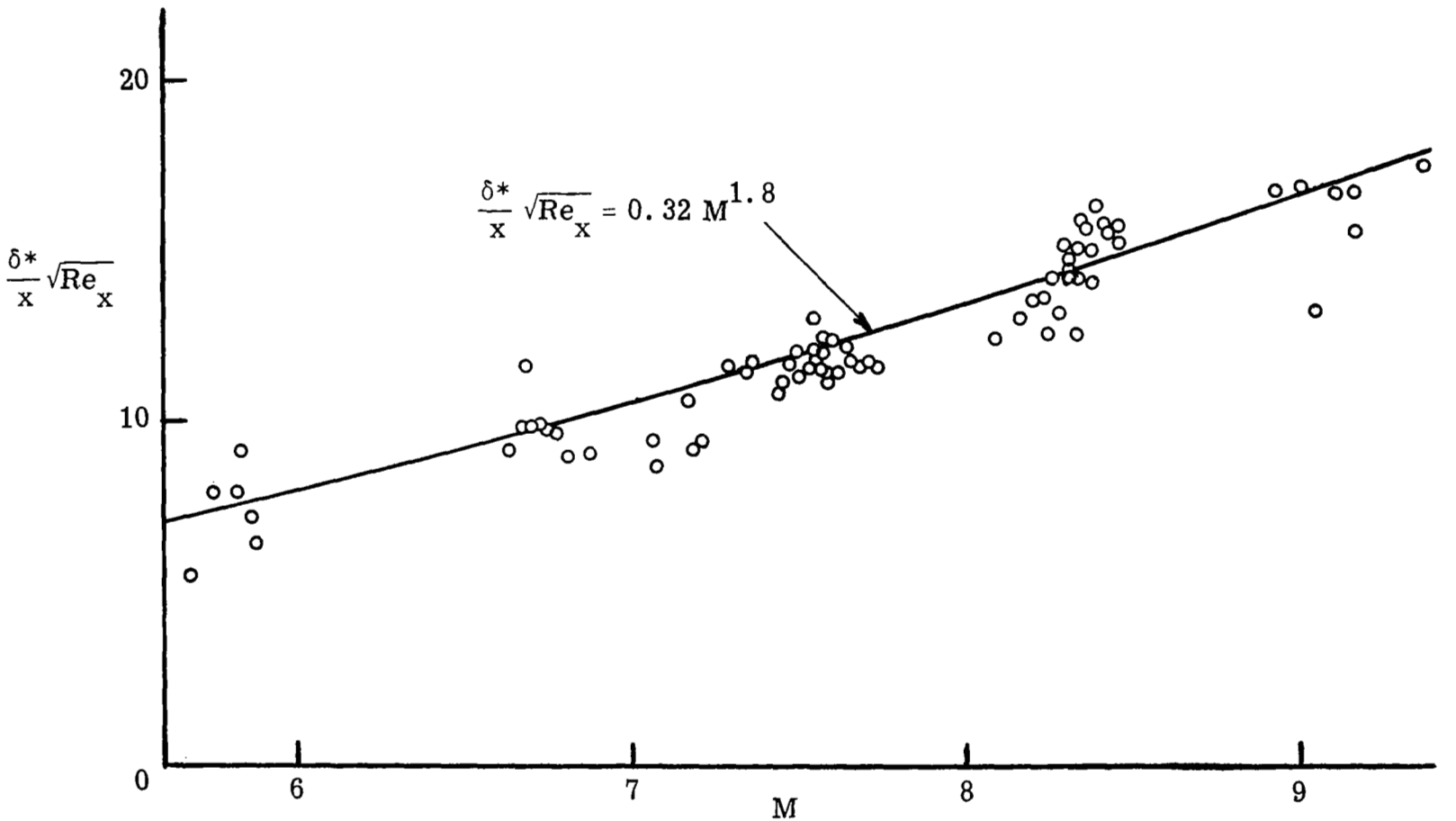


Figure C26. Variation of Laminar Boundary Layer Displacement Thickness with Mach Number, for Conical Nozzle.

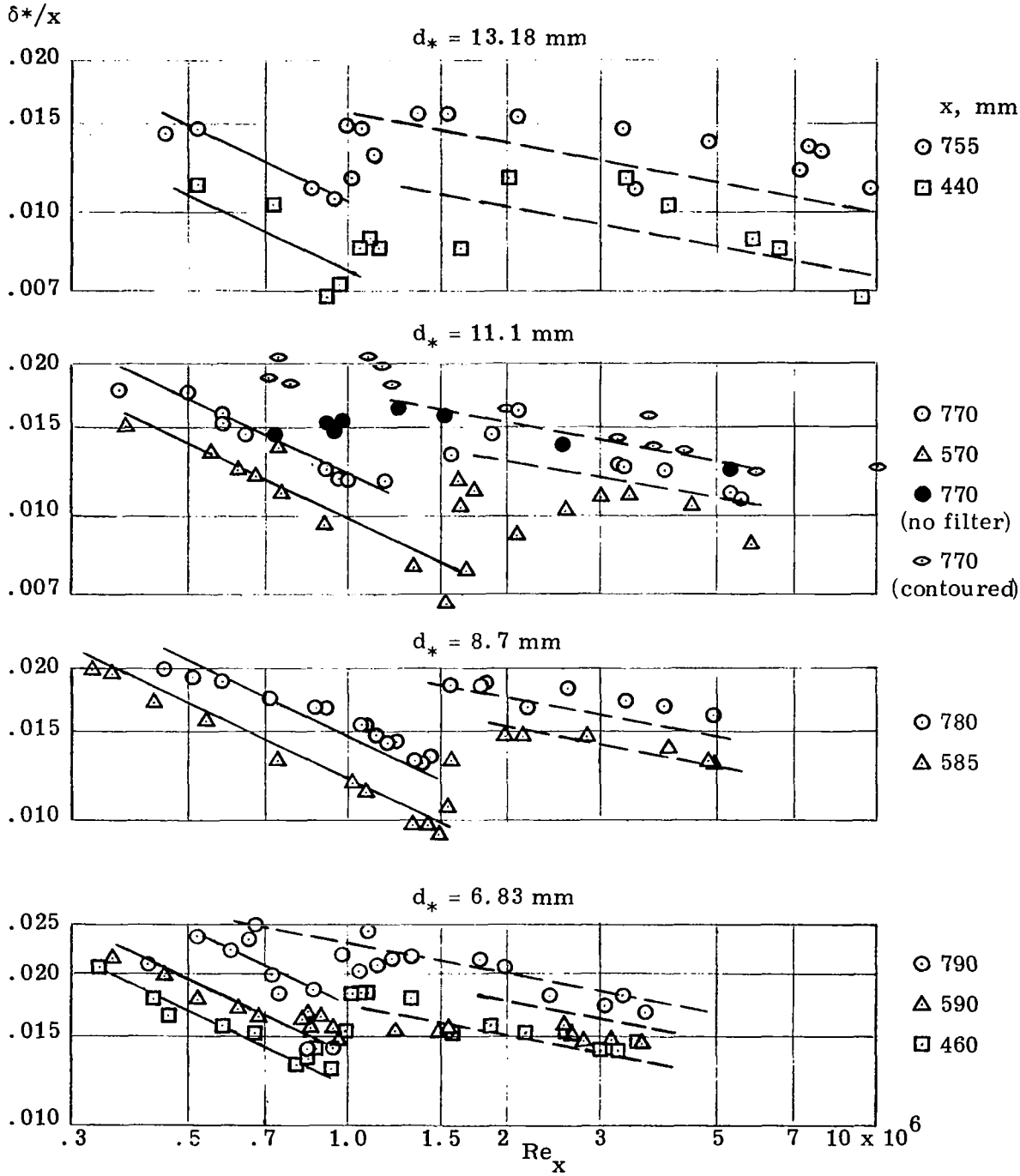


Figure C27. Variation of Displacement Thickness with Reynolds Number.

——— $\delta^*/x = 0.32\ M^{1.8}/\sqrt{Re_x}$ (Laminar)

— — — $\delta^*/x = 0.0133\ M^{1.5}/(Re_x)^{1/5}$ (Turbulent)

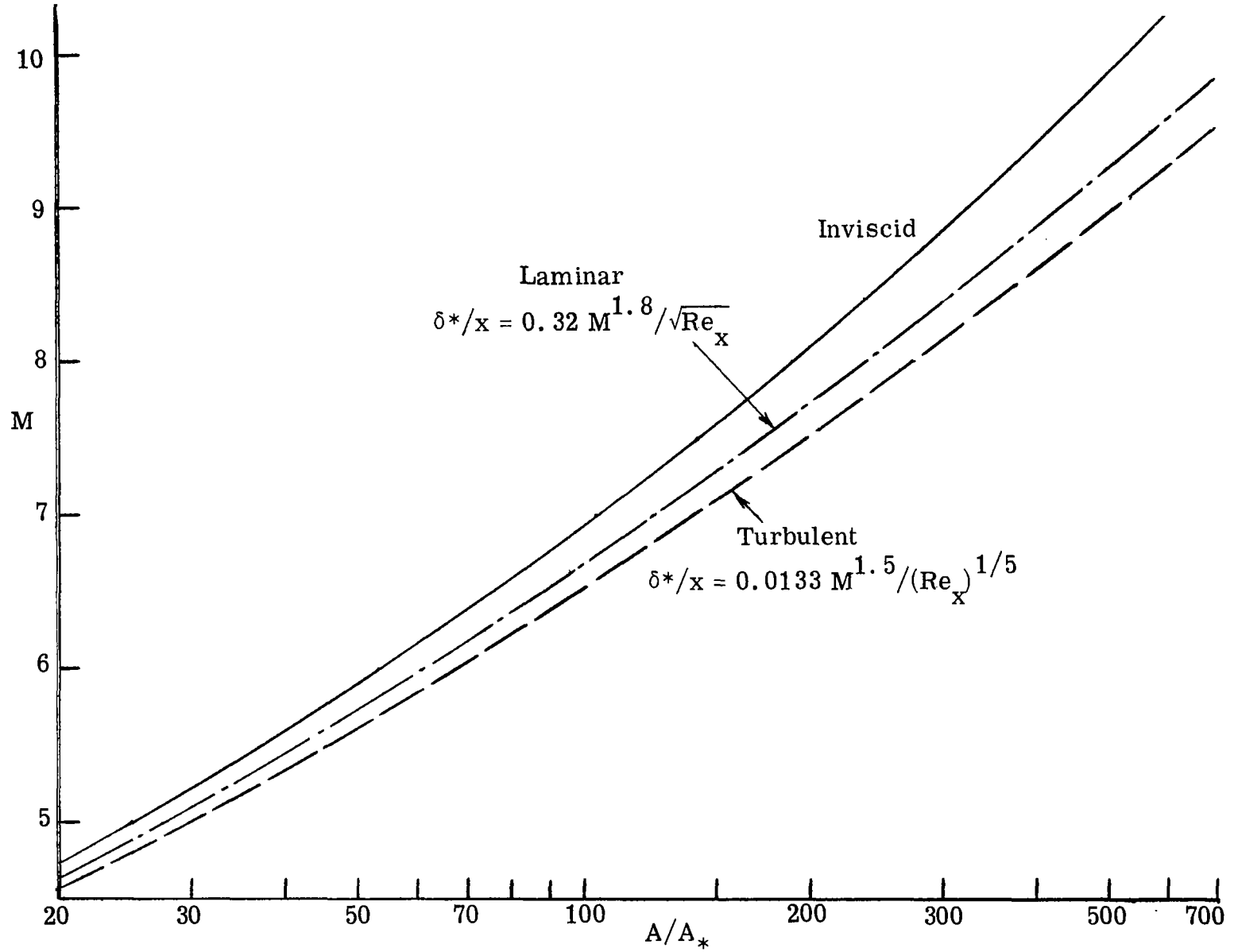


Figure C28. Core Mach Number as a Function of Area Ratio

$Re_x = 1.5 \times 10^6$